University of Alberta

A Study Of The Mechanisms Of Internal Cake Formation During Drilling, Well Completion And Hydraulic Fracturing Operations

By

Riaz Khan 

A thesis submitted to the Faculty of Graduate Studies and Research in partial fulfilment of the requirement for the degree of Master of Science

In

Petroleum Engineering

Department of Civil and Environmental Engineering

Edmonton, Alberta

Spring 2004

Your file Votre référence
ISBN: 0-612-96500-7
Our file Notre référence
ISBN: 0-612-96500-7

ABSTRACT

Xanthan gum (XG) and partially hydrolyzed polyacrylamide (PHPA) are used extensively as viscosifiers in the oil industry for different applications due to their unique rheological properties. An experimental study has been conducted to investigate formation damage characteristics of XG and PHPA based fluids.

Formation of internal cake due to the invasion of reservoir rock by drilling, completion, and fracturing fluids is one of the major causes of productivity reduction. A detailed investigation of the role of the rheology of viscoelastic fluids on the formation of "internal cake" has, therefore, been conducted in this study.

Extensional and shear viscosity measurements, and API filtration tests have been conducted by using fluids of 3 different XG and PHPA concentrations (0.5, 1.5, and 3.0 lb/bbl).

A series of core flow experiments have been conducted by using XG and PHPA solutions to investigate the effects of polymer concentration, fluid extensional and shear viscosity, and filtration loss characteristics on the original permeability of the porous media.

ACKNOWLEDGMENTS

I would like to express my sincere appreciation to my academic supervisor, Dr. Ergun Kuru for his guidance and supervision of this research study.

I am also grateful to Dr. Bernard Tremblay for his help in conducting the extensional viscosity measurements at Alberta Research Council (ARC). My heartiest thank to Mr. Sean Watt for his help in the construction of physical model and calibration of the transducers for measuring the pressure losses across the core.

Finally, I would like to extend my thanks and appreciations to my loving mother and late father, wife, and brothers for their patience and support during my studies.

TABLE OF CONTENTS

LIST OF TABLES

LIST OF FIGURES

NOMENCLATURE

A	cross-sectional area of porous medium, m^2
G	mass velocity, gram-cm^{-2}-sec^{-1}
k	permeability, m^2 (1Darcy = 1μm^2)
K	consistency index, dynes-sec^n-cm^{-2}
L	length of porous medium, m
n	flow behavior index
ΔP	pressure difference, Pa
q	volumetric flow rate, m^3/s
ε	extensional rate, 1/sec
ϕ	void fraction
γ	shear rate, sec^{-1}
γ_ω	wall shear rate, sec^{-1}
μ	fluid viscosity, cp
ρ	fluid density, gr/cc
τ	shear stress, Pa
η	shear viscosity, cp
η_e	extensional viscosity, cp
σ_{11}	stress in the axial direction, Pa
σ_{33}	stress in radial direction, Pa

CHAPTER 1

INTRODUCTION

1.1 Overview

Formation damage is defined as any type of a process, which results in a reduction of the flow capacity of an oil, water or gas bearing formation. Formation damage has long been recognized as a source of substantial productivity reductions in many oil and gas reservoirs and as a cause of water injectivity problems in many waterflood projects.

Most hydrocarbon reservoirs are exposed to multiple forms of formation damage including sand and fines migration, clay swelling, organic precipitation, scale and formation alteration caused by thermal recovery methods.

Optimizing production in field with multiple formation damage mechanisms can be an enormously expensive task. There are many factors to be considered including proper identification of the damage mechanisms, remedial testing and design, data interpretation, and implementation of preventive measures.

The economic impact of poor productivity of open-hole wells has pushed operators, service companies, and other research institutions towards spending significant research efforts in recent years to investigate drilling, completion and stimulation induced formation damage [1].

Development of meaningful laboratory testing and data interpretation techniques for assessment of the formation damage potential of petroleum bearing formations under actual scenarios of field operations, and for evaluations of techniques for restoration and stimulation of damaged formations are essential for exploitation of petroleum reservoirs economically [2].

Correct fluid composition, bridging material selection, and good maintenance of the wellbore fluid systems are the keys to success for better productivity [3].

Despite all the efforts, questions still remain regarding the formulation of optimum fluid composition to minimize, if not eliminate completely, productivity impairment due to formation damage.

1.2 Statement of The Problem

The pressure of the fluid column in the wellbore is usually higher than the formation pore fluid pressure and, therefore, some filtration of the wellbore fluid into the formation is always anticipated.

The rate of fluid filtration into the reservoir rock (leak-off rate) is one of the most critical parameters that needs to be controlled carefully during drilling, completion and stimulation operations. A strict control of fluid filtration characteristics is required to limit borehole instability, excessive torque and drag, pressure differential sticking and formation damage [4]. The problem becomes even more critical when drilling/completing horizontal wells with water based fluids where the fluids remain in contact with the pay zone for a long period.

Fluid loss control is generally achieved by; increasing the viscosity of the fluid [5-6] and developing internal/external filter cake using fluid loss control additives [7]. If the viscosifiers and fluid loss control additives are not selected properly, both mechanisms may lead to significant reduction of permeability [4, 8].

The rheology of drilling, completion and fracturing fluids is complex. These fluids must have the right yield stress in order to suspend cuttings without impeding flow. They must be shear thinning (viscosity decreases with shear rate) when pumped down the well and through the drill bit. These fluids often contain emulsifiers, breakers (fracturing fluids) and flocculants. Controlling the filtration rate of these rheologically complex fluids requires a comprehensive understanding of the viscoelastic properties of these fluids and their impact on the pressure drop as they flow through porous media.

One of the most common features associated with the flow of viscoelastic fluids in packed beds is that, much higher-pressure losses are observed than that can be attributed

to the shear flow of these fluids in the porous media. Such excessive pressure losses for viscoelastic fluids are well documented in the literature for a variety of aqueous polymer solutions and polymer melts. It has been recognized that the excess pressure drop may be due to the substantial extensional component present in this flow configuration [8-17]. Durst et al [11], for example, suggested that as much as 75 % of the pressure losses in the formation might result from extensional viscosity.

The pressure drop observed during the flow of viscoelastic fluids flow through porous media is a strong function of the fluid shear and extensional viscosities. As a fluid element moves forward through the tortuous channels in a porous medium, variations in cross-sectional area lead alternately to tensile and compressive deformations of the fluid element along its longitudinal axis. On each contraction and expansion, the fluid experiences shear (close to the walls) as well as extension (along the flow axis). The apparent viscosity as defined by the Darcy's law is, therefore, a mixture of shear and extensional viscosities.

The extensional viscosity for pure liquids without any structure is three times the shear viscosity. For these liquids, contribution of the extensional viscosity to the pressure loss is, therefore, constant and often neglected. However, for viscoelastic fluids such as typical drill-in and fracturing fluids, the extensional viscosity may be several orders of magnitude larger than the shear viscosity. This will lead to a tremendous increase in pressure loss, which is very often attributed to the development of internal cake during drilling, well completion, and hydraulic fracturing operations [18].

Formation of internal cake following the invasion of reservoir rock by drilling, completion, and fracturing fluids is known to be one of the major causes of productivity reduction. Actual physical mechanisms leading to internal cake development are not well known. In particular, there is a need for better understanding of quantitative relationship between viscoelastic properties of drilling, completion, and fracturing fluids and the degree of productivity impairment.

Understanding the mechanisms of internal cake formation and their quantitative relation to fluid properties will help to design of optimum drill-in, completion, and fracturing

fluid composition and hence, to minimize the productivity reduction associated with the application of these fluids in oil and gas wells. Correct fluid composition, bridging material selection, and good maintenance of the drilling fluid system are the keys to success for better productivity.

This research, therefore, calls for a preliminary investigation of the factors controlling the formation of "internal filter cakes". It is anticipated that better understanding of the flow of viscoelastic fluids in porous media would facilitate formulation of optimum drilling, well completion and fracturing fluid compositions with minimum formation damage effect.

1.3 Objective and Scope of Study

The primary objective of this research study is to investigate the formation damage characteristics of xanthan gum and partially hydrolized polyacrylamide based fluids.

A secondary objective of this study was to investigate the extensional viscosity of polymer based fluids as a possible mechanism of internal cake formation. In order to achieve these objectives the following tasks have been accomplished:

i-) Measure the shear viscosities of XG and PHPA based solutions with three different polymer concentrations (0.5, 1.5, 3.0 lb/bbl).

ii-) Measure the API filtration loss characteristics of XG and PHPA based solutions with three different polymer concentrations (0.5, 1.5, 3.0 lb/bbl).

iii-) Measure the extensional viscosities of XG and PHPA based solutions with three different polymer concentrations (0.5, 1.5, 3.0 lb/bbl).

iv-) Conduct core-flow experiments to investigate the possible relationship among the polymer concentration, fluid extensional viscosity, shear viscosity, filtration loss characteristics, and pressure drop across the core samples.

1.4 Structure of Thesis

Chapter 1 gives an overview of the research work. It outlines the background and statement of the research problems, the objectives and the scope of the work.

Chapter 2 gives a comprehensive literature review of the subject area.

Chapter 3 describes the methodology followed throughout this study. A detailed description of experimental set-up and procedure for core flow experiments, description of the equipment and used procedure for shear and extensional viscosity measurements are given.

Chapter 4 presents the results of rheology measurements, filtration tests and core flow experiments using xanthan gum solutions.

Chapter 5 presents the results of rheology measurements, filtration tests and core flow experiments using partially hydrolyzed polyacrylamide solutions.

Chapter-6 provides the detailed discussion and comparison of the results from XG and PHPA solutions.

Finally, the Chapter-7 includes the conclusions of this study and the recommendations for further research.

CHAPTER 2

LITERATURE REVIEW

2.1. Formation Damage

Formation damage is a generic terminology referring to the impairment of the permeability of petroleum bearing formations by various adverse processes. Formation damage is an undesirable operational and economic problem that can occur during the various phases of oil and gas recovery from subsurface reservoirs including production, drilling, hydraulic-fracturing and workover operations [2]. As expressed by Amaefule et al. (1988) [19] "Formation damage is an expensive headache to the oil and gas industry". Bennion (1999) [20] described formation damage as: "The impairment of the invisible, by the inevitable and uncontrollable, resulting in an indeterminate reduction of the unquantifiable!" Formation damage assessment, control, and remediation are among the most important issues to be resolved for efficient exploitation of hydrocarbon reservoirs (Energy Highlights, 1990) [21].

Formation damage is caused by physico-chemical, chemical, biological, hydrodynamic, and thermal interactions of porous formation, particles, and fluids and mechanical deformation of formation under stress and fluid shear. These processes are triggered during the drilling, production, workover, and hydraulic fracturing operations. Formation damage indicators include permeability impairment, skin damage, and decrease of well performance. As stated by Porter (1989) [22], "Formation damage is not necessarily reversible" and "What gets into porous media does not necessarily come out." Porter (1989) called this phenomenon "the reverse funnel effect." Therefore, it is better to avoid formation damage than to try to restore it.

The consequences of the formation damage are the reduction of the oil and gas productivity of reservoirs and noneconomic operation. Therefore it is essential to develop experimental and analytical methods for understanding and preventing and/or controlling formation damage in oil and gas bearing formations. The laboratory experiments are important steps in reaching understanding of the physical basis of formation damage

phenomena. "From this experimental basis, realistic models which allow extrapolation outside the scalable range may be considered" (Energy Highlights, 1990). These efforts are necessary to develop and verify accurate mathematical models and computer simulators that can be used for predicting and determining strategies to avoid and/or mitigate formation damage in petroleum reservoirs [2].

2.1.1. Factors Affecting Formation Damage

Amaefule et al. [19] classified the various factors affecting formation damage as follows: (1) Invasion of foreign fluids, such as water and chemicals used for improved recovery, drilling mud invasions, and workover fluids; (2) Invasion of foreign particles and mobilization of indigenous particles, such as sand, mud fines, bacteria, and debris; (3) Operation conditions such as well flow rates and well bore pressures and temperatures; and (4) Properties of the formation fluids and porous matrix.

2.1.1.1. Formation Damage Mechanisms

Bishop (1997) [23] summarized the seven formation damage mechanisms described by Bennion and Thomas (1991, 1994) [20,24] as follows: (1) Fluid-fluid incompatibilities, for example, emulsion generated between invading oil based mud filtrate and formation water; (2) Rock-fluid incompatibilities, for example, contact of potentially swelling smectite clay or deflocculatable kaolinite clay by non-equilibrium water based fluids with the potential to severely reduce near wellbore permeability; (3) Solids invasion, for example, the invasion of weighting agents or drilled solids; (4) Phase trapping/blocking, for example, the invasion and entrapment of water based fluids in the near wellbore region of a gas well; (5) Chemical adsorption/wettability alteration, for example, emulsifier adsorption changing the wettability and fluid flow characteristics of a formation; (6) Fines migration, for example, the internal movement of fine particulates within a rock's pore structure resulting in the bridging and plugging of pore throats; (7) Biological activity, for example, the introduction of bacterial agents into the formation

during drilling and the subsequent generation of polysaccharide polymer slimes which reduce permeability.

2.1.1.2. Formation Damage by Fines Migration Including Effects of Internal Filter Cake

The infiltration and/or migration of fluids in porous media has long been a problem to petroleum industry. The consequences of these fluid invasions are numerous and have been identified in many field operations [1, 25, 26]. In oil and gas reservoirs, such an invasion of foreign fluids and their consequent interaction with the in-situ fluids and formation causes drastic reduction in production [27, 28]. For example, the in-situ release and subsequent migration of indigenous fines in sandstone reservoir cause drastic permeability reduction when fresh and low salinity water replaces the brine commonly present in reservoirs [29, 30].

Filtrate invasion of a drilling fluid and the accompanying invasion and migration of solids may come directly from the fluid system or from the formation itself. The intrusion and deposition of these mobile particles lead to the blockage of pore throats, which include a reduction in permeability of the rock. [31]. Deeper invasion into the formation is favoured by large pore size and small particle size. The depth of invasion can be significant if the formation is highly fractured. Once the formation near wellbore becomes totally filled or plugged by particles, an internal filter cake begins to establish in the formation. [32].

2.1.2. Formation Damage in Different Oilfield Operations

Formation damage and its effect on well productivity may result from drilling mud filtrate interaction with formation minerals and from invasion of drilling fluid solids. Penetration of filtrate damage depends on the effectiveness of fluid-loss control and may range from a few inches to several feet [33].

Production rates normally decline with the natural depletion of a field; accelerated decline from formation plugging is a common problem during production operations that must be dealt with to maintain an adequate return on investment. Detection and diagnosis, critical factors in remedying a well-plugging problem, often are not simple [1].

Formation permeability damage from fracturing fluids can sometimes be a serious problem, possibly because of deep penetration of the damage during prolonged pumping. The characteristic of a good fracturing fluid includes ability to withstand high shear rates in the wellbore (up to 1300 sec^{-1}) and high viscosities at low shear rates (below about 50 sec^{-1}) for proppant transport in the fracture.

The extensional viscosity of polymer solutions may reduce leakoff, thus reducing potential formation damage in gravel pack and hydraulic fracturing applications [16].

Two main factors affect the fluid loss of fracturing fluids; (1) an early high leakoff phase before a component filter cake is established across the face of the formation, typically referred to as spurt loss, and (2) a phase where all fluid loss is controlled by the leakoff through the filter cake.

The major factors that influence the spurt loss and filter cake behavior are; (1) shear rate in the fracture; (2) permeability of the reservoir; (3) pressure difference between the bottom hole fracturing pressure and the reservoir pressure; (4) fluid properties and; (5) temperature [34].

Fluid quality is particularly critical in treating perforated completions. We must keep in mind that deeply penetrating workover damage will create a condition similar to perforating with insufficient penetration into a previously damaged zone. Well productivity can easily drop to a small fraction of the undamaged productivity [1].

2.1.3. Laboratory Evaluation of Formation Damage

Laboratory testing is a critical component of the diagnostic procedure followed to characterize the damage. To properly characterize the formation damage, a complete

history of the well is necessary [35]. Development of meaningful laboratory testing and data interpretation techniques for assessment of the formation damage potential of petroleum bearing formations under actual scenarios of field operations, and for evaluations of techniques for restoration and stimulation of damaged formations are essential exploitation of petroleum reservoirs.

Experimental systems and procedures should be designed to extract meaningful and accurate experimental data. The data should be suitable for use with the available analytical interpretation methods. This is important to develop reliable empirical correlations, verify mathematical models, identify the governing mechanisms, and determine the relevant parameters. These are then used to develop optimal strategies to mitigate the adverse processes leading to formation damage during reservoir exploitation [2].

Formation damage in petroleum-bearing formation as described above, occurs by various mechanisms and/or processes, depending on the nature of the rock and fluids involved, and the in-situ conditions. The commonly occurring processes involving rock-fluid and fluid-fluid interactions and their affects on formation damage by various mechanisms have been reviewed by numerous studies, including Mungan (1989), Gruesbeck and Collins (1982), Khilar and Fogler (1983), Sharma and Yortsos (1987), Civan (1992, 1994, 1996), Wojtanowicz et al. (1987, 1988), Masikewich and Bennion (1999), and Doane et al. (1999) [24].

Laboratory test are designed to determine, understand and quantify the governing processes, their parameters, and dependency on the in-situ and various operations conditions, and their effect on formation damage. Laboratory tests help determine the relative contributions of various mechanisms of formation damage.

2.1.4. Selection of Reservoir Compatible Fluids

Masikewich and Bennion (1999) [36] described the typical information, tests and processes necessary for laboratory testing and optimal design, and selection of fluids for

reservoir compatibility. Hence, they classify the effort necessary for fluid testing and design into six steps: (1) identification of the fluid and rock characteristics, (2) speculation of the potential formation damage mechanisms, (3) verification and quantification of the pertinent formation damage mechanisms by various tests, (4) invasion of the potential formation damage mitigation techniques, (5) development of the effective bridging systems to minimize and/or avoid fluids and fines invasion into porous media, and (6) testing of candidate fluids for optimal selection.

2.1.5. Experimental Set-up for Formation Damage Testing

The design of apparatus for testing of reservoir core samples with fluids varies with specific objectives and applications. Typical testing systems include core holders, fluid reservoirs, pumps, flow meter, sample collectors, control system for temperature, pressure or flow, and data acquisition systems. The degree of sophistication of the design of the core testing apparatus depends on the requirements of particular testing conditions and expectations (Doane et al. 1999 [37]).

2.2. Viscoelastic Effects of Fluids Flowing Through a Porous Media

The analysis of viscoelastic effects of fluids flowing through porous media is not a new subject. Several authors, from different areas including fundamental rheology, EOR and drilling/completions have made qualitative observations about the fact [38].

Data presented by Dauben and Menzie [39], Cakl et al. [40] and Marshall e Metzner [41] indicate higher friction losses than the ones predicted by Darcy's Law. The authors attribute the fact to normal stresses effects, typical of viscoelastic flow.

Durst et al. [11] present a broad discussion on the nature of non-Newtonian flows through porous media. The main motivation is the deviation found in the well-known Darcy Law for the flow of some diluted polymeric solutions. The authors propose that the total strain experimented by the fluid is a composition of shear and elongation efforts.

Jones and Walters [42] introduce the importance of the extensional components in polymer injection through porous media, aiming EOR applications. Saasen et al [13] correlated fluid invasion with linear viscoelastic parameters. Later, Svendsen et al. [43] show results of extensional viscosity as indicators of fluid invasion governing parameters. Young et al. [16] show similar correlation for fracturing fluid invasion. These authors suggest that the Trouton Ratio (a ratio of extensional viscosity to shear viscosity at the same shear/extensional rates) would be the major rheological parameter governing fluid invasion. Bird et al. [44] describe in detail the several material functions, which can characterize the viscoelastic steady and unsteady flow of fluids in several geometries.

The Trouton ratio is the established method of comparing extensional and shear viscosities. By definition extensional viscosity is always 3 times greater than shear viscosity at Newtonian conditions. Therefore a Trouton ratio of 3 indicates Newtonian behaviour. Thus, any deviation away from 3 leading to greater values indicates that there is viscoelasticity in the sample [43].

2.2.1. Flow Behavior of Polymer Based Fluids in Porous Media

With the growing interest in the oil field applications of polymer based solutions, it becomes increasingly important to have a proper understanding of the flow behavior of high concentration of polymer-based solutions in porous media

Newtonian fluids, such as brines and mineral oils, exhibit a linear relationship between the shear stress, τ, and the shear rate, γ:

$$\tau = -\mu\gamma \qquad (2.1)$$

where the coefficient μ represents the fluid viscosity. Aqueous polymer solutions, however, do not show such linear relationship. Instead, a non-linear relationship is found approximated by the empirical expression:

$$\tau = -K[\gamma]^{n} \qquad (2.2)$$

where K represents the consistency index and n the flow behavior index.

Darcy's law describes the laminar flow of Newtonian fluids through porous media:

$$\frac{q}{A} = \frac{k}{\mu} \cdot \frac{\Delta P}{L} \quad \text{.....(2.3)}$$

To describe the flow of polymer solutions their non-Newtonian behavior must be taken into account. In principle, this behavior can be determined in core flow experiments by recording the pressure drop as a function of flow rate, making allowance for the dimensions of the test sample and the viscosity of the fluid. The interpretation of the experimental results are complicated by the influence of several phenomena [45]:

1. aqueous polymer fluids exhibit non-Newtonian flow behavior; their viscosity is not constant but depends on the applied flow rate [39, 46-47],

2. the fluid may also show pseudoplastic behavior resulting in an additional pressure drop [39,41,48],

3. shear degradation of polymer molecules may occur when a certain critical flow rate is exceeded, in which case the fluid viscosity will be decreased irreversibly [49, 50],

4. adsorption/retention of polymer molecules on the rock surface [51-53],

5. part of the pore volume is virtually inaccessible to polymer flow [52, 54-55].

All these phenomena affect the pressure drop across the core sample, and the evaluation of the complex overall behavior would be greatly facilitated if the contribution of the different phenomena could be accessed.

In order to account for the effect of shear-thinning characteristics of polymer based fluids on the pressure losses, Darcy equation (equation 2.3) can be modified by using the power-law model (equation.2.2). Many authors have attempted to develop macroscopic relationships between the velocity of the fluid in the rock and the apparent shear rate of the fluid. This shear rate represents an average shear rate in the porous media, since the

actual shear rate on each individual pore is a strong function of the diameter of the pore-throat and each rock has a pore-throat size distribution leading to a shear rate distribution.

The modified Blake-Kozeny equation was derived to estimate shear rates for the flow of power law fluids in porous media [56].

$$\dot{\gamma}_w = \frac{3n+1}{4n} \frac{12G}{\rho(150k\phi)^{1/2}}. \quad \text{.....(2.4)}$$

2.3. Fluid Loss (Leak-off) Control

The rate of leakoff is of critical importance during drilling, completion operations (i.e. sand control) and stimulation treatments, such as acid treatments and hydraulic fracturing. In all of these cases, fluid loss control has been achieved by two basic mechanisms [7]:

Increasing the overall viscosity of the fluid using high polymer concentrations or by crosslinking the polymer [5, 6],

Developing an internal and/or external filter cake using fluid loss additives (starch, sized $CaCO_3$, mica silica flour, oil soluble resins, etc) to plug the pore throats of the formation [57].

Both fluid loss control mechanisms may result in a loss of permeability when flow is initiated in the production mode. Furthermore, if fluid loss additives are not used properly, they can cause significant loss of permeability due to their plugging mechanism if they enter the formation [58, 59].

Two distinct phases of fracturing fluid loss appear to exist: (1) an early high leakoff phase before a component filter cake is established across the face of the formation, typically referred to as spurt loss, and (2) a phase where all fluid loss is controlled by the leakoff through the filter cake [34].

The effect of the parameters that influence fluid leakoff have been investigated by many authors [5-7, 60]. However, it is clear that fluid leakoff is a complex phenomenon that is

not fully understood and poorly modelled. Penny and Conway [7] and McGowen and Vitthal [34] provide comprehensive reviews of fracturing fluid-loss, thus only literature relevant to discussion of the effects of shear rate, permeability, and pressure will be reviewed here.

2.3.1. Effect of Shear Rate on Fluid Loss

Many researchers have investigated the effect of shear rate on the buildup of filter cake [34, 5-7, 60]. Although most researchers agree about the qualitative trends, such as higher leakoff at higher shear rates, different researchers have different conclusions regarding the importance of the dynamic flow conditions.

Gulbis [61, 62] reported no shear rate effects with crosslinked fluids for shear rates below 80 sec^{-1}. In contrast, Penny et al. [7, 63] reported no shear effects at less than 40 sec^{-1}.

Recently Navarette et al. [5, 64] have reported large differences between static and dynamic conditions (conflicting most previous investigators). They reported that spurt loss can be reduced by either using more viscous fluids (such as crosslinked guars instead of HEC) or by using fluid-loss additives. However, the use of more viscous fracturing fluids or fluid-loss additives or both can adversely affect the conductivity of the proppant pack, which becomes a critical factor on the postproduction of the well because of the higher permeability of the formation.

Vitthal et al. [34] conducted experimental work and reported that the fluid loss of linear gels is independent of the shear rate and can be lower than that of crosslinked gels on low permeability formations. The fluid loss for crosslinked fluids increases as the shear rate increases, primarily because of the creation of a filter cake that is in equilibrium with the fluid shear stress. Higher shear rates result in thinner equilibrium filter cakes and increased steady-state leakoff velocities. Shear rate has a negligible effect on early-time filtration data [34, 65].

2.3.2. *Effect of Permeability on Fluid Loss*

Roodhart [66] conducted some of the earliest work on the effect of permeability of cores with hydroxyethylcellulose (HEC) fluids with silica flour up to 100 md at a pressure of 1,500 psi. He found that the spurt loss was proportional to the square root of the permeability and that C_w (wall-building coefficient, $ft/min^{0.5}$) was independent of core permeability for all fluids that generated a filter cake.

Penny and Conway [63] likewise report spurt loss to be proportional to the square root of the permeability for linear HPG fluids in cores up to 100 md; however, they also show spurt-loss data that is directly proportional to permeability for crosslinked HPG fluids.

McMechan [67] similarly shows data that indicate a linear relationship between spurt loss and core permeability. McGowen et al. [68] introduced the first detailed study of static fluid leakoff of fracturing fluids into very high permeability cores (up to 5,000 md). This research has been supported by subsequent studies [6, 64, 67]. Parlar et al. [6] indicated a linear spurt-loss relationship with permeability in their testing with high-permeability cores (up to 1,000 md).

Vitthal et al. [34] reported that high-permeability cores are less sensitive to shear rate effects because of internal pore plugging. This internal pore plugging increases significantly as permeability or pressure increases, and causes a reduction in the C_w and v_n (dynamic leakoff coefficient, ft/min). Linear gels transition from building filter cakes to whole gel leakoff, with, increasing core permeability and increasing filtration. The major effect of permeability on the fluid loss of crosslinked gels is an increase in the spurt loss.

2.3.3. *Effect of Differential Pressure on Fluid Loss*

Several studies have been performed regarding the effect of differential pressure on fluid loss [6,7, 66 & 69]. The results of these studies have also been conflicting. In Roodhart's study [66], he reported that filter cakes were compressible up to 300 psi (filter cake

compressibility, $\alpha = 0.0$) but incompressible ($\alpha=0.5$) thereafter. He did not report a trend of spurt loss vs. pressure.

Mayerhofer [70, 71] performed static measurements on filter paper and also reported that the degree of filter-cake compressibility varied with pressure. He found in his study that α was lower while the pressure was increasing.

Penny et al. [7, 63, 72] showed that filter cakes were compressible ($\alpha=0.17$ to 0.25) for pressure drops up to 2,000 psi, while no data on the spurt dependency was presented. Whereas Vitthal et al. [34] mentioned that increased filtration pressure results in an increase in the spurt loss for all fluids. The filter cakes of linear and crosslinked fluids are highly compressible; therefore, the C_w increases slightly with increasing pressure. The relaxation times for filter cakes are small and the filter cakes adjust quickly to pressure changes. The product of the formation permeability and the pressure drop (also called driving force) drives fluid loss; a strong linear relationship exists between the driving force and the spurt loss for a fluid.

2.4. Selection of Non-Damaging/Optimum Drill in Fluids Composition

Correct fluid composition, bridging material selection, and good maintenance of the drilling fluid system are the keys to success for better productivity. A filter cake that allows a better flow profile along the entire wellbore reduces the risks of water coning or erosion associated with non-uniform flow and pressure drop. Very often, the cost of a specialized reservoir drilling fluid system is less than that of any treatment required to remove a standard filter cake and restore the original permeability along the entire borehole [3]. The productivity of openhole completions can be increased by the use of reservoir drilling fluids that are properly designed to minimize formation damage [73, 74].

Investigations have shown that rapid formation of a thin, impermeable, external filter cake reduces formation damage [74, 75]. To achieve this goal, careful design is required to minimize spurt loss and invasion during drilling and completion operations. Selection

of the correct chemicals and defining their concentration in use is paramount to obtaining the desired properties [3]. An area of particular importance is the choice of bridging solids. It has been demonstrated that bridging solids play a critical role in the rapid formation of the filter cake [75, 76].

Another dominant factor in the productivity of openhole completions is the compatibility of the filter cake with the formation and completion hardware. Bailey et al. [77] found that filter cake yield strength plays a significant role in the removal of filter cake during drawdown and that the yield stress is affected by the type and size of particles in the fluid.

When adsorbed in the near-well region, polymers formed by long flexible chainlike molecules, like polyacrylamides, help reducing water production in mature wells suffering from excessively high water cut [78, 79].

Several studies [80-82] have shown that a bridging adsorption phenomenon occurs in low permeability porous media due to a combination of chain elongation and adsorption. Zitha [82] developed a theory for polymer flow in porous media honouring the layer and bridging adsorption phenomena (canonical filtration theory) and proved that the bridging adsorption phenomenon includes a strong filtration of the longest polymer molecules.

Designing drill-in fluids, which can guarantee minimum invasion into the reservoir rock, is a must for openhole completion wells. The industry has proposed several ideas to deal with the problem, most of them based on adding bridging agents to the fluid formulation. Such agent would block pores near the well bore and, consequently, prevent additional fluid to invade the rock [38].

Several authors (Xiao et al. [83] Peng et al [84], Carlson et al. [85], Longeron et al. [86], Clark et al. [87], Gallino et al. [88], Audibert et al. [89] and Navarrete et al. [90] present relevant theoretical and experimental studies on the filtration properties of water based fluids. Those test were run both in dynamic and static conditions for several types of fluid, pH, solids size, shape and concentration, pressure and shear stresses.

Lomba et al. [91] introduced a discussion on additional mechanisms, besides bridging, which could minimize fluid invasion. Among them, there is a topic on how polymers of different rheological properties would behave while flowing through a non consolidated sand bed in a static filtration apparatus specifically designed to evaluate invasion. The authors concluded that shear viscosity was not the only factor, which governs invasion, since some less viscous fluids presented less invasive behaviour, for the same conditions, than high viscosity fluids. The authors postulate several hypotheses on the role of the viscoelastic properties of such fluids on the invasion behaviour. The role of rheology on fluid invasion in the reservoir is still not clearly stated. Main points, which arise, are: to what nature of efforts the fluid is submitted when flowing through the porous media? Which shear rates characterize the well-reservoir boundary? Which rheological properties govern the invasion phenomenon?

A different concept was proposed by Martins et al. [38] for controlling invasion in their article: designing a polymer based fluid which would generate extremely high friction losses when flowing through a porous medium without generating extra losses while flowing in the well. In this case the fluid would present proper flow and solids transport properties in the well and would not invade the rock formation. They conducted some experimental work and their results indicate that Newtonian fluids, CMC (Carboximethyl Cellulose) solutions and low concentration XC (Xanthan Gum) and PHPA (Partially Hydrolyzed Polyacrylamide) solutions were properly fit by Darcy law. On the other hand, the highly concentrated solution presented relevant deviations. Such deviations tended to increase with the increase of deformation rate (or differential pressure). This fact indicates that there is a need for applying viscoelastic constitutive models to account for the extra friction losses.

Svendsen et al. [43] reported, in a clear fluid without solid bridging material, it becomes necessary to use polymeric additives to create a sufficient extensional viscosity to prevent fluid from flowing into the formation. The extensional viscosity, also called the shear free viscosity [45], is known to be the major factor controlling the flow of polymeric liquids into porous formations [11]. The reason is that the fluid resists changing to a shape similar to a rod thickening under compression [92, 93]. Thus, for regular flow in a porous

medium, it contributes about 75% of the resistance to flow. In this case, because the extensional viscosity and the shear viscosity are proportional, the empirical determination of the permeability will hide the effect of the extensional viscosity. For polymeric liquids the case is completely different, as in Non-Newtonian flow the extensional viscosity can be several magnitudes larger than the shear viscosity [93]. Thus optimum filtration control is achieved by the use of a fluid with a high extensional viscosity.

2.5. Extensional Viscosity

When a fluid flows through a porous rock, it experiences a series of contractions and expansions as it goes from pore-bodies into pore-throats and then into pore-bodies again. On each contraction and expansion the fluid experiences shear close to the wall and extension away from the walls. The extensional rate (or rate of stretching) is the product of the converging flow into the pore-throat (accelerating) and expansion exiting the pore-throat (decelerating). Based on the type of deformation, shear and extensional viscosity can be defined as [18]:

Shear Viscosity:

$$\eta = \frac{\sigma_{12}}{\gamma} \quad \text{.....(2.5)}$$

Extensional viscosity:

$$\eta_e = \frac{\sigma_{11} - \sigma_{33}}{\varepsilon} \quad \text{.....(2.6)}$$

Where σ_{11} and σ_{33} are the stresses in the axial and radial directions respectively for uniaxial elongation and σ_{12} is the shear stress. The shear rate is γ and the extensional rate is ε.

The apparent viscosity obtained from Darcy's law is the result of the contributions of both the shear and extensional viscosities [42, 7]

The elongational / extensional viscosity is that parameter which is at the base of elongational flow. The elongational viscosity regards the strength of polymer melt in tensile stress while the shear viscosity is related to the shear flow.

Two types of axisymmetrical elongational flows exist. The most investigated type of extensional flow is simple extension (uniaxial). The other axisymmetrical flow is biaxial extension. Planar extension on the other hand is a non-axisymmetrical elongational flow since it is deformed only in two directions [94] (Figure 2.1).

The shear and elongational viscosities of a Newtonian fluid are constant. For an axisymmetric flow of Newtonian fluid, the Trouton ratio ($Tr = \eta_e/\eta$) is 3.

For polymers, shear and elongational viscosities depend upon strain rate. At low value of strain rate, the shear and elongational viscosities of a polymer are typically constant. For axisymmetrical flow, Trouton ratio for the zero strain rate, shear and elongational viscosities of a polymer is generally 3. As the strain rate is increased beyond the Newtonian limit, the shear viscosity of a polymer decreases with increasing strain rate, whereas the elongational viscosity may actually increase or decrease followed by a decrease or increase as the strain rate is further increased, depend upon the polymer type and its concentration [95].

2.6. Extensional Viscosity of Polymer Melts

There are several existing models that can be used to estimate the extensional / elongational viscosity of polymer melts. The processing of polymer melts involves both shear and extensional deformations. In simple shear flow the velocity changes in the direction perpendicular to the flow direction. Material elements are not stretched along the streamlines contrary to elongational flow. As mentioned before, two types of axisymmetrical elongational flows exist. The most investigated type of extensional flow is simple extension (uniaxial). The other axisymmetrical flow is biaxial extension. Planar extension on the other hand is a non-axisymmetrical elongational flow since it is deformed only in two directions (Figure 2.1). All these flows are shear free which greatly

complicates the design of the extensional rheometers to replicate these flows since the polymer must not adhere to any surfaces other than those which transmit the stretching force [94].

There are two basic approaches for the determination of the elongational flow properties of polymer melts: using either tensile testing method or converging flow methods.

The flow near an abrupt contraction in a channel (entrance flow) is highly extension dominated. Therefore, entrance flow is a good benchmark test for analyzing the effect of elongational viscosity on polymer flows. Besides being a good test case, entrance flow is often encountered in polymer-processing applications, such as extrusion dies and the runners in injection modelling.

For Newtonian fluids it has been established experimentally and by numerical simulation that the main cause of vortex near the abrupt contraction is the fluid inertia. In contrast, for creeping flow of polymers, it has been experimentally demonstrated by many researchers that a recirculating vortex near the abrupt contraction, which can grow significantly with the flow rate in the channel. Furthermore, at certain flow rates, experiments have shown the formation of a second vortex, called lip vortex, near the entrant corner. Since the flow near an abrupt contraction is highly extension dominated, in addition to the pressure drop for fully developed flow in the upstream and downstream channels, an extra pressure loss is encountered in the entrance flow. Due to the high elongational viscosity of polymers, this extra pressure loss, called the entrance loss, can be particularly large for polymers [95].

Several entrance flow models were developed to estimate the extensional viscosity of a fluid from the entrance pressure and shear viscosity measurements [94]. A critical issue in applying entry flow analysis techniques to estimate the elongational viscosity is to obtain entrance pressure measurements.

Bagley [96] observed that the flow of polymer melts into a capillary generates an extra pressure at the entrance, which is higher than for a Newtonian fluid (up to 10 times). A method was developed by Bagley to determine this entrance pressure.

A potential source of error exists in applying entry flow analysis when the entrance pressure measurements are made under melt fracture conditions. Melt fracture is the name given to an unstable flow regime which occurs upstream of a contraction (Piau et al. [97]). This instability is believed to occur at a critical entrance pressure (Cogswell [98]) due to excessive tensile stresses in the converging flow at the entrance to a contraction. This critical entrance pressure depends on the polymer investigated, its molecular weight and temperature and on the geometry of the die.

2.6.1. Cogswell Analysis

The assumptions for the velocity field into a contraction are quiet different on the entry flow model chosen. The Cogswell model [98] assumes that the velocity on the surface of the recirculation vortices shown in Figure 2.2 is zero. This assumption is based on flow observations by Cogswell [99, 100] who claims that the velocity on the surface of the vortices is equal to only 10% of the velocity on the flow axis. The method by which Cogswell arrived at this measurement was not specified however. The measurements of Cogswell may have been for small vortices. A streak photograph (Figure 2.2) of the flow of a branched Polydimethylsiloxane (PDMS) into an orifice shows that the velocity on the surface of a vortex is approximately 40% of the axial velocity at the same distance away from the orifice. According to Cogswell [99, 100], the generation of vortices minimizes the pressure drop at the entrance to a contraction.

The following expression was then obtained for the extensional viscosity:

$$\eta_E = (9 / 32)(n + 1)^2 (P_o / \gamma_A)^2 / \eta \quad \text{.....(2.7)}$$

where:

P_o = entrance pressure, η = Viscosity = $k\gamma_A^{(n-1)}$, n = power law index, k = power law coefficient, γ_A = apparent shear rate = $4Q/(\pi R_o^3)$, R_o = radius of Capillary, Q = flow rate

The average extensional rate was derived to be:

$$\varepsilon = 4\gamma_A 2\,\eta / (3\,(n+1)\,P_o) \quad \text{.....(2.8)}$$

The entrance angle, θ, of the converging flow funnel, in Figure 2.3, was calculated by Cogswell [99, 100]:

$$\tan(\theta) = (8/3)\eta\gamma_A / ((n+1)P_o) \quad \text{.....(2.9)}$$

2.6.2. Gibson Model

The Gibson model neglects completely the upstream vortices by claiming that their contribution to the pressure drop is of second order. Gibson [101, 102] argues that the viscous dissipation in extension is the major contribution to the entrance pressure drop for dies with large entry angles and that the extensional contribution is not very sensitive to differences in the flow between the case of small vortices and large vortices.

Shear stress, τ, and the extensional stress, σ_E, were written as power law expressions and the following expression was then derived for the extensional viscosity:

$$\sigma_E = l\,\varepsilon^t \quad \text{.....(2.10)}$$

$$\tau = \kappa\gamma^n \quad \text{.....(2.11)}$$

where:

$$\gamma = (3n+1)/(4n) * \gamma_A$$

$$\gamma_A = 4Q / (\pi R_o^3)$$

The coefficients l and k are constant and n and t are called power law indices. The shear contribution to the total pressure drop across the flow regime was calculated by Gibson [101, 102].

$$P_s = 2K\,(\sin(\alpha))^{3n} / 3n\alpha^{(1+3n)} * ((1+3n)/(4n))^n * (1 - R_0/R_b)^{3n})\,\gamma_A{}^n \quad \text{.....(2.12)}$$

Where:

α = converging angle of die (half angle)

R_o =radius of Capillary

R_1 = radius of upstream conduit

The elongation contribution, P_e, to the entrance pressure, P_o, was calculated by subtracting P_s (equation 2.14) from the total measured entrance pressure, P_o:

$$P_e = P_o - P_s \quad \text{.....(2.13)}$$

The following expression was obtained for the extensional component of the entrance pressure:

$$P_e = l\gamma_A^t [(2 / (3t)(\sin(\alpha)(1+\cos(\alpha))/4)^t (1 - R_o / R_1)^{(3t)}) + \phi(t, \alpha) / 4^t] \quad \text{....(2.14)}$$

Where:

$$\phi(t, \alpha) = \text{Int}(0\text{-}\alpha) (\sin(\beta))^{(t-1)} (1+\cos(\beta))^{(t-1)} d\beta$$

The average strain rate, ε, was calculated to be:

$$\varepsilon = \gamma_A \sin(\alpha)(1 + \cos(\alpha)) / 4$$

2.6.3. Binding Model

The analysis of Binding [103] differs significantly from that of Gibson [101, 102]. Binding [103] assumes in his analysis that the entrance pressure is dominated by the shear contribution to the total viscous dissipation as postulated by Cogswell [99, 100]. This difference can be understood by the different assumptions used by Gibson [101, 102] and Binding [103] regarding the boundary conditions and location in the converging flows. Binding [103] assumes as Cogswell [99, 100] that the velocity at the surface of the upstream vortices is zero. The entrance angle θ, (Figure 2.3) of polymers melt such as low density polyethylene (LPDE) can be quite small (15°). The entrance angles calculated by both Cogswell [99, 100] and Binding [103] were compared by Tremblay [94] to the

entrance angle measured from photographs of the flow of LDPE, linear low-density polyethylene (LLDPE) and 50/50 blend of the two. It was found that both the Cogswell and Binding models underestimate significantly the entrance angle.

The following expression was then obtained by Binding for the extensional viscosity:

$$\eta_E = l\,\varepsilon^{(t-1)} \quad \text{.....(2.15)}$$

Where the power law coefficient l for the elongation viscosity can be written as:

$$l = k / (t\,(1 + 3n) n^t I_{nt})\,[(C3t^2\,(1 + n)^2 / (2k\,(1 + t)^2 *$$

$$(1 - (R_o / R_1)^{(3t\,(1 = n)/\,(1 + t)}))]^{(1 + t)} \quad \text{.....(2.16)}$$

$$\varepsilon = (n + 1)\,(k / (lt\,(3n + 1) n^t I_{nt}))^{(1 / (1 + t))}\,\gamma^{((1 + n) / (1 + t)} \quad \text{.....(2.17)}$$

Where $\gamma = (3n + 1) / (4n)\,\gamma_A$

2.6.4. Tremblay Model

Tremblay model [94] describes the velocity along the surface of the upstream vortex decreases rapidly as it approaches the lip of the die. The total viscous dissipation due to the flow of a fluid into a capillary is then assumed to be given by the sum of the dissipation due to elongational stresses within the converging flow region and the dissipation due to stagnation flow around the lip of the die.

The following expression was then obtained for the extensional viscosity:

$$P_o = l\,(\gamma_A / 4)^t\,(2 - \cos\theta) t\,(2 - \cos\theta + \cos\theta\,(1 + \cos\theta)\,(t + 1) /$$

$$((1 + 2\cos\theta)\,(n + 1))) \quad \text{.....(2.18)}$$

$$\varepsilon = Q / (\pi R_o^3)\,(2 - \cos\theta)$$

In order to calculate the extensional viscosity of a polymer melt, the entrance pressure is first plotted as a function of the apparent shear rate. This data is then fitted to a power law function to obtain C (coefficient in the power law expression for the entrance pressure) and the power law index s in the equation:

$$P_o = C\,(4Q / (\pi R_o^3)^s \quad \text{.....(2.19)}$$

The power law index t in the elongation viscosity:

$$\eta_E = l\,\varepsilon^{(t-1)}$$

is equal to the power law index s. The coefficient l is then obtained simply as:

$$l = C\,4^t / 2.2 \quad \text{.....(2.20)}$$

In conclusion, the Gibson [101, 102] and Tremblay [94] models follow more closely the slope of the uniaxial elongational viscosity in the power law regime. The Cogswell [98] and Binding [103] models do not follow as well the slope of the uniaxial elongational viscosity for certain polymers since both of these latter models follow the same relation [99] in the power law regime. The Gibson and Tremblay equations [94, 101, 102] appear to predict well the slope of the uniaxial elongation viscosity versus strain rate curve for all six polymers investigated by Laun and Schuch [104]. The Gibson model [101, 102] can be used with dies of any converging angle. The elongational viscosity estimated by the Gibson [101, 102] model coincides with the Cogswell [98] model for capillary dies of low convergence angle and is close to the Tremblay [94] model at high convergence angles (greater than 120^0). The Gibson and Tremblay models however predict fairly accurately the slope of the uniaxial elongational viscosity curves in the power law regime. The Tremblay model is the easiest to use among the entry flow models.

2.6.5. Tremblay's Method of Measuring Elongational Viscosity

Tremblay's method is based on the measurement of the pressure required to push the gel through an orifice. The apparatus consists of a hollow cylinder (barrel) and a moving

piston (Figure 2.4). An orifice was located at the centre of the piston. The cylinder was filled with approximately one litre of polymer solution and the piston was allowed to move at a controlled speed from the top of the cylinder to the bottom. The pressure measured at the bottom of the barrel was corrected for hydrostatic head of the gel within the barrel in order to get orifice entrance pressure values at different deformation rate.

Entrance pressure values and shear viscosities were used in Gibson model [101,102] to calculate extensional viscosities of the test fluids. A brief description of the Gibson model is given in the Appendix-A.

2.7. Xanthan Gum and Partially Hydrolyzed Polyacrylamide

In this study, Xanthan Gum and Partially Hydrolyzed Polyacrylamide (PHPA) were selected because of their extensive use as a viscosifier in the oil industry for different applications due to their unique rheological properties. A brief description of both polymers is given in the following section:

2.7.1. Xanthan Gum

Xanthan gum, an exocellular heteropolysaccharide produced in fermentation by bacteria (Xanthomonas campestris), is a cream-coloured powder that dissolves in water to produce solutions with high viscosity at low concentration [105].

Xanthan gum was discovered in the 1950s by scientists of the Northern Regional Research Laboratory of the U.S. Department of Agriculture in the course of a screening, which aimed at identifying microorganisms that produced water-soluble gums of commercial interest. The first industrial production of xanthan was carried out in 1960, and the product first became available commercially in 1964.

Xanthan gum is produced by the microorganism Xanthomonas campestris, originally isolated from the rutabaga plant. The gum is produced commercially by culturing X. campestris purely under aerobic conditions in a medium containing commercial glucose,

a suitable nitrogen source, dipotassium phosphate, and appropriate essential elements. When the fermentation is complete, the gum is recovered from the fermentation broth by precipitation with isopropyl alcohol, and dried, milled, tested, and packed [113].

Xanthan gum has relatively stable viscosity properties as a function of salt concentration, pH, temperature and shear degradation [106].

Xanthan gum solutions are rheologically characterized as shear thinning typed fluids i.e. shear viscosity of xanthan gum solutions decreases as shear rate increases [42].

Jones and Walters developed a macroscopic media model where they flowed Xanthan solution. They characterized xanthan gum solutions as extensional thinning fluids. They also mentioned that the flow of xanthan gum solution was dominated by shear viscosity as compared to extensional viscosity [42,12].

Xanthan gum's high viscosifying ability, coupled with excellent stability under high salinity, high temperature, and mechanical shear conditions makes the use of xanthan gum favourable for various drilling, drill-in, completion, fracturing and even in enhanced oil recovery (EOR) operations in the oil field [105, 106, 107]. In a recent study, however, Saasen and Loklingholm [108] reported that poor whole cleaning is obtained if xanthan gum is used as a primary viscosifying additive in standard water based drilling fluids. They suggested that xanthan gum should primarily be used to control barite sag and not be used as general viscosifier.

2.7.2. Polyacrylamide

The polyacrylamides are versatile synthetic polymers, readily water-soluble over a broad range of conditions. These polymers are unique in their strong hydrogen bonding, linearity, and very high molecular weight.

The polyacrylamide can be modified by changing some of the amide groups to carboxyl groups. This technique, known as hydrolysis, is accomplished by treating a polyacrylamide solution with a strong base. When only part of the amide groups are

modified, the process is called partial hydrolysis, forming partially hydrolysed polyacrylamide (PHPA). The typical PHPA used in drilling muds is comprised of 70% primary amide groups and 30% carboxylic groups [109].

Solutions of Polyacrylamide polymers have good temperature stability. This is true only so long as there are no sources of free radicals in the system [110].

In porous media the flow of biopolymer solutions changes from Newtonian to shear thinning at increasing flow rates, the behavior of Polyacrylamide solutions undergoes transitions from Newtonian flow via shear thinning into shear thickening beyond a certain critical flow rate.

This dual rheological behavior comprising both viscous and elastic responses complicates significantly the description of flow in porous media and has moreover a number of important implications.

Viscoelasticity of Polyacrylamide solutions may put constrains in field applications. At the high flow rates around the injection well the shear thickening effect can lead to excessive pressure build-up or consequently low maximum injection rates. This emphasis the needs for quantification of the effects of viscoelasticity on reservoir flow [95].

Jones and Walters characterized Polyacrylamide solutions as extensional thickening. Most coiled molecules become extensional thickening at high-enough extensional rates for polyacrylamide. The results of their experiments indicated that the flow of polyacrylamide solution was dominated by extensional viscosity [42,12].

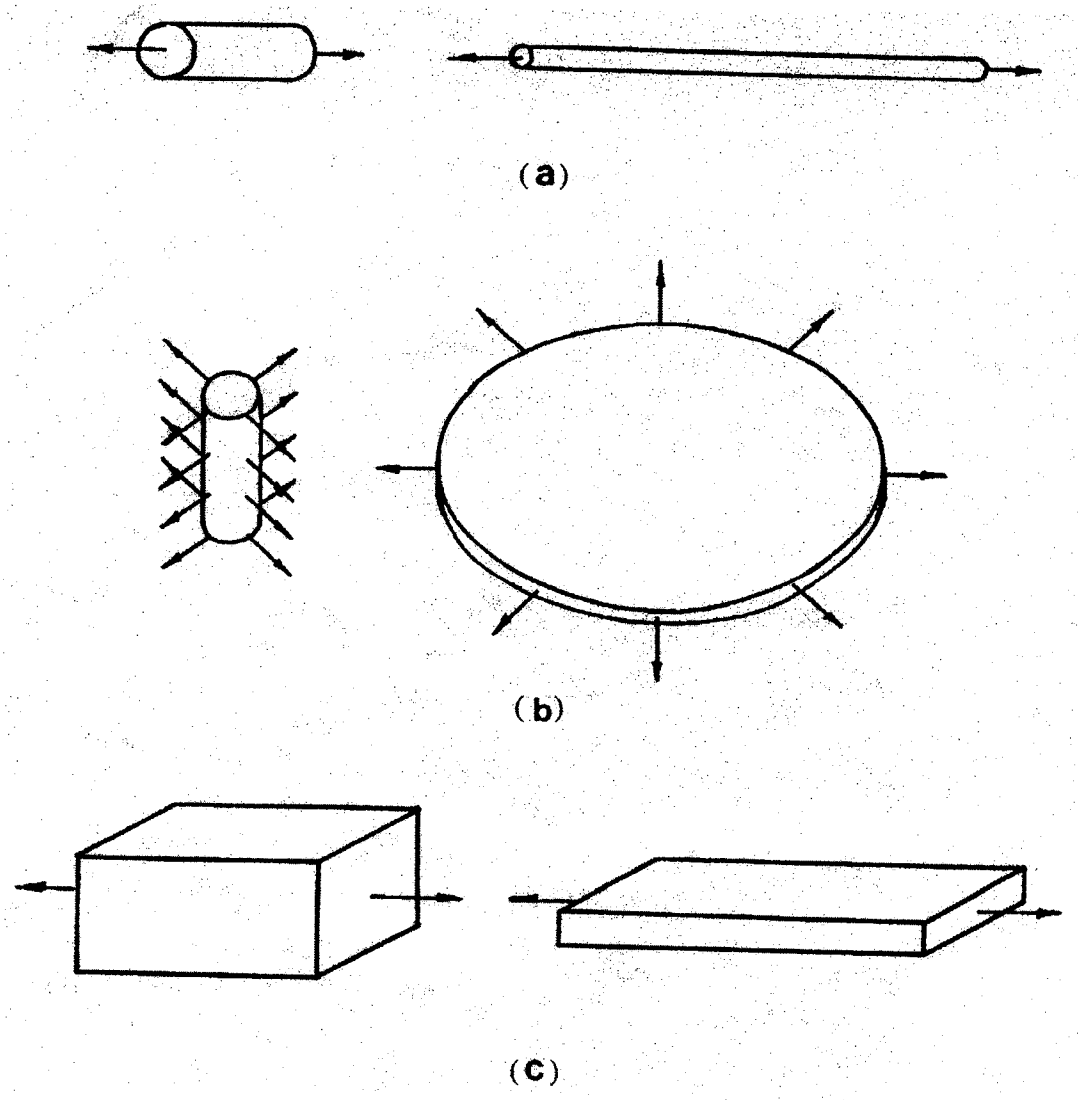

Figure 2.1: Deformation of Polymer Sample in: (a) uniaxial extension (b) biaxial extension, and (c) planar extension (Ref. 94)

Figure 2.2: Visualization of the Flow of a Branched Polydimethylsiloxane (PDMS) through a submerged orifice. U = upstream, D = downstream, a= length of streak before impinging on surface c (Ref. 94)

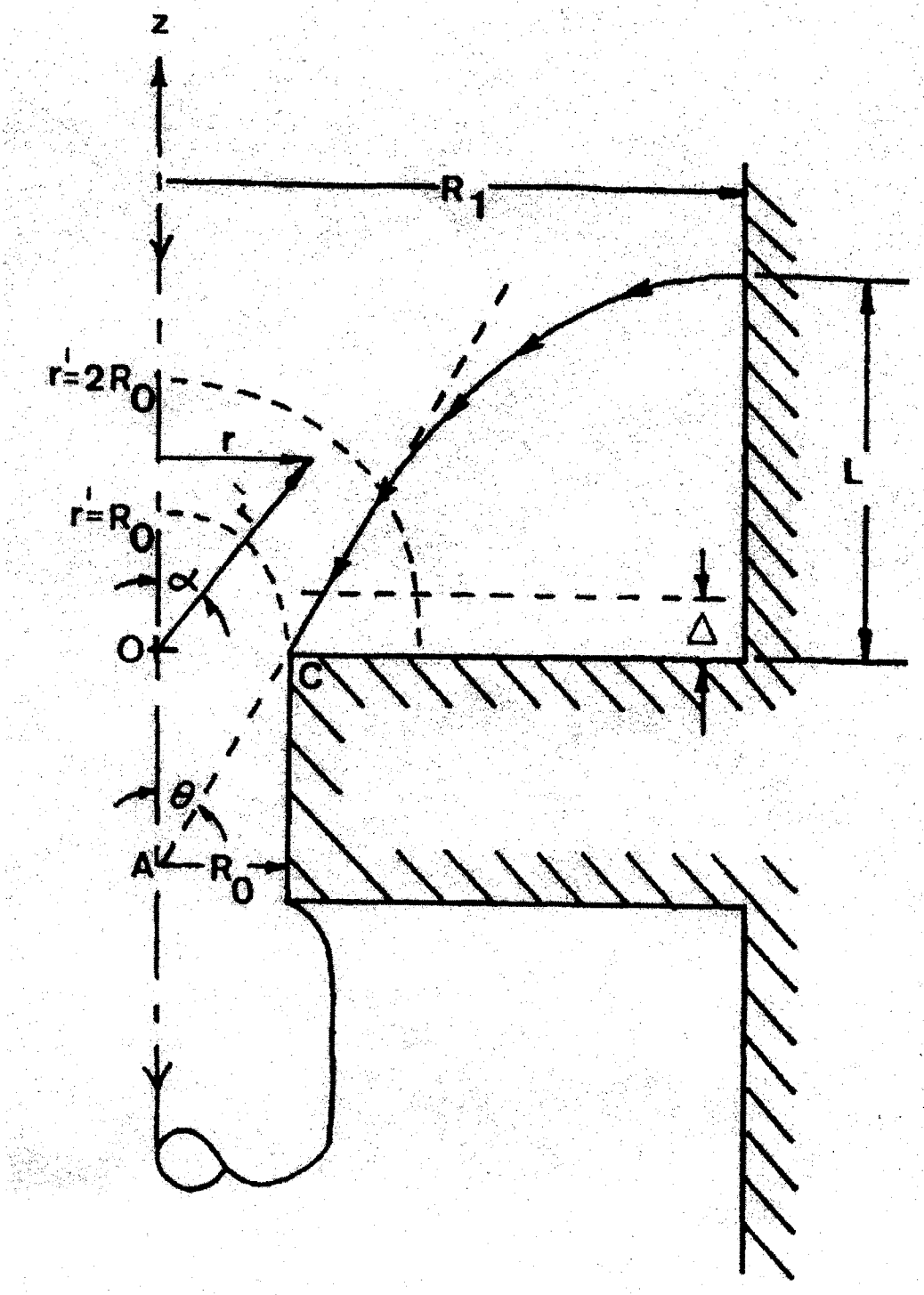

Figure 2.3: Details of control volume used in Tremblay Analysis. θ = entrance half angle, Δ = velocity redistribution thickness. (Ref. 94)

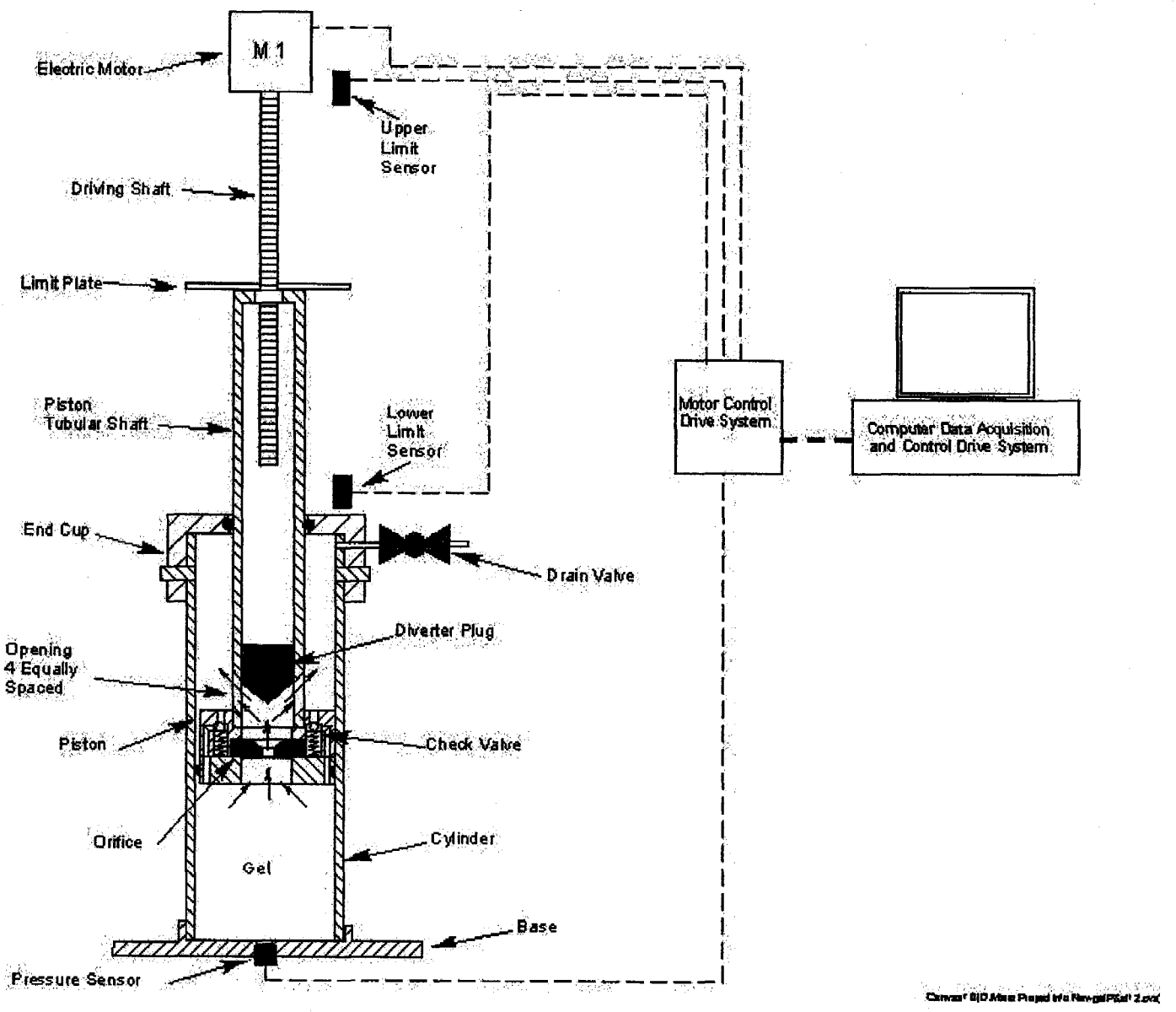

Figure 2.4: Gel Tester (Ref. 94)

CHAPTER 3

EXPERIMENTAL PROGRAM

Experimental program consists of: (1) Rheological characterization of the XG and PHPA solutions (2) Determination of filtration characteristics of XG and PHPA solutions (3) Core flow experiments to determine formation damage characteristics of the XG and PHPA solutions.

The following sections provide a detailed description of the methodology, materials and the equipment used for the experimental study.

3.1. Materials Used for the Preparation of Polymer-Based Fluids

The polymers used in this research study; were supplied at no cost by Baroid International Canada Limited. These polymers were xanthan gum (XG) and partially hydrolyzed polyacrylamide (PHPA) and their commercial names are Barazan D Plus and Barafloc respectively.

Barazan D Plus is a powdered dispersant-added biopolymer (xanthan gum): provides viscosity and suspension in fresh water, sea water, sodium bromide, potassium bromide, potassium chloride, and sodium chloride-based fluids. It has been specially formulated for enhanced dispersibility. It viscosifies fresh water and brine-based fluids used in drilling, milling, under-reaming, and gravel packing operations. It suspends bridging agents and weighting materials in fresh water and brine systems.

Barazan D Plus disperses easily in fresh water or brine with shear, provides thixotropic properties and non-Newtonian flow characteristics over a wide salinity range at low concentrations. It provides excellent suspension without the need for clays, minimizes the potential for formation damage, it is stable up to 250°F (121°C).

Barazan D Plus is a yellow to white powder with specific gravity of 1.6 and molecular weight of 2 million. The pH of 1% aqueous solution of Barazan D Plus is 6.3.

Barafloc is a versatile PHPA polymer for use as a flocculant, viscosifier, and encapsulator in conventional and polymer based drilling muds and water treatment and clarification.

Barafloc's typical advantages are; (1) Aids in the maintenance of drilling fluids (2) Decreases filtercake thickness (3) Allows for increased rate of penetration (4) Reduces water requirements for controlling mud weight and keeping the solids concentration low (5) Effective in small concentrations.

The appearance of the Barafloc polymer powder is white and opaque white in liquid form. Its pH (0.5% aqueous solution) is 7.0 and molecular weight is 15 million. It is very sensitive to mechanical degradation therefore careful measures should be taken during the preparation of PHPA solutions to eliminate the mechanical degradation effect.

3.2. Shear Viscosity Measurements

The main purpose of these measurements was to determine the shear stress-shear rate behavior, shear viscosities and the yield strength of the polymer solutions. A Haake RotoVisco RT 20 shear Rheometer (Figure 3.1) and a Brookfield DV II Cone/Plate Viscometer (Figure 3.2) were used for shear viscosity measurements. Polymer concentrations, ranging from 0.5 to 3.0 lb/bbl, were used for preparing polymer solutions.

The shear viscosity values measured from Haake viscometer, at Alberta Research Council (ARC), were used to obtain the extensional viscosity of polymer-based solutions.

Whereas shear viscosity values measured with Brookfield viscometer, at the University of Alberta Laboratory, were used to estimate the concentration profile, across the core length, during core flow experiments.

Brief descriptions of the both viscometers and measurement procedures are given in the next sections.

3.2.1 Shear Viscosity Measurements with Haake Rheometer

The RotoVisco RT20 is a controlled rate/stress rheometer manufactured by HAAKE (Figure 3.1). The Rheo Win Pro software package was provided with the rheometer for data acquisition and analysis.

The temperature of the cooling bath was set at 22 °C. Polymer solution was pre-sheared for a period of four minutes for each measurement at a controlled shear rate of $0.7sec^{-1}$. Two shear rate sweeps were set for each measurement cycle; first sweep in which the shear rate increased in twenty steps from 0 to the maximum rate of $2300sec^{1}$ followed by a sweep in which the shear rate was decreased in twenty equal steps back to zero. A fresh sample was used for each measurement. The sample was poured into the sample cup and placed onto the cup holder. The sample cup was automatically lifted to the rotor and the measurement was performed.

3.2.2 Shear Viscosity Measurements with Brookfield DV II Cone/Plate Viscometer

The Brookfield DV II is a Digital Cone/Plate Viscometer (Figure 3.2). The Viscometer rotates a sensing element in a fluid and measures the torque necessary to overcome the viscous resistance to the induced movement. This is accomplished by driving the immersed element, which is called a spindle, through a beryllium copper spring. The degree, to which the spring is wound, detected by a rotational transducer, is proportional to the viscosity of the fluid. It is able to measure over a number of ranges since, for a given spring deflection, the actual viscosity is inversely proportional to the spindle speed and shear stress is related to the spindle's size and shape.

Measurements made using the same spindle at different speeds are used to detect and evaluate the rheological properties of the test materials. Cone/Plate viscometer is useful especially when small sample is available to analyze. It needs sample volume range from 0.5 to 2.0 ml, depends upon the spindle size. With the cone spindle # CP-41 and CP-52 it

gives shear rate range from 0.6 to 120 sec^{-1}. The viscosity range is form 3840 cp to 19.2 cp for CP-41 and from 31,065.6 cp to 155.33 cp for CP-52 respectively.

Brookfield DV II Cone/Plate Viscometer gives viscosity values directly in centipoises. It was used to examine the samples collected during the core flow tests, for shear rates ranging from 0.6 to 120sec^{-1}. These shear viscosity values were used to determine the concentration profile of polymer solution across the core length during core flow tests.

3.3. Extensional Viscosity Measurements

Extensional viscosity measurements were conducted at Alberta Research Council (ARC) Laboratories. A unique method recently developed by Tremblay et al. [94] was used to determine the extensional viscosity of polymer-based solutions. The method is based on the measurement of the pressure required to push the gel through an orifice (Figure 3.3). The apparatus consists of a hollow cylinder (barrel) and a moving piston. An orifice was located at the centre of the piston. The cylinder was filled with approximately one litre of Polymer solution and the piston was allowed to move at a controlled speed from the top of the cylinder to the bottom. The pressure measured at the bottom of the barrel was corrected for hydrostatic head of the gel within the barrel in order to get orifice entrance pressure values at different deformation rate. Entrance pressure values and shear viscosities (measured using Haake viscometer) were used in Gibson model [101,102] to calculate extensional viscosities of the test fluids. A brief description of the Gibson model is given in the Appendix-A.

3.4. API Filtration Test – Static Filtration

The filter press (Figure 3.4) is used to determine the filtration rate through a standard filter paper. The standard American Petroleum Institute (API) filter press has an area of 45 cm^2 and is operated at a pressure of 6.8 atm (100 psig). A standard Wattman 40 filter paper is placed at the bottom of the sample cup. The cup is then filled up with the test fluid and the sample cup lid is fixed on the top. A 100-psig pressure is applied and filtrate sample is collected into a graduated cylinder.

The detailed description of the API filtration test procedure is available in the "Standard Procedure for Testing Drilling Fluids (API R.P. 13B, Dallas, 1974)". The filtrate volume collected in a 30-min time period is reported as the standard API filtration loss values.

API filtration tests were performed for three different concentrations (0.5, 1.5 and 3.0 lb/bbl) of XG and PHPA solutions. The discussion of the results of API filtration tests is given in chapters 4 and 5.

3.5. Core Flow Experiments

The experimental set-up and procedure used for core flow tests are described in the following sections.

3.5.1. Experimental Set-Up

A schematic of the experimental set-up is shown in Figure 3.5. A 12-inch long and 2-inch diameter stainless steel core holder (Figure 3.6) was used for linear core flow experiments. Two flanges were fitted on each end of the coreholder. A sintered screen was fitted into the inside wall of the cap flanges to act as a distributor for the fluids injected. The core holder was packed with glass beads simulating the porous media with an average permeability of 11-13 Darcy and porosity of 38 %.

Four pressure transducers (one differential pressure transducer across the whole core and three absolute pressures transducers in the middle of the core at equal distances) were used to measure the pressure drop across the core holder (Figure 3.6).

Intermediate pressure measurement ports were also equipped with syringe valves to allow fluid sample collections at any time during the flow experiments.

3.5.1.1. Materials and Fluids

The material used to pack the coreholder was glass beads with a US mesh size of 60-80. The porosity of the pack was around 37-38% and the absolute permeability of the pack varied between 11 to 13 Darcy.

Polymers solutions prepared by using three different concentrations of Barazan D Plus (XG) and Barafloc (PHPA) were used in core flow tests. A detailed description of polymers is given in chapter 2, section 2.7.

3.5.1.2. Injection and Production System

A progressive cavity pump with variable frequency drive control was used to inject the test fluid into the core sample.

The fluid samples were collected at the outlet end of the core holder. Samples were also collected at different time intervals through the syringe valves located at the three intermediate pressure transducers.

3.5.1.3. Data Acquisition System

The data acquisition system had two parts: hardware and software systems. The hardware consisted of four Validyne transducers and a Validyne UPC601-L sensor interface card. The card came with its own sensor excitation and carrier demodulation, which meant that no external signal conditioning was required. The card could accommodate a maximum of sixteen single-ended or 8 differential input channels.

The software used for data acquisition was StabView, a menu driven data acquisition program that supports real time logging of data to excel files. All set-up parameters were available through pull-down window selections.

3.5.2. Model Preparation

The first step in preparing the model was making sure that all parts of the apparatus were clean and working properly. Then the coreholder was isolated from the transducer connections, and the injection and production system. The core holder was placed vertically in preparation for packing. Then the model was evacuated with a vacuum pump, and was saturated with water. After saturation, the model was placed horizontally and connected to the injection and production system, and to the transducers. At this stage the absolute permeability was measured.

3.5.2.1. Packing Procedure

The dry packing method was used in all experiments in this study. The packing process started with the coreholder mounted vertically, with the injection end pointing upwards and the production end pointing downwards. A mechanical vibrator was strapped onto the core. In the same time a transparent extension of the same core holder size was attached to the inlet end. This extension helped to maintain more consistent packing throughout the core and insured that the glass beads pack level flushed with the top of the end flange. The glass beads were loaded into the coreholder while vibrating. The core was vibrated for five hours. The top extension was removed and an end flange was installed. The model was subjected to a vacuum of 6.89 kPa for three hours. After drawing the vacuum, tab water was allowed to imbibe into the glasspack core from the bottom end. At this stage, the core was 100% saturated. The amount of imbibed water was then taken to be the pore volume of the glass beads pack. Porosity was then determined by dividing the pore volume by the bulk volume.

3.5.3. Experimental Procedure

Experimental procedure consists of following steps: (1) Preparation of Polymer Solutions (2) Absolute Permeability Measurements (3) Core Flow Experiments-Assessment of

Formation Damage (4) Core Cleaning Procedure (5) Data Reduction for Core Flow Experiments.

3.5.3.1. Preparation of Polymer Solutions

Xanthan Gum: Test fluids were prepared by mixing (tap) water with powdered xanthan gum at three different concentrations, 0.5, 1.5, and 3.0 lb/bbl. A Hamilton-Beach overhead malt mixer was used to prepare the solutions in 400 ml batches. Water was added to the mixing cup and the required amount of polymer added slowly. The solution was then mixed at 10,000 rpm for 15 min.

The initial batch fluid viscosity profile was determined using Brookfield DV-II viscometer at 22 ° C. In order to eliminate any micro bubbles (possibly formed during the mixing process), the batch fluid was filtered through Wattman 40 filter paper by using standard filter press. After the filtration test, the viscosity of the fluid was again measured at 22° C to ensure that the polymer was not being removed during the filtration step.

Partially Hydrolyzed Polyacrylamide: PHPA solutions were prepared by sprinkling the dry polymer uniformly into the (tap) water where an ordinary laboratory magnetically driven stirrer was used for mixing. As soon as the entire polymer is added, the stirrer is slowed to a speed of 60-80 rpm to avoid mechanical degradation. The solutions were allowed to stir overnight so that it can soak and dissolve all of the dry polymers.

The initial batch fluid viscosity profile was determined using Brookfield DV-II viscometer at 22 ° C. In order to eliminate any micro bubbles (possibly formed during the mixing process), the batch fluid was filtered through Wattman 40 filter paper by using standard filter press. After the filtration test, the viscosity of the fluid was again measured at 22° C to ensure that the polymer was not being removed during the filtration step.

3.5.3.2. *Absolute Permeability Measurements*

The core holder was put in a horizontal position for absolute permeability measurement. The core initially was 100% water saturated, and the pressure inside the core pack was atmospheric. Water was injected at different flow rates from the inlet end and produced at the outlet end of the core. When the pressure across the core stabilized, the flow rate and the absolute pressures at the three intermediate transducers were recorded. For differential pressure reading difference of two intermediate pressure transducers reading, and the corresponding core length was used.

Darcy's law for linear flow was used to calculate the absolute permeability for each experiment.

$$q = -1.127k\left(\frac{A\Delta P}{\mu L}\right) \quad \text{.....(3.1)}$$

Given that

L = Length of the sand pack, ft

μ = Viscosity, cp

A = Cross-sectional area of the core pack, ft^2

q = Water flow rate, bbl/day

ΔP = Pressure difference, Psi

k = Absolute permeability, Darcy

A plot of q μ L / A*1.127 versus ΔP gives a straight line passing through the origin with a slope equal to k (darcy). Three to five points of pressure and their corresponding flow rates were used to construct this line. The least square fit method was used to determine the best straight line across the test data points. The slope of the line was calculated as the

permeability, k. The absolute permeability measurement was conducted for each core flow test in this study.

3.5.3.3. Core Flow Experiments-Assessment of Formation Damage

Before the injection of polymer-based solutions core was dried using air injection. The core was then put into the oven for over night. The Corepack was cooled down using air before the fluid injection. All transducers were calibrated and installed on the core holder before each flow test and then connected to the data acquisition system. Polymer solutions were injected at different flow/shear rates using injection pump starting from lower to higher flow rates. Samples were collected upon first production through the outlet end. Samples were also collected at the three syringe valves (Figure 3.6) located at three intermediate transducers and at the outlet end. Polymer solution was allowed to flow for about an hour and four samples were collected during this time period. Real time pressure data was recorded throughout the flow test using the data acquisition system.

After the flow test, the core was flushed with water for about 24 hours to clean the core from polymer solutions. Permeability of the core pack was measured again using the tab water. Difference in the permeability before and after the core flow tests were taken as the formation damage induced due to polymer flow. Permeability data before and after core flow tests and their discussions are given in chapters 4, 5 and 6.

3.5.3.4. Core Cleaning Procedure

Core was cleaned using acetone. Acetone was pumped using accumulator for about 30 minutes at 30-psi differential pressure across the core, 15 minutes from each directions. Core was then flushed with air and then with hot water to clean the core from the acetone. Permeability of core was measured again using tab water to make sure that the original permeability of the core has been retrieved. An average of 95- 98% permeability was retrieved using core-cleaning procedure.

3.5.3.5. Data Reduction for Core Flow Experiments

Upon the completion of an experiment, the pressure data was retrieved from the data acquisition system and plotted on Microsoft Excel. Viscosity of the fluid samples was measured using the Brookfield Digital DVII Cone/Plate Viscometer and the data was entered manually into a spreadsheet and then plotted.

Pressure drop across the core sample was calculated using Darcy's equation and compared with the measured ones. Formation damage was calculated using the absolute permeability data before and after the flow test.

A calibration curve was plotted using the viscosity values for different fluid concentrations of polymer-based solutions. This calibration curve was used to estimate the fluid concentration across the core sample.

Extensional viscosities of the polymer based solutions and their Trouton ratios were plotted and compared with the pressure data and fluid concentrations.

API filtration loss values were measured for different concentrations of polymer-based solutions and compared to see the effect of fluid loss on the formation of internal filter cake i.e. formation damage.

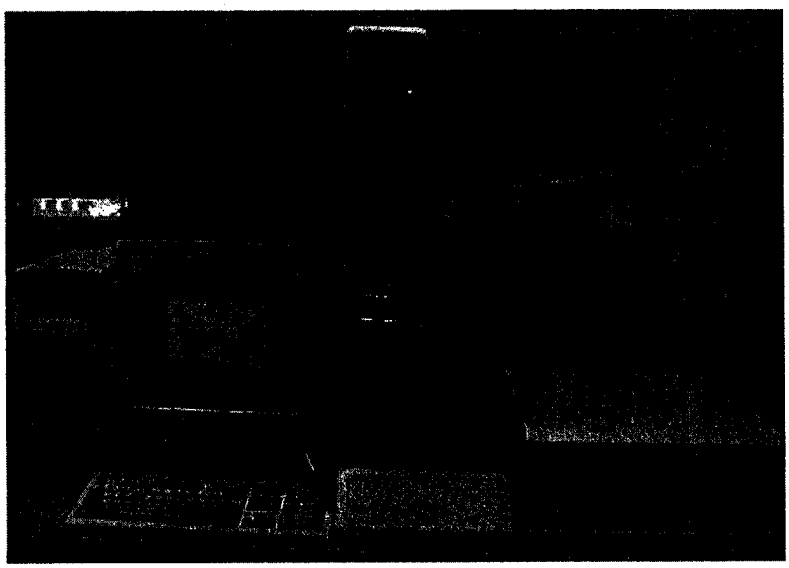

Figure 3.1: Haake Rheometer RotoVisco RT 20

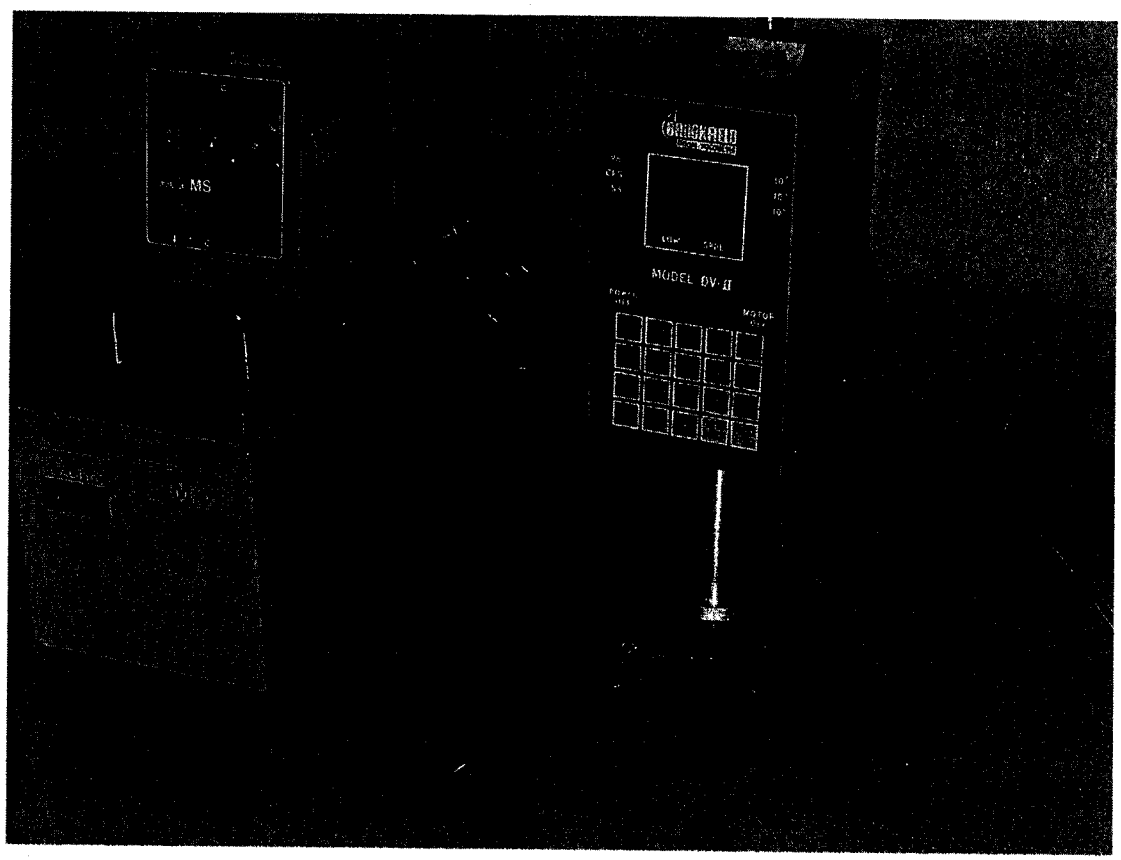

Figure 3.2: Brookfield DV II Cone/Plate Viscometer

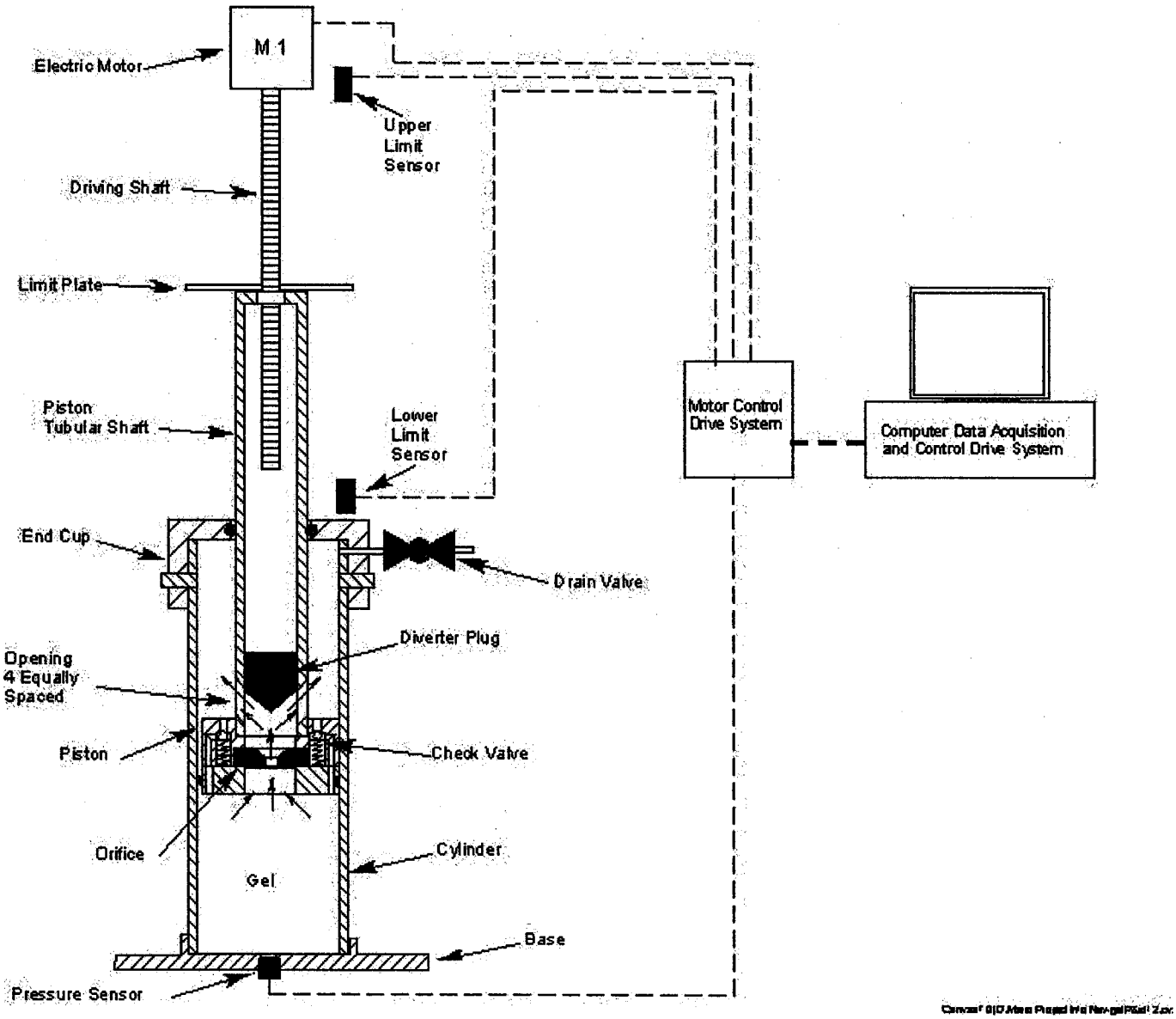

Figure 3.3: Gel Tester (Ref. 94)

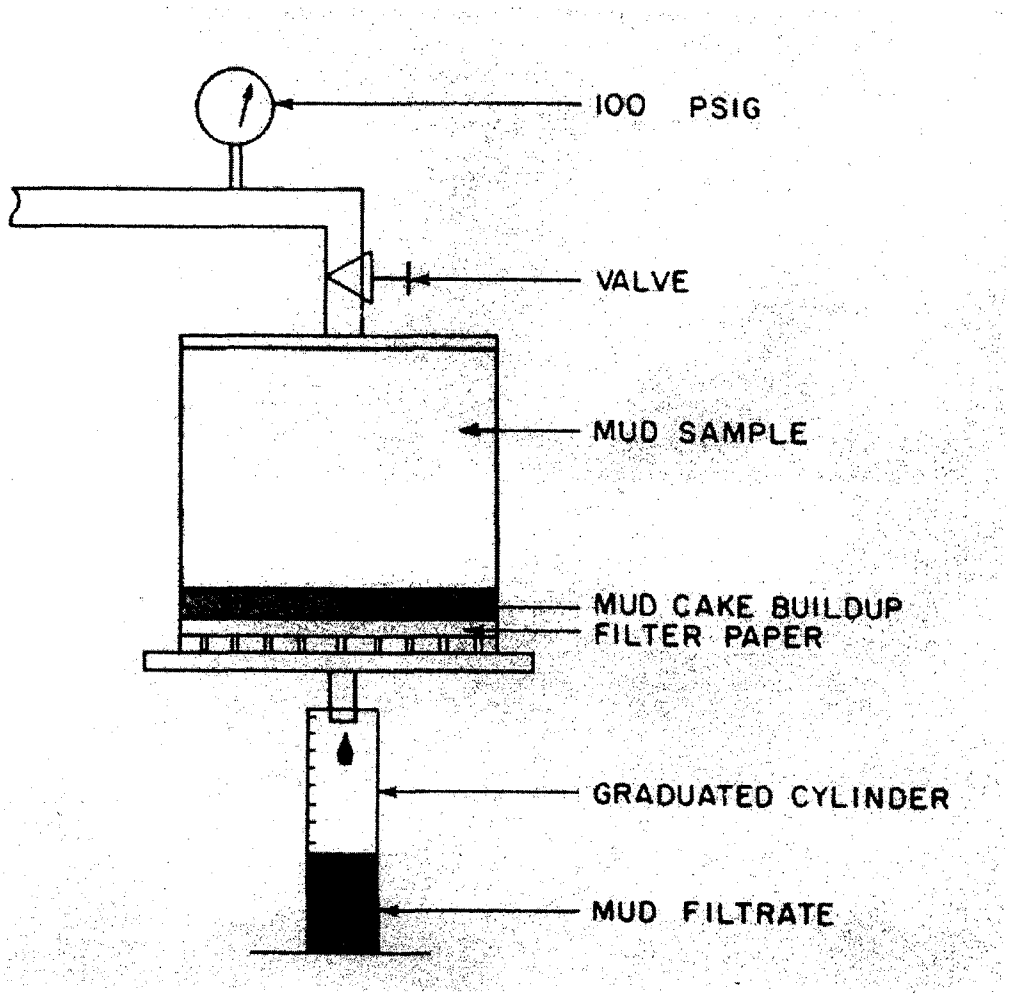

Figure 3.4: API Filter Press (Bourgoyne et al., 1991)

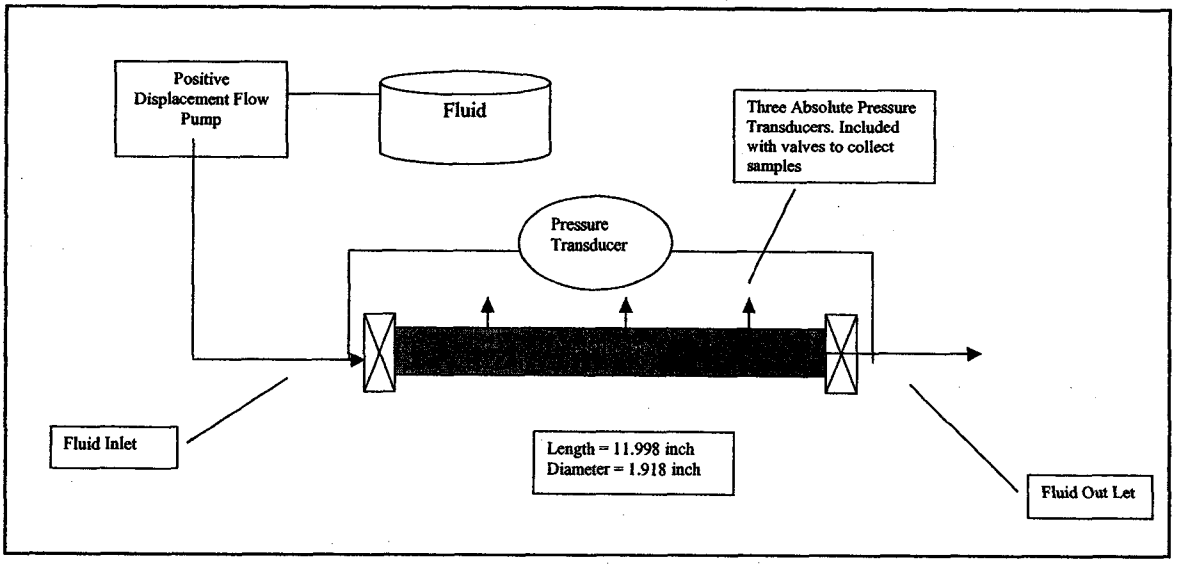

Figure 3.5: Flow Diagram of Core Flow Experiment

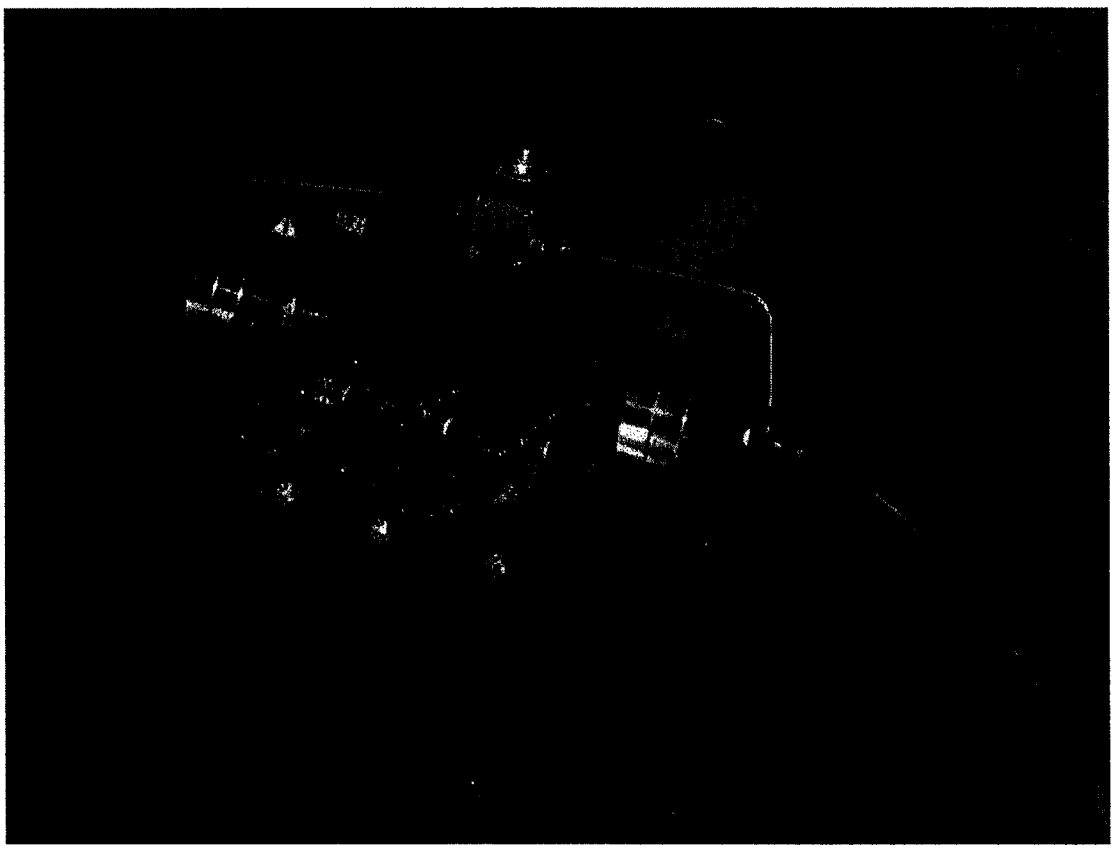

Figure 3.6: Metallic Core Holder

CHAPTER 4

EXPERIMENTAL RESULTS OF XANTHAN GUM SOLUTIONS

4.1. Rheological Characterization of Xanthan Gum Solutions

A full-scale rheological characterization of xanthan gum solutions was carried out by measuring the shear and extensional viscosities.

4.1.1. Shear Viscosity Measurements

Shear viscosities of the test fluids were measured by using Haake viscometer. The shear stress vs. shear rate plots of xanthan gum solutions are shown in Figure 4.1 (Appendix N). The shear stress vs. shear rate diagram (Figure 4.1) shows that xanthan gum solutions have low yield stress values and can be rheologically characterized as Power law type fluids. Power law model coefficients of xanthan gum solutions are given in Table 4.1.

The shear viscosity vs. shear rate curves for three different concentrations of xanthan gum solutions are shown in Figure 4.2. The shear viscosity vs. shear rate diagram (Figure 4.2) confirms the shear thinning characteristics of xanthan gum solutions.

A calibration curve relating the shear viscosity to xanthan gum concentration (at a base shear rate observed at pore level; 105 sec^{-1}) was developed (Figure 4.3). The polymer concentration calibration curve was later used to determine the variation of polymer concentration along the core. Figure 4.3 shows that the shear viscosity of xanthan gum solutions increases significantly as the polymer concentration increases.

4.1.2. Extensional Viscosity Measurements

Extensional viscosity values for two xanthan gum solutions (1.5 and 3.0 lb/bbl) are shown in Figures 4.4. As shown in Figure 4.4 (Appendix H) extensional viscosities of 1.5 and 3.0lb/bbl xanthan gum solutions decrease with increasing strain/extensional rate,

however, the rate of decline is much steeper at low shear rate regions (less than 800 sec^{-1}).

Trouton ratio values for two xanthan gum solutions (1.5 and 3.0 lb/bbl) are shown in Figure 4.5. Figure 4.5 shows that the Trouton ratios of xanthan gum solutions increase with increasing strain/extensional rate.

It is anticipated that the biaxial extensional viscosity at small elongation rates becomes three times the zero shear rate viscosity (Trouton ratio =3) [93]. However, it is seen from Figure 4.5 that Trouton ratio values at low strain rates are higher than 3, suggesting that these zero strain rate values can be inaccurate. However, at larger strain rates we expect these values to be more correct.

It is possible that the deformation rates in the gel tester were still too high. These polymers can sometimes show flow instabilities at high deformation rates called melt fracture. This type of instability can be observed as a pulsating flow at the entrance to a contraction. This type of flow can physically degrade the polymer chains. It is possible that the higher concentration xanthan gum is more affected by this type of flow. This might explain why the elongational viscosity seems to decline more with increasing deformation rate.

Gibson model [101, 102] was used to calculate the extensional viscosity for all strain rates. We therefore, used this calculated extensional viscosity also for small strain rates without bringing in any theoretical speculations about the correct values.

In general, xanthan gum solutions (Figure 4.4) can be considered as fluids with extensional thinning characteristics i.e. extensional viscosity decreases as the strain rate increases. Whereas extensional viscosities of xanthan gum solutions increase significantly with the increase in fluid concentration (Figure 4.4).

4.2. API Filtration Tests

API filtration test results have shown that xanthan gum solutions have high filtration loss values (Table 4.2). However, API filtration loss volume decreased significantly (59%) when xanthan gum concentration is increased from 1.5 to 3.0lb/bbl.

The exact reason of reduction in filtration rate is, however, not clear. The increase in shear viscosity and extensional viscosity were expected to control the reduction of leak-off rate.

A comparison of the fold of increase of extensional and shear viscosities might be useful to find out which one of the viscosities has dominant effect on the reduction of filtration rate.

The shear viscosities of xanthan gum (at $105sec^{-1}$) were measured as 71 cp and 175 cp for 1.5 and 3.0lb/bbl XG polymer solutions respectively. The fold of increase in the shear viscosity is 2.46.

The extensional viscosities of XG solutions were measured (at $105sec^{-1}$) as 756 cp and 3105 cp for 1.5 and 3.0lb/bbl solutions respectively. The fold of increase in this case is 4.1.

The fold of increase in extensional viscosity (4.1) is higher than the fold of increase in shear viscosity (2.46), suggesting that the extensional viscosity might play more significant role in the reduction of leak-off rate.

4.3. Core-Flow Experiments - Assessment of Formation Damage

The main objectives of core flow tests were:

i-) To determine if there is any reduction in the original permeability of the pack after flowing xanthan gum solutions, and if there is any damage occurred, to determine the effect of xanthan gum concentration on the severity of the permeability reduction,

ii-) To determine if the extensional viscosity of the fluids influence the pressure drop along the pack.

Fluids with three different xanthan gum concentrations (0.5, 1.5, and 3.0 lb/bbl) were used for the core flow tests.

Measurements from three intermediate pressure transducers (located at equal distance from each other) were used to determine absolute permeability of the glass bead pack before and after the flow of xanthan gum solution through the pack.

Xanthan gum solutions were injected at certain rates to generate a base shear rate of $105sec^{-1}$ in the core.

4.3.1. Pressure Losses Measurements Along the Core

Pressure losses along the core were measured (Appendix J) and compared with the ones calculated from Darcy equation for linear flow. The use of Darcy equation for pressure loss estimation requires the values of shear viscosities determined at shear rates, which prevail within the porous media. Shear rates in the mechanically packed core were estimated using modified Blake-Kozeny equation (Equation 2.4). A comparison of measured and calculated pressure loss values for fluids with two different xanthan gum concentrations (1.5, 3.0 lb/bbl) at $105sec^{-1}$ shear rate are given in Table 4.3.

The results shown in Table 4.3 indicate that calculated pressure loss values are 11.6 % and 27.3 % lower than the measured pressure loss values for 1.5 lb/bbl and 3.0 lb/bbl solutions respectively. Shear viscosity values measured at the shear rate of 105 sec^{-1} and original core permeability values were used in the Darcy equation (equation 2.3) for pressure loss calculations. Both shear and extensional viscosity values seemed to be decreasing as the fluid flows from inlet to outlet. Therefore, it is postulated that any possible reduction in the permeability due to the flow of xanthan gum solutions might have caused measured pressure drops to be higher than the calculated ones.

Core flow experiments were also conducted using 1.5-lb/bbl solution at different flow rates to see the effect of fluid injection rate (shear rate) on the pressure losses (Table 4.4). Measured pressure losses were also higher than calculated pressure losses with slight increase in percent difference as the flow rate increased.

4.3.2. Assessment of Formation Damage

Formation damage was calculated (Appendix L) by measuring the permeability before and after the core flow test. Initial permeability of the pack was measured by flowing water through the pack. The flow test was conducted by injecting xanthan gum solutions through the core. After the flow test was completed, the core was flushed with water for about 24 hours. The permeability of the pack was then measured again. The percent reduction of the original pack permeability was recorded as an indicator of the damage in each case. Table 4.5 summarizes the results of permeability measurements before and after core flow tests.

Core flow tests were actually conducted to see if the original permeability of the core would be reduced due to the flow of xanthan gum solutions. Permeabilities measured before and after the flow tests are shown in Table 4.5. The results have shown that original core permeability was reduced by 25 % and 28 % due to the flow of 1.5 and 3.0 lb/bbl solutions respectively.

Adsorption and retention of polymer molecules on the rock surface is suggested as one of the primary reasons of observed formation damage in the case of xanthan gum solutions.

4.3.3. Change in Polymer Concentration Along the Core

Shear viscosities of the fluid samples collected at the inlet, at the three middle pressure measurement ports and at the outlet of the core were measured. The samples were collected as soon as the first fluid comes out of the core and after that, the fluid samples were collected at various time intervals until the flow reaches to steady state (i.e. pressure

stabilizes). The shear viscosity values at the inlet and at the outlet are given in Table 4.6. Figure 4.6 shows the variation of shear viscosities along the core.

The results in Table 4.6 show that the shear viscosities at the outlet decreased by about 9.7 % and 11.5 % for 1.5 lb/bbl and 3.0 lb/bbl xanthan gum solutions respectively, as soon as the first fluid comes out of the core during the core flow tests.

Xanthan gum concentrations corresponding to measured inlet and outlet shear viscosities were estimated by using the calibration curve (Figure 4.3). The results shown in Table 4.7 indicate that the polymer concentration reduced by about 10 and 12% as the 1.5 lb/bbl and 3.0 lb/bbl solutions flew through the core sample respectively.

The reduction in fluid concentration, permeability, and API filtration loss values indicate that the xanthan gum solutions have formation damage characteristics during the core flow tests.

Table 4.1: Power Law Model Coefficients of Xanthan Gum Solutions

Xanthan Gum	Consistency Index	Flow Behavior Index
Concentration	K	n
lb/bbl	N-s/m^2 or pa-sec	
0.50	0.1264	0.5898
1.50	2.1142	0.2616
3.00	6.9703	0.1769

Table 4.2: API Filtration Loss vs. Xanthan Gum Concentration

Xanthan Gum Concentration lb/bbl	API Filtration Loss ml
0.5	N/A
1.5	187.0
3.0	76.0

Table 4.3: Comparison of Measured Pressure Loss vs. Estimated Pressure Loss of Xanthan Gum Core Flow Tests (at 105 sec^{-1} flow rate)

Xanthan Gum Concentration lb/bbl	Measured Pressure Loss psi	Calculated Pressure Loss psi	% Difference
1.5	17.2	15.4	11.6
3.0	37.3	29.3	27.3

Table 4.4: Comparison of Measured Pressure Loss vs. Estimated Pressure Loss at Different Flow Rates (Xanthan Gum Concentration, 1.5 lb/bbl)

Flow Rate ml/min	Shear Rate 1/sec	Measured Pressure Loss psi	Calculated Pressure Loss psi	% Difference
15.6	105	17.2	15.4	11.6
17.8	120	18.4	15.9	15.7
22.2	150	19.5	16.8	16.1
29.7	200	21.4	18.1	18.2
44.4	300	24.7	20.1	22.9

Table 4.5: Permeability Measurements for Xanthan Gum Flow Test

Xanthan Gum Concentration, lb/bbl	Permeability before the test Darcy	Permeability after the test Darcy	Permeability Reduction %
1.5	12.86	9.59	25.41
3.0	11.81	8.46	28.39

Table 4.6: Variation of Shear Viscosity Between the Inlet and the Outlet of the Core

Initial Xanthan Gum Concentration lb/bbl	Shear Viscosity at the Inlet cp	Shear Viscosity at the Outlet cp	% Reduction in Shear Viscosity
1.5	70.8	63.9	9.7
3.0	174.9	154.7	11.5

Table 4.7: Variation of Xanthan Gum Concentration Between the Inlet and the Outlet of the Core

Xanthan Gum Concentration at the Inlet lb/bbl	Xanthan Gum Concentration at the Outlet lb/bbl	% Reduction in Xanthan Gum Concentration
1.5	1.35	10
3.0	2.65	12

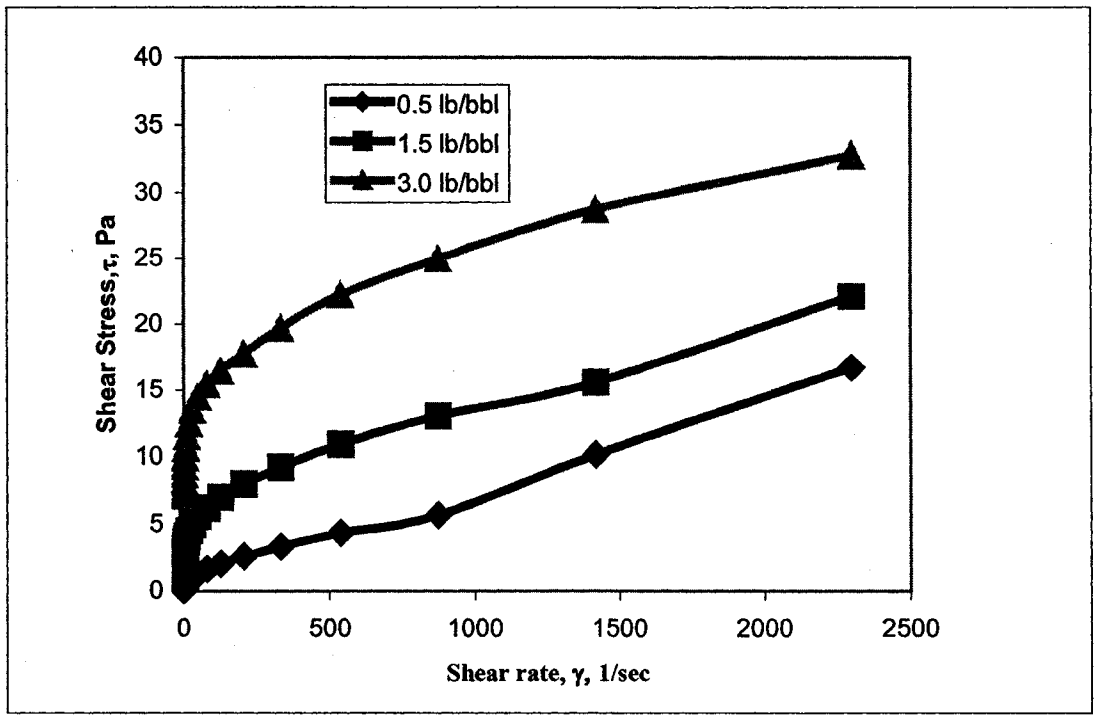

Figure 4.1: Shear Stress vs. Shear Rate Diagram for Xanthan Gum Solutions

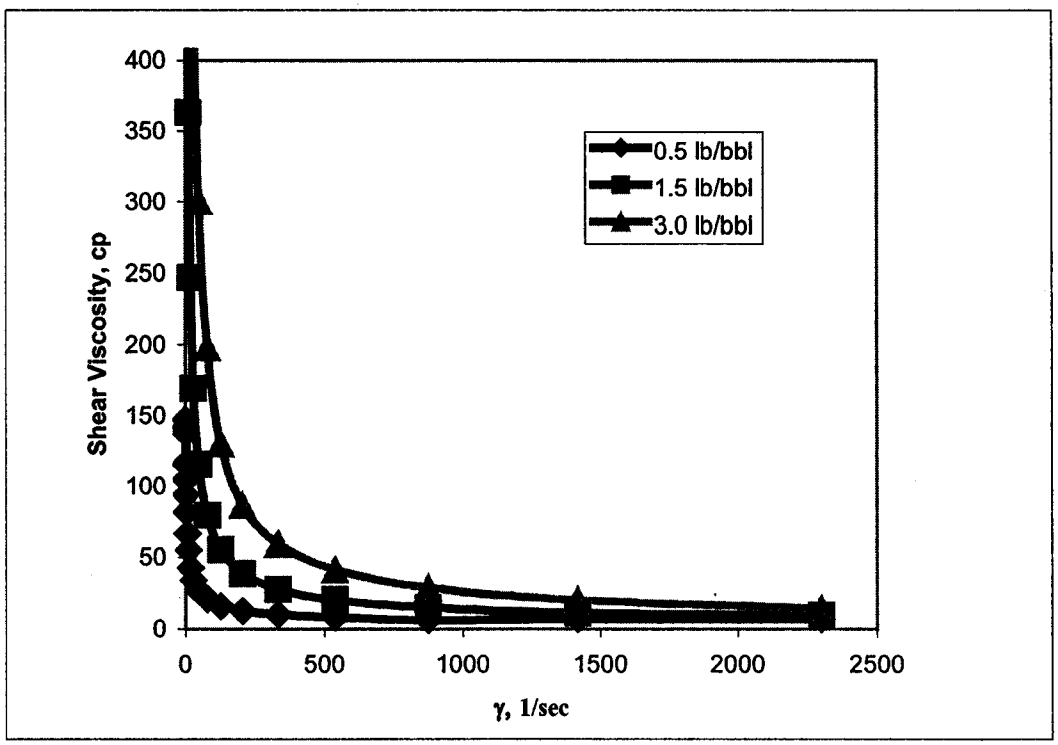

Figure 4.2: Shear Viscosity vs. Shear Rate of Xanthan Gum Solutions

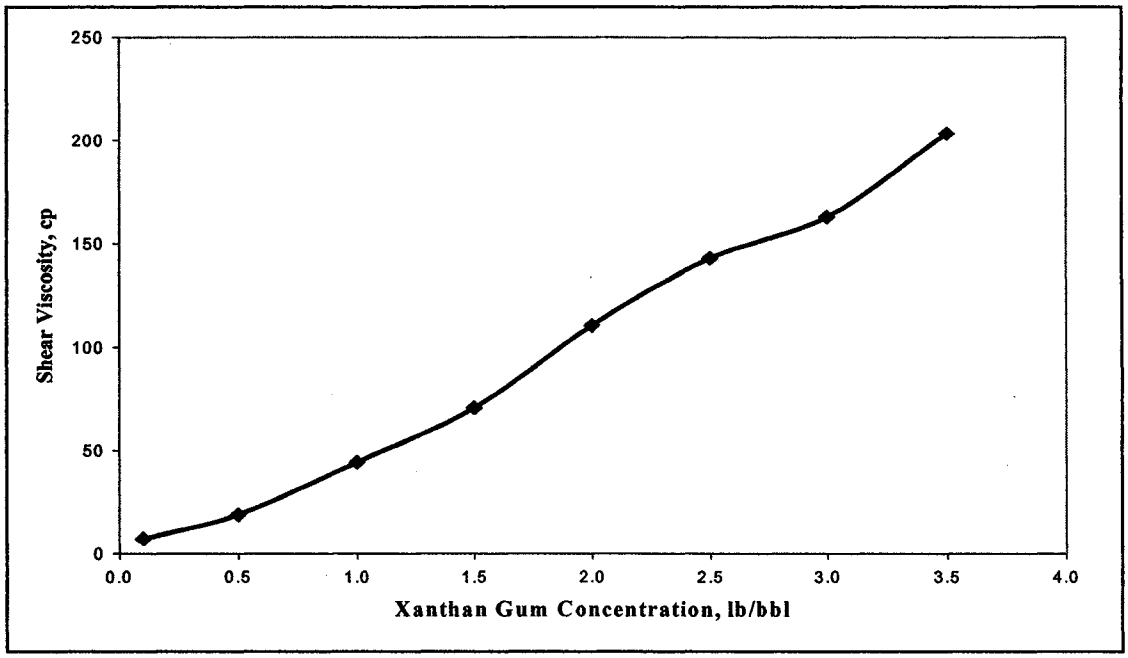

Figure 4.3: Measured Shear Viscosity vs. Xanthan Gum Concentration Calibration Curve (Measured at 105 1/sec)

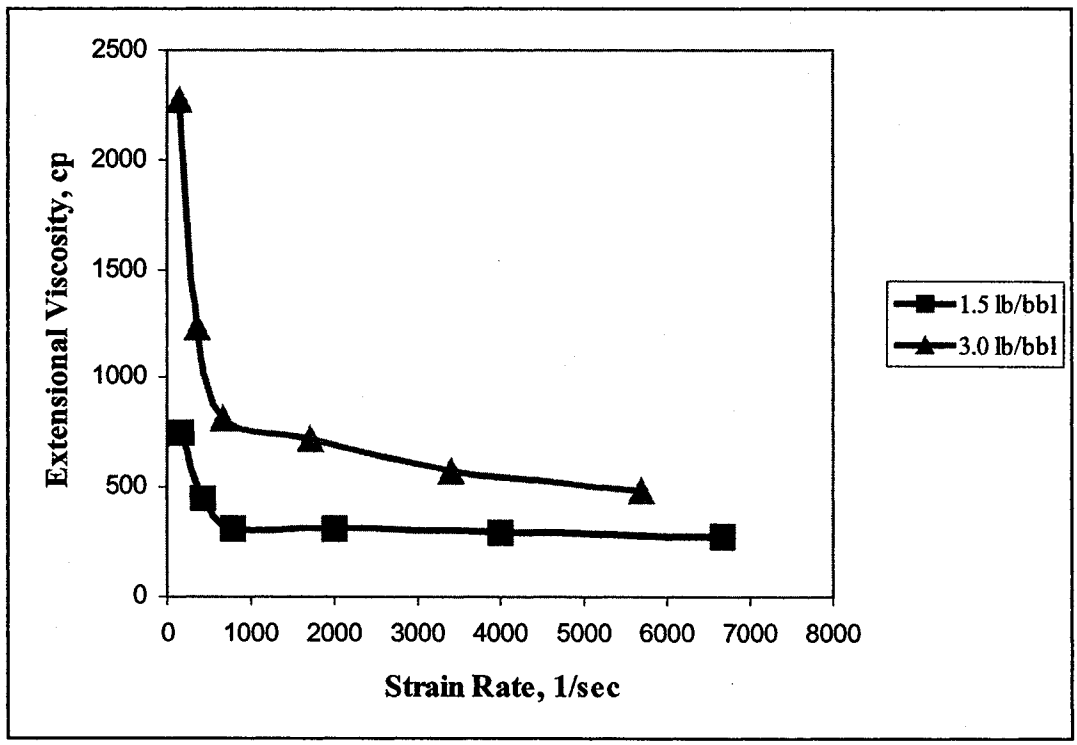

Figure 4.4: Extensional Viscosity vs. Strain/Extensional Rate of Xanthan Gum Solutions

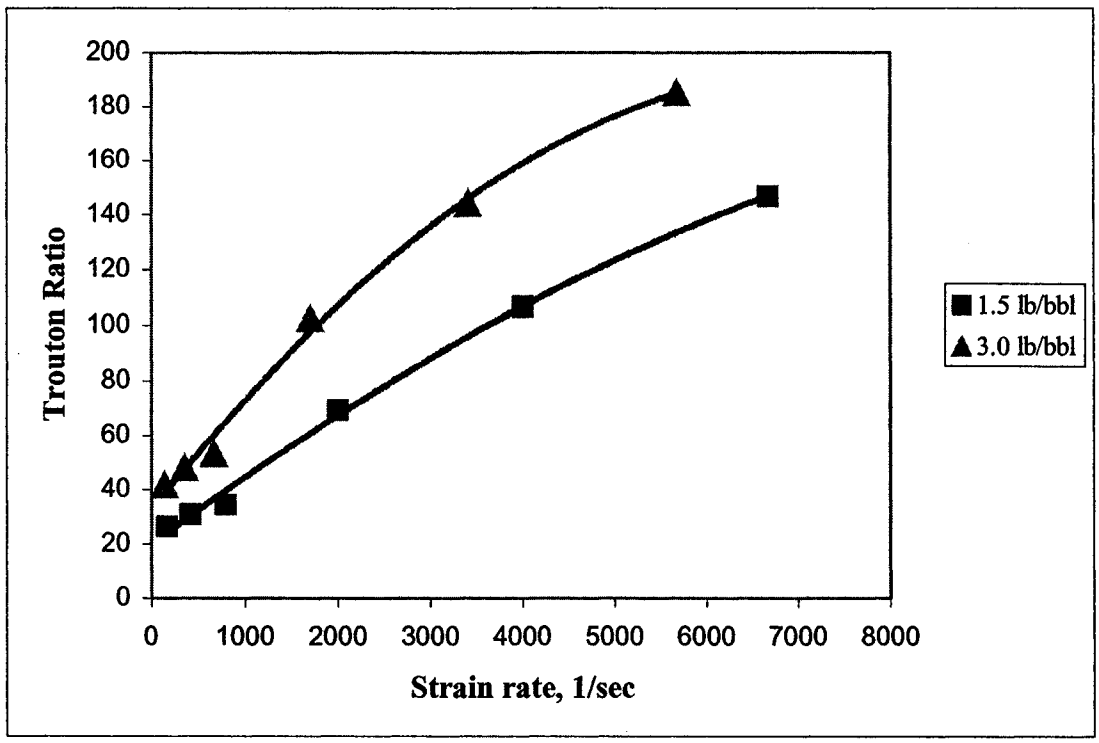

Figure 4.5: Trouton Ratio vs. Strain/Extensional Rate of Xanthan Gum Solutions

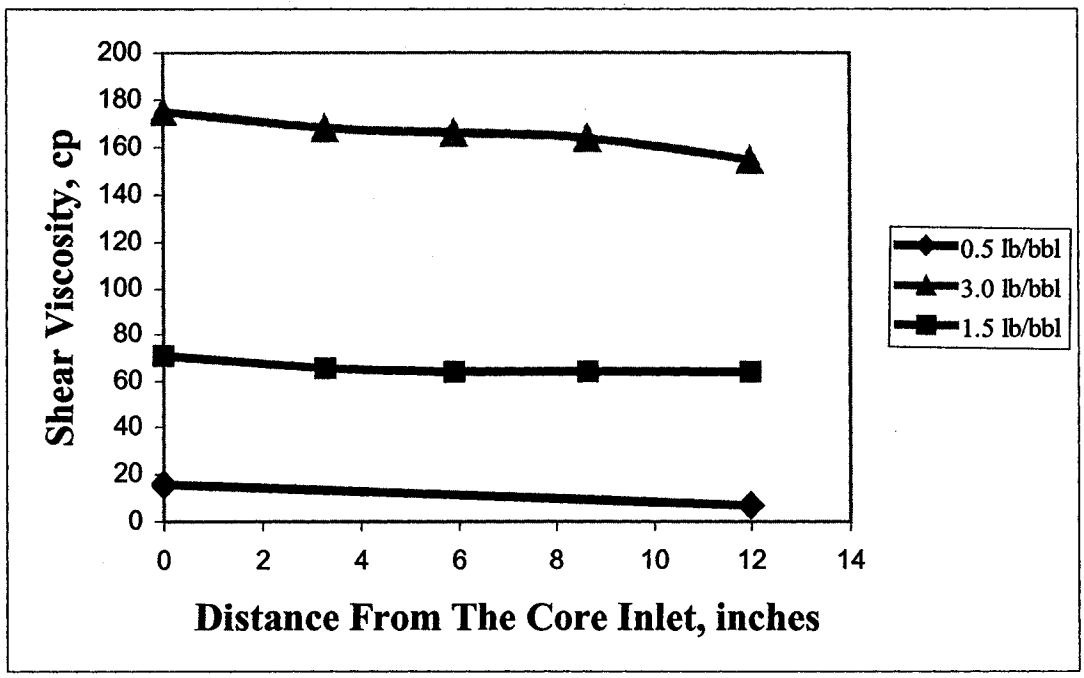

Figure 4.6: Variation of Shear Viscosity Along The Core (measured at 105 sec^{-1}) for Xanthan Gum Core Flow Test

CHAPTER 5

EXPERIMENTAL RESULTS OF PARTIALLY HYDROLYZED POLYACRYLAMIDE (PHPA) SOLUTIONS

5.1 Rheological Characterization of PHPA Solutions

A full-scale rheological characterization of PHPA solutions was carried out by measuring the shear and extensional viscosities.

5.1.1 Shear Viscosity Measurements

Shear viscosities of the fluids were measured by using the Haake (RotoVisco RT-20) viscometer. The shear stress vs. shear rate diagram of three different PHPA solutions (0.5 to 3.0 lb/bbl) is shown in Figure 5.1 (Appendix O). Shear stress-shear rate diagram (Figure 5.1) indicates that the PHPA solutions have very low yield strength and their rheological behavior can be characterized by power law model (Figure 5.1). Power law model coefficients of PHPA solutions are given in Table 5.1.

The shear viscosity vs. shear rate curves of the PHPA solutions (0.5 to 3.0 lb/bbl) is shown in Figure 5.2. Shear viscosity versus shear rate measurements show that the PHPA solutions have shear thinning characteristics (Figure 5.2).

A calibration curve relating the shear viscosity of PHPA solutions (measured at the shear rate observed at pore level; 105 sec^{-1}) to polymer concentration was developed (Figure 5.3). This calibration curve was later used to determine the variation of polymer concentration along the core. The shear viscosities of PHPA solutions increase with increasing polymer concentrations (Figure 5.3).

5.1.2 Extensional Viscosity Measurements

The extensional viscosities were measured (Appendix I) by using the Gel Tester developed by Tremblay et al. [94]. Figure 5.4 shows extensional viscosity versus strain

rate plots of 1.5 and 3.0 lb/bbl PHPA solutions. The extensional viscosities of PHPA solutions increase with the increase in extensional rate (Figure 5.4), which indicates extensional thickening characteristics of PHPA solutions. Whereas xanthan gum solutions showed extensional thinning characteristics. The extensional viscosities of PHPA solutions increase as the polymer concentration increases (Figures 5.4).

Trouton ratio vs. strain rate plots of 1.5 and 3.0 lb/bbl PHPA solutions are shown in Figure 5.5. The Trouton ratios of 1.5 and 3.0 lb/bbl PHPA solutions increase with the increase in strain/extensional rate.

5.2 API Filtration Tests

API filtration tests were performed to determine the effect of PHPA concentrations on the total filtration volume. The results of API filtration tests are given in Table 5.2.

API filtration test results have shown that PHPA solutions have high filtration loss values (Table 5.2). However, API filtration volume decreased (15.2%) with the increasing PHPA concentration from 1.5 to 3.0 lb/bbl.

The actual cause of filtrate reduction is not known. The increase in shear and extensional viscosities were both expected to control rate to the reduction of filter loss.

A comparison of the fold of increase of extensional and shear viscosities might be useful to find out which one of the viscosities has dominant effect on the reduction of filtration rate.

The shear viscosities of 1.5 and 3.0lb/bbl PHPA solutions, at $105sec^{-1}$ shear rates, were measured. Shear viscosity of 1.5lb/bbl PHPA solution was 27 cp and 3.0lb/bbl was 67 cp (at $105sec^{-1}$). The fold of increase in shear viscosity of PHPA solution was 2.5 when the PHPA polymer concentration was increased from 1.5 to 3.0 lb/bbl.

The extensional viscosities of 1.5 and 3.0lb/bbl PHPA solutions, at $105sec^{-1}$ strain rates, were measured. Extensional viscosity of 1.5lb/bbl PHPA solution was 43 cp and

3.0lb/bbl was 200 cp. The fold of increase in extensional viscosity of PHPA solution was 4.6 when the PHPA polymer concentration was increased from 1.5 to 3.0 lb/bbl.

API filtration loss values for 1.5lb/bbl PHPA solution is 249ml and for 3.0lb/bbl PHPA solution is 211ml. The 15% reduction in the filtration loss values with the increase in polymer concentration suggesting that extensional viscosity might play an important role in controlling the filtration loss values of PHPA solutions as compared to shear viscosity, as it can be seen that increase in the extensional viscosity with the increase in PHPA polymer concentration is 4.6 fold, whereas increase in the shear viscosity is only 2.5 fold.

5.3 Core Flow Tests-Assessment of Formation Damage

Fluids with three different polymer concentrations (0.5, 1.5, and 3.0 lb/bbl) were used for the core flow tests.

Measurements from three intermediate pressure transducers (located at equal distance from each other) were used to determine absolute permeability of the glass bead pack before and after the flow of xanthan gum solution through the pack.

PHPA solutions were injected at certain rates to generate a base shear rate of 105sec^{-1} in the core.

5.3.1 Pressure Losses Measurements Along the Core

Pressure losses along the core were measured (Appendix K) and compared with the ones calculated from Darcy equation for linear flow. The use of Darcy equation for pressure loss estimation requires the values of shear viscosities determined at shear rates, which prevail within the porous media. Shear rates in the mechanically packed core were estimated by using the modified Blake-Kozeny equation (Equation 2.4).

Results shown in Table 5.3 indicate that there is a significant difference in measured and calculated pressure losses observed during the flow of PHPA solutions (9.3, 46.4, and 31.4%, corresponding to 0.5, 1.5 and 3.0lb/bbl PHPA concentrations respectively).

Core flow experiments were also conducted using 0.5 and 1.5-lb/bbl PHPA solutions at different flow rates to see the effect of fluid injection rate (shear rate) on the pressure losses (Table 5.4). Measured pressure losses were higher than the calculated pressure losses with slight increase in percent difference as the flow rate increased.

In a previous study by Enevoldsen et al. [111], it was demonstrated that the pressure loss due to the flow of aqueous PHPA solutions through a sand pack could be more than twice of that predicted by Darcy calculations. They suggested that this effect was caused by the very high extensional viscosity of the PHPA solutions. In their case, they used a PHPA concentration of 1.58 lb/bbl. It is, however, likely that they used PHPA with a much higher molecular weight than in the present case. This would lead to higher extensional viscosity values, which may act as an internal filter cake causing higher pressure drops.

5.3.2 Assessment of Formation Damage

Formation damage was calculated (Appendix M) by measuring the permeability before and after the flow test. Initial permeability of the pack was measured by flowing water through the pack.

The flow tests were conducted by injecting PHPA solutions through the core. After a flow test was completed, the core was flushed with water for about 24 hours. The permeability of the pack was then measured again. The percent reduction of the original pack permeability was recorded as an indicator of the damage in each case.

Table 5.5 summarizes the results of permeability measurements before and after core flow tests with PHPA solutions. It was observed that permeability of the core was reduced slightly after the flow of PHPA solutions. The magnitude of permeability reduction increased from 2.5% to 5.3% as the PHPA concentration was changed from 0.5 lb/bbl to 3.0 lb/bbl.

5.3.3 Change in Polymer Concentration Along the Core

Samples of PHPA solutions were collected during the flow tests at the inlet, at the three intermediate stations along the core, and at the outlet. Shear viscosities of these samples were measured. As shown in Figures 5.6, shear viscosities of PHPA solutions were reduced slightly as the fluid flew between inlet and outlet of the core. Depending on the initial PHPA concentration, the reduction in the shear viscosities of the PHPA solutions varied from 4.9% to 8.4% as the fluid flew between inlet and outlet of the core (Table 5.6).

In order to see if adsorption/retention of PHPA molecules play any role on the permeability reduction, PHPA concentrations corresponding to measured inlet and outlet shear viscosities were estimated by using the calibration curve (Figure 5.3).

Figure 5.7 shows the change in polymer concentration of the PHPA solutions as they flow along the core. The results summarized in Table 5.7 show that the PHPA concentration was reduced slightly as the fluid flew between the inlet and outlet of the core. The measured concentration changes were 4.2 %, 5.9% and 6.4% corresponding to fluids with initial PHPA concentrations of 0.5 lb/bbl, 1.5 lb/bb/ and 3.0 lb/bbl respectively. These results are in agreement with the observation that original pack permeability was reduced slightly after the flow of PHPA solutions indicating low rate adsorption/retention of PHPA molecules in the porous media (Table 5.5).

Table 5.1: Power Law Model Coefficients of PHPA Solutions

PHPA Concentration lb/bbl	Consistency Index K $N\text{-}s/m^2$ or pa-sec	Flow Behaviour Index n
0.50	0.0152	0.8896
1.50	0.0401	0.8745
3.00	0.3214	0.6616

Table 5.2: API Filtration Loss vs. Polymer Concentration for PHPA Solutions

	PHPA
Polymer Concentration lb/bbl	API Filtration Loss ml
0.50	N/A
1.50	249.0
3.00	211.0

Table 5.3: Measured Pressure Loss vs. Calculated Pressure Loss for Flow of PHPA Solutions (at 105 1/sec Shear Rate)

PHPA Concentration lb/bbl	Measured Pressure Loss Psi	Calculated Pressure Loss Psi	% Difference
0.50	3.29	3.01	9.3
1.50	13.69	9.35	46.4
3.00	32.72	24.9	31.4

Table 5.4: Comparison of Measured Pressure Loss vs. Calculated Pressure Loss at Different Flow Rates (PHPA Concentration, 0.5 and 1.5 lb/bbl)

0.5 lb/ bbl				
Flow Rate ml/min	Shear Rate 1/sec	Measured Pressure Psi	Calculated Pressure Psi	Difference %
24.70	105.00	3.29	3.01	9.3
28.20	120.00	3.63	3.32	9.3
35.20	150.00	4.44	3.92	13.3
46.90	200.00	5.55	4.87	13.9
70.30	300.00	8.33	6.59	26.4

1.5 lb/bbl				
Flow Rate ml/min	Shear Rate 1/sec	Measured Pressure Psi	Calculated Pressure Psi	Difference %
26.40	105.00	14.00	9.39	49.1
30.10	120.00	15.30	10.23	49.6
37.60	150.00	18.12	12.02	50.1
50.20	200.00	22.56	14.84	57.02

Table 5.5: Permeability Measurements After Flow of PHPA Solutions

PHPA Concentration lb/bbl	Permeability Before The Test Darcy	Permeability After The Test Darcy	Permeability Reduction %
0.50	13.19	12.86	2.50
1.50	13.61	13.09	3.79
3.00	13.36	12.64	5.33

Table 5.6: Variation of Shear Viscosity Between the Inlet and Outlet of the Core

Initial PHPA Concentration lb/bbl	Shear Viscosity at the Inlet cp	Shear Viscosity at the Outlet cp	% Reduction in Shear Viscosity
0.50	10.10	9.60	4.95
1.50	26.78	25.16	6.05
3.00	66.88	61.26	8.40

Table 5.7: Variation of PHPA Concentration Between the Inlet and the Outlet of the Core

PHPA Concentration at the Inlet lb/bbl	PHPA Concentration at the Outlet lb/bbl	% Reduction in PHPA Concentration
0.5	0.480	4.17
1.5	1.416	5.93
3.0	2.820	6.38

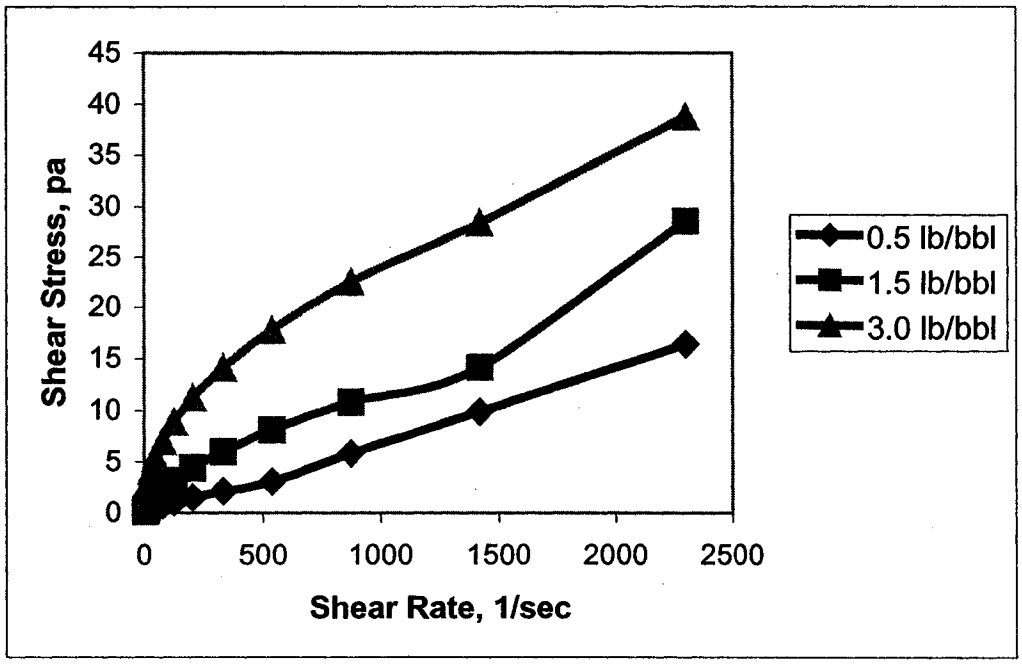

Figure 5.1: Shear Stress vs. Shear Rate Diagram for PHPA Solutions

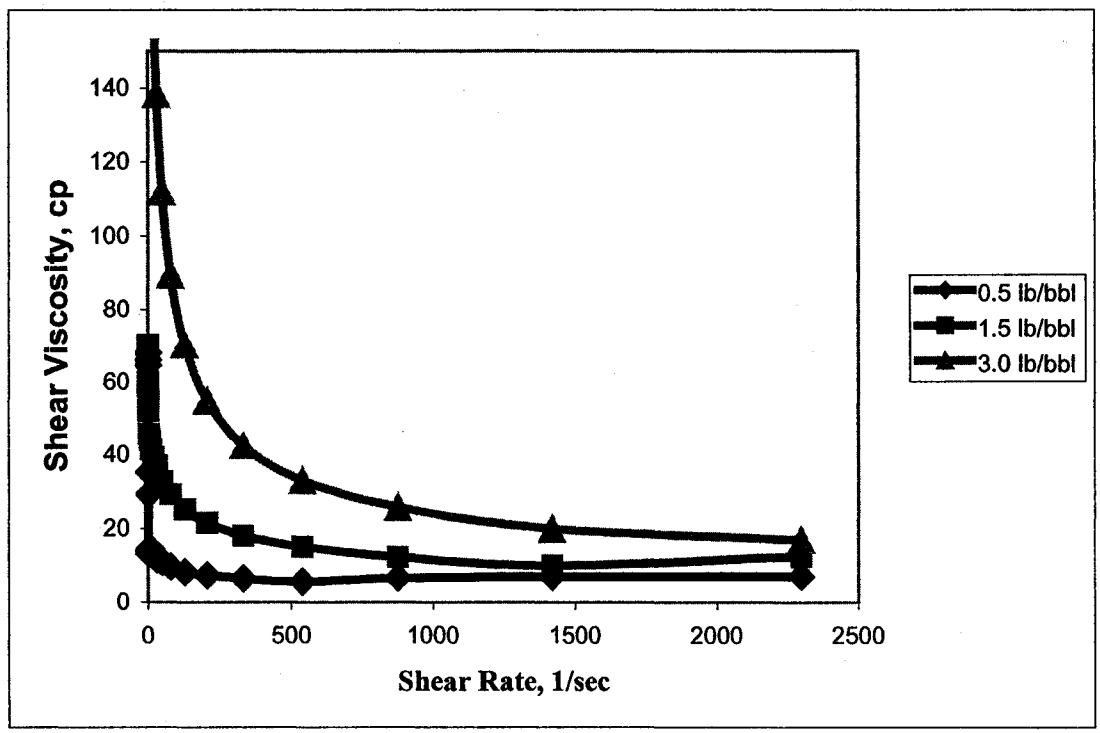

Figure 5.2: Shear Viscosity vs. Shear Rate for PHPA Solutions

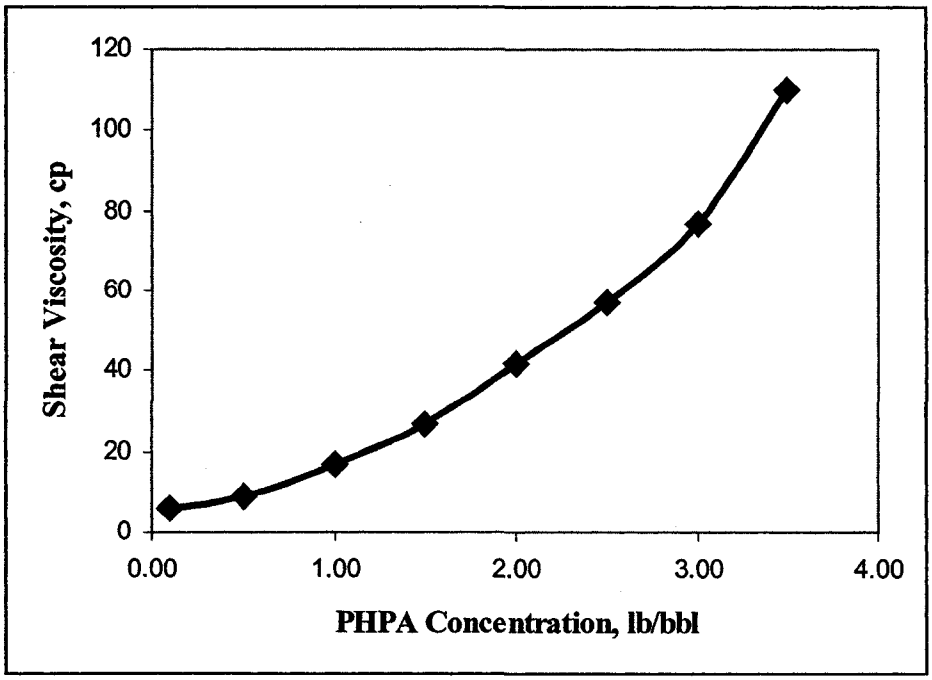

Figure 5.3: Measured Shear Viscosity vs. PHPA Concentration Calibration Curve (Measured at 105 sec^{-1})

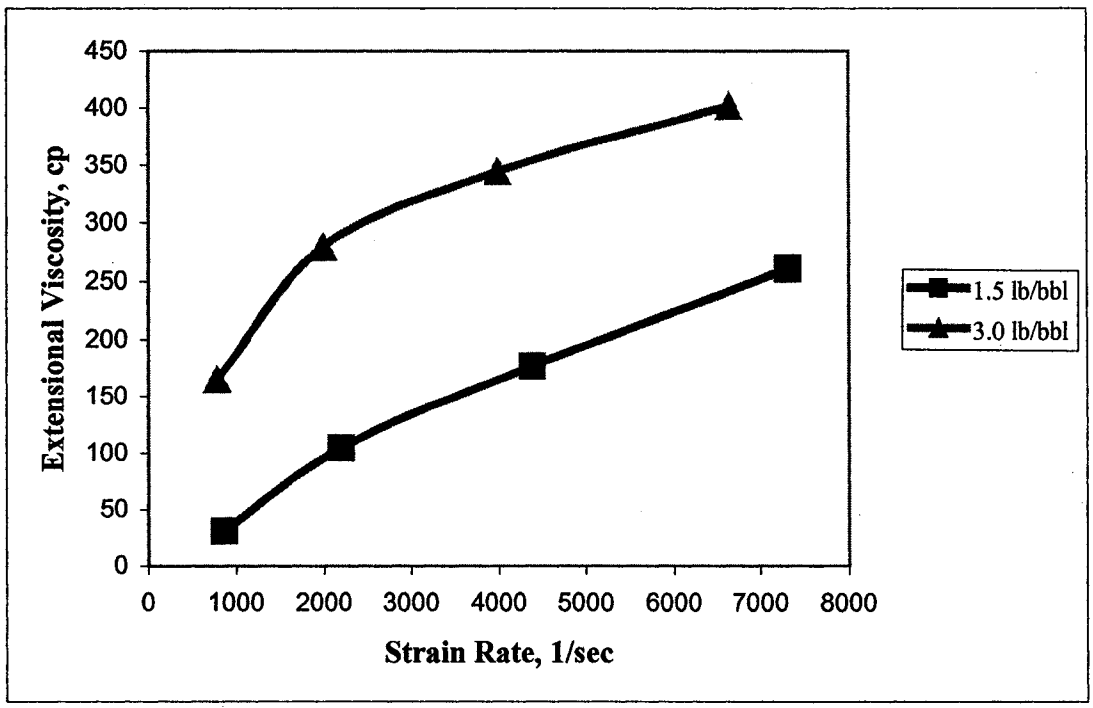

Figure 5.4: Extensional Viscosity vs. Strain/Extensional Rate for PHPA Solutions

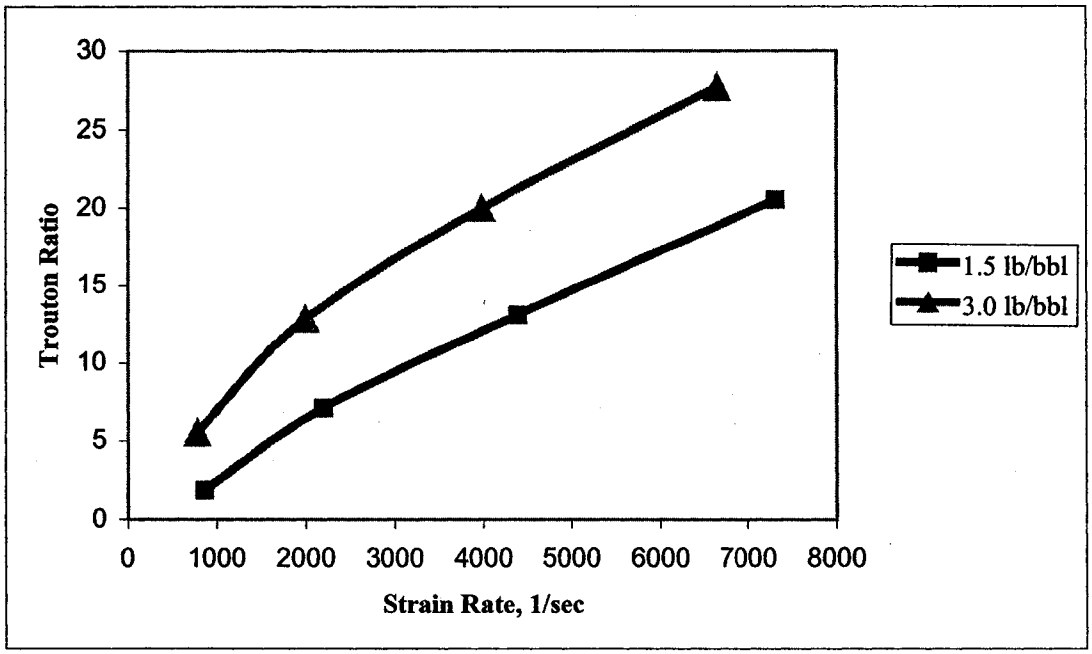

Figure 5.5: Trouton Ratio vs. Strain/Extensional Rate for PHPA Solutions

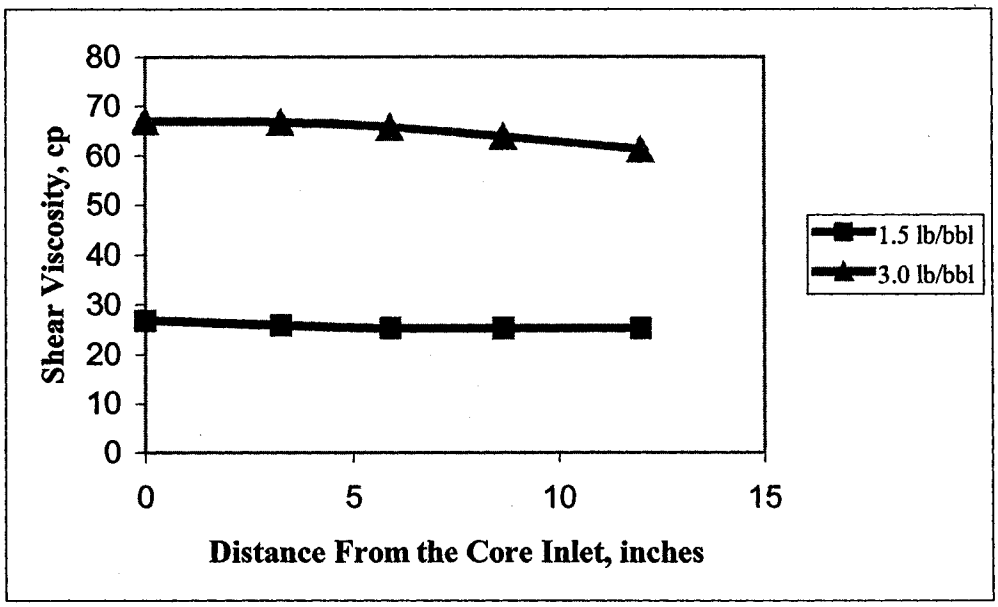

Figure 5.6: Variation of Shear Viscosity of PHPA Solutions along the Core (Measured at 105 sec^{-1})

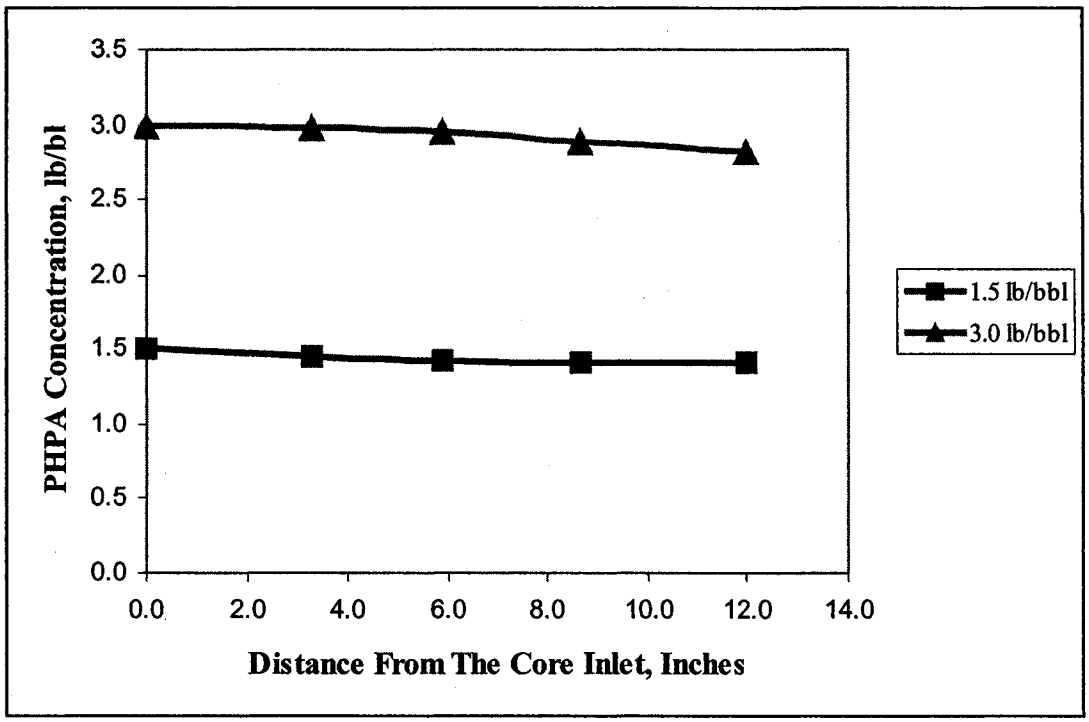

Figure 5.7: Variation of PHPA Concentration along the Core

CHAPTER 6

COMPARISON OF XANTHAN GUM AND PARTIALLY HYDROLYZED POLYACRYLAMIDE SOLUTIONS TEST RESULTS

6.1 Comparison of Shear Viscosity Measurements

Comparison of the shear stress-shear rate diagram of 1.5lb/bbl XG and PHPA solutions is shown in Figure 6.1. Figure 6.1 indicates that XG and PHPA solutions of 1.5lb/bbl concentrations have very low yield stresses, however, XG solution indicates slightly higher yield stress value as compared to PHPA solution.

Comparison of the shear stress-shear rate diagram of 3.0lb/bbl XG and PHPA solutions is shown in Figure 6.2. Figure 6.2 indicates that XG and PHPA solutions of 3.0lb/bbl concentrations have low yield stresses, however, XG solution shows higher yield stress value as compared to PHPA solution.

Figure 6.3 shows the comparison of shear viscosity-shear rate diagram of 1.5lb/bbl XG and PHPA solutions. Figure 6.3 shows that both XG and PHPA solutions are shear thinning in characteristics i.e. shear viscosity decreases as the shear rate increases. The XG solution (Figure 6.3) indicates higher shear viscosity values than that of PHPA solution, especially for the shear rate values from 0 to 500sec^{-1}.

Figure 6.4 shows the comparison of shear viscosity-shear rate diagram of 3.0lb/bbl XG and PHPA solutions. The XG and PHPA solutions of 3.0lb/bbl are shear thinning in characteristics (Figure 6.4), whereas XG solution (Figure 6.4) has high shear viscosity values as compared to PHPA solution, especially for the shear rate values from 0 to 1000sec^{-1}.

The shear viscosities of PHPA and XG solutions (at 105sec^{-1}) are given in Table 6.1. The shear viscosities (at 105sec^{-1}) of 1.5lb/bbl PHPA and XG solutions are 27 cp and 71cp respectively and the shear viscosities (at 105sec^{-1}) of 3.0lb/bbl PHPA and XG solutions

are 67 cp and 175 cp respectively. The difference in shear viscosities is 2.6 fold for both 1.5 and 3.0lb/bbl polymer concentrations.

6.2 Comparison of Extensional Viscosity Measurements

Comparison of the extensional viscosity of 1.5lb/bbl XG and PHPA solutions is shown in Figure 6.5. The extensional viscosity of XG solution shows extensional thinning characteristics whereas PHPA solution indicates extensional thickening characteristics. Figure 6.5 also indicates that XG solution has higher extensional viscosity values as compared to PHPA solutions.

Figure 6.6 shows the comparison of the extensional viscosity of 3.0lb/bbl XG and PHPA solutions. Figure 6.6 shows the extensional thinning characteristics for 3.0lb/bbl XG solution and extensional thickening characteristics for 3.0lb/bbl PHPA solution.

Therefore the xanthan gum solutions, in general, can be characterized as extensional thinning, whereas PHPA solutions as extensional thickening, similar behavior was also reported by Jones and Walters [12]. The 3.0lb/bbl XG solution has high extensional viscosity values as compared to the same concentration of PHPA solution (Figure 6.6).

The extensional viscosities (at $105sec^{-1}$) of PHPA and XG solutions are given in Table 6.2. The extensional viscosities (at $105sec^{-1}$) of 1.5lb/bbl PHPA and XG solutions are 43 cp and 756 cp respectively and the extensional viscosities (at $105sec^{-1}$) of 3.0lb/bbl PHPA and XG solutions are 200 cp and 3104 cp respectively. The difference in extensional viscosities is 17.5 fold for 1.5lb/bbl polymer concentrations and 15.5 fold for 3.0lb/bbl polymer concentrations.

Figure 6.7 shows the comparison of Trouton ratio of 1.5lb/bbl XG and PHPA solutions. Xanthan gum solution of 1.5lb/bbl concentration indicates high Trouton ratio values as compared to the same concentration of PHPA solutions (Figure 6.7).

Comparison of Trouton ratio of 3.0lb/bbl XG and PHPA solutions is given in Figure 6.8. Xanthan gum solution of 3.0lb/bbl concentration has high Trouton ratio values as compared to the same concentration of PHPA solutions.

Table 6.3 shows that the Trouton ratios (at $105sec^{-1}$) of 1.5lb/bbl PHPA and XG solutions are 1.6 and 10.7 respectively and the Trouton ratio (at $105sec^{-1}$) of 3.0lb/bbl PHPA and XG solutions are 2.9 and 17.7 respectively. The difference in Trouton ratio is 6.6 fold for 1.5lb/bbl polymer concentrations and 5.9 fold for 3.0lb/bbl polymer concentrations.

In conclusion, XG solutions have high extensional viscosity and Trouton ratio values as compared to the same concentration of PHPA solutions. Whereas XG is extensional thinning in characteristics while PHPA is extensional thickening.

6.3 API Filtration Tests

API filtration test results have shown that PHPA solutions have much higher filtration loss values than that of XG solutions (Table 6.4). Powell et al. [112] reported that when using "solids free" xanthan gum solutions, filtration rate was controlled by high values of shear viscosities measured at low shear rates and also by the true yield stress of these fluids.

Svendsen et al. [43] argued that Powell et al.'s [112] explanation was incomplete mainly because xanthan gum solutions have low yield stress and they suggested that major factor controlling the fluid loss would be the extensional viscosity of these fluids.

Polymer solutions used in this study have low yield stresses (Figures 6.1 & 6.2) and their extensional viscosities increase significantly as the polymer concentration increases (Figures 4.4 & 5.4). Therefore, results from this study seem to be in agreement with Svendsen et al's [43] conclusion suggesting that the filtration volume is controlled by extensional viscosity.

The fact that XG solutions have much higher extensional viscosities than PHPA solutions suggest that the extensional viscosities may play more significant role than shear viscosities in controlling filtration loss.

For example; the shear viscosity of 3.0lb/bbl XG solution at 105sec^{-1} shear rate is 175 cp while shear viscosity of PHPA solution is 67 cp. The difference in shear viscosity is 2.6 fold.

The extensional viscosity of 3.0lb/bbl XG solution (at 105sec^{-1} strain/extensional rate) is 3104 cp while the extensional viscosity of 3.0lb/bbl PHPA solution is 200 cp. The difference in extensional viscosity is 15.5 fold.

The API filtration loss value of 3.0lb/bbl XG solution is 76 ml while API filtration loss value of 3.0lb/bbl PHPA is 211 ml. The difference is 2.78 fold. Therefore it can be suggested that fluid loss value is more affected by extensional viscosity rather than shear viscosity.

6.4 Core Flow Tests-Assessment of Formation Damage

The main objectives of core flow tests were:

i-) To determine if there is any reduction in the original permeability of the pack after flowing xanthan gum solutions, and if there is any damage occurred, to determine the effect of xanthan gum concentration on the severity of the permeability reduction,

ii-) To determine if the extensional viscosity of the fluids influence the pressure drop along the pack.

6.4.1 Pressure Losses Measurements Along the Core

A comparison of measured and calculated pressure loss values at 105 sec^{-1} shear rate for fluids with three different concentrations (0.5, 1.5 and 3.0 lb/bbl) of PHPA and XG solutions are given in Table 6.5.

Results indicate that the differences in measured and calculated pressure losses are much higher in the case of PHPA solutions (9.3, 46.4, and 31.4 %) as compared to XG solutions (4.7, 11.6, and 27.3%).

Results indicate that using shear viscosity in Darcy equation leads to underestimation of pressure losses significantly. It seems that excess pressure loss observed, particularly, in the case of PHPA solutions might be due to the extensional viscosity component present in this flow configuration, as these solutions have very less formation damage effect (2.5 to 5.5%). These results seem to be in agreement with the results of Naverrete et al [17], where they suggested that for the PHPA solutions, the flow was dominated by the extensional viscosity effect.

6.4.2 Assessment of Formation Damage

Table 6.6 provides comparison of the permeability data obtained after the flow of PHPA and XG solutions. Results indicate that the flow of XG solutions caused significantly higher permeability reduction (up to 28%) than that of the PHPA solutions (up to 5.3%).

Adsorption and retention of polymer molecules on the rock surface is suggested as one of the primary reasons of observed formation damage in core flow tests especially in the case of xanthan gum solutions.

It is also shown in API filtration tests results that PHPA solutions have higher filtration loss values (Table 6.4), for 30 minutes time period, than xanthan gum solutions. Figures 6.9 and 6.10 show comparison of filtration loss versus time plots for PHPA and XG solutions respectively. As seen from Figures 6.9 and 6.10 that filtration profile of PHPA is linear (straight line) with respect to time. Whereas in the case of xanthan gum, filtration volume decreased significantly after 5 minutes indicates that xanthan gum solutions have higher spurt losses and cake-building characteristics.

The rate of leakoff is of critical importance during drilling, completion operations (i.e. sand control) and stimulation treatments, such as acid treatments and hydraulic fracturing. In all of these cases, fluid loss control has been achieved by two basic mechanisms [7]:

1. Increasing the overall viscosity of the fluid using high polymer concentrations or by crosslinking the polymer [5, 6],

2. Developing an internal and/or external filter cake using fluid loss additives (starch, sized $CaCO_3$, mica silica flour, oil soluble resins, etc) to plug the pore throats of the formation [57].

Both fluid loss control mechanisms may result in a loss of permeability when flow is initiated in the production mode. Furthermore, if fluid loss additives are not used properly, they can cause significant loss of permeability due to their plugging mechanism if they enter the formation [58, 59].

Therefore, after evaluating the degree of formation damage, especially in the case of xanthan gum, it can be concluded that xanthan gum solutions have higher formation damage characteristics as compared to PHPA solutions.

Although it can be said, for both types of fluids, the fluid loss can be controlled by increasing the fluid viscosity, but the effect of increasing viscosity results higher formation damage values (Table 6.6).

It can also be concluded that the effect of extensional viscosity may play significant role on the pressure losses. This is true especially for PHPA solutions where higher difference in pressure losses (Table 6.5) is observed while the degree of formation damage (Table 6.6) is low.

6.4.3 Change in Polymer Concentration Along the Core

The results in Tables 6.7 indicate that change in polymer concentration during the flow of PHPA solutions (5.9 and 6.3%, corresponding to 1.5 and 3.0lb/bbl PHPA concentrations respectively) is less than the one observed during the flow of XG solutions (10 and 12%, corresponding to 1.5 and 3.0lb/bbl XG concentrations respectively).

The small change in PHPA concentration indicates that polymer retention/adsorption does not occur in this case. This result is also in agreement with the fact that relatively

low formation damage is observed due to the flow of PHPA solutions (2.5, 3.8, and 5.3% permeability reduction, corresponding to 0.5, 1.5, and 3.0lb/bbl PHPA concentrations respectively).

The significant change in XG polymer concentration (10 and 12%, corresponding to 1.5 and 3.0lb/bbl) indicates that polymer retention/adsorption does occur in this case. This result is also in agreement with the fact that relatively high formation damage is observed due to the flow of XG solutions (21.2, 25.4, and 28.4% permeability reduction, corresponding to 0.5, 1.5 and 3.0lb/bbl XG solutions respectively).

Table 6.1: Comparison of Shear Viscosities of Xanthan Gum and PHPA Solutions (at 105sec^{-1})

Polymer Conc. lb/bbl	Shear Viscosity, cp (@ 105sec^{-1})		Fold of Increase
	PHPA	XG	
1.5	27	71	2.6
3.0	67	175	2.6

Table 6.2: Comparison of Extensional Viscosities of Xanthan Gum and PHPA Solutions (at 105sec^{-1})

Polymer Conc. lb/bbl	Extensional Viscosity, cp (@ 105sec^{-1})		Fold of Increase
	PHPA	XG	
1.5	43	756	17.5
3.0	200	3104	15.5

Table 6.3: Comparison of Trouton Ratios of Xanthan Gum and PHPA Solutions (at 105sec^{-1})

Polymer Conc.	Trouton Ratio		Fold of Increase
lb/bbl	(@ 105sec^{-1} extensional rate)		
	PHPA	XG	
1.50	1.6150	10.6774	6.6
3.00	2.9904	17.7473	5.9

Table 6.4: API Filtration Loss vs. Polymer Concentration for PHPA and Xanthan Gum

	PHPA	Xanthan Gum
Polymer Concentration lb/bbl	API Filtration Loss ml	API Filtration Loss ml
0.50	N/A	N/A
1.50	249.0	187.0
3.00	211.0	76.0

Table 6.5: Comparison of Measured Pressure Loss and Calculated Pressure Loss Values (at 105 1/sec Shear Rate) Between PHPA and Xanthan Gum

	PHPA			Xanthan Gum		
Fluid	**Measured**	**Calculated**		**Measured**	**Calculated**	
Concentration	**Pressure Loss**	**Pressure Loss**	**% Difference**	**Pressure Loss**	**Pressure Loss**	**% Difference**
lb/bbl	**Psi**	**Psi**		**Psi**	**Psi**	
0.50	3.29	3.01	9.3	7.09	6.77	4.72
1.50	13.69	9.35	46.4	17.24	15.39	11.6
3.00	32.72	24.9	31.4	37.33	29.26	27.3

Table 6.6 Comparison of Formation Damage Measured After Flow of PHPA and Xanthan Gum Solutions

	PHPA	Xanthan Gum
Fluid Concentration lb/bbl	**Formation Damage %**	**Formation Damage %**
0.50	2.50	21.19
1.50	3.79	25.41
3.00	5.33	28.39

Table 6.7: Comparison of Change in Polymer Concentration Along the Core

Polymer Concentration	Reduction in Polymer Concentrations, %	
lb/bbl	PHPA	XG
1.5	5.930	10.00
3.0	6.380	12.00

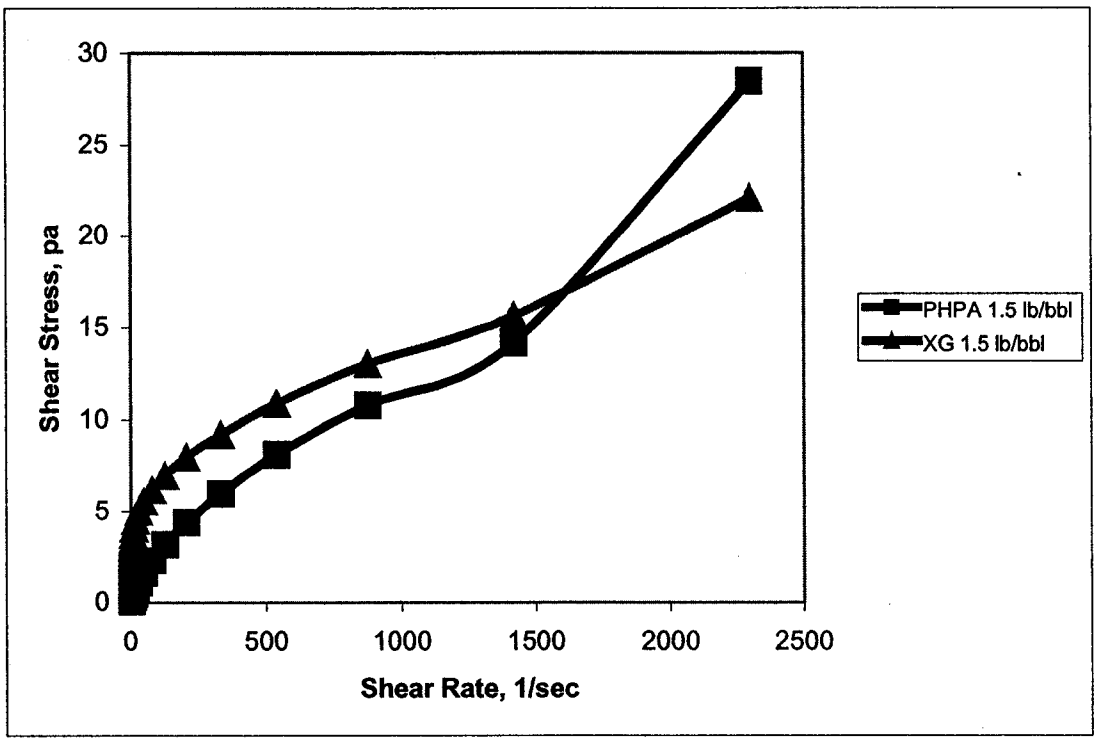

Figure 6.1: Shear Stress vs. Shear Rate of 1.5 lb/bbl PHPA and Xanthan Gum Solutions

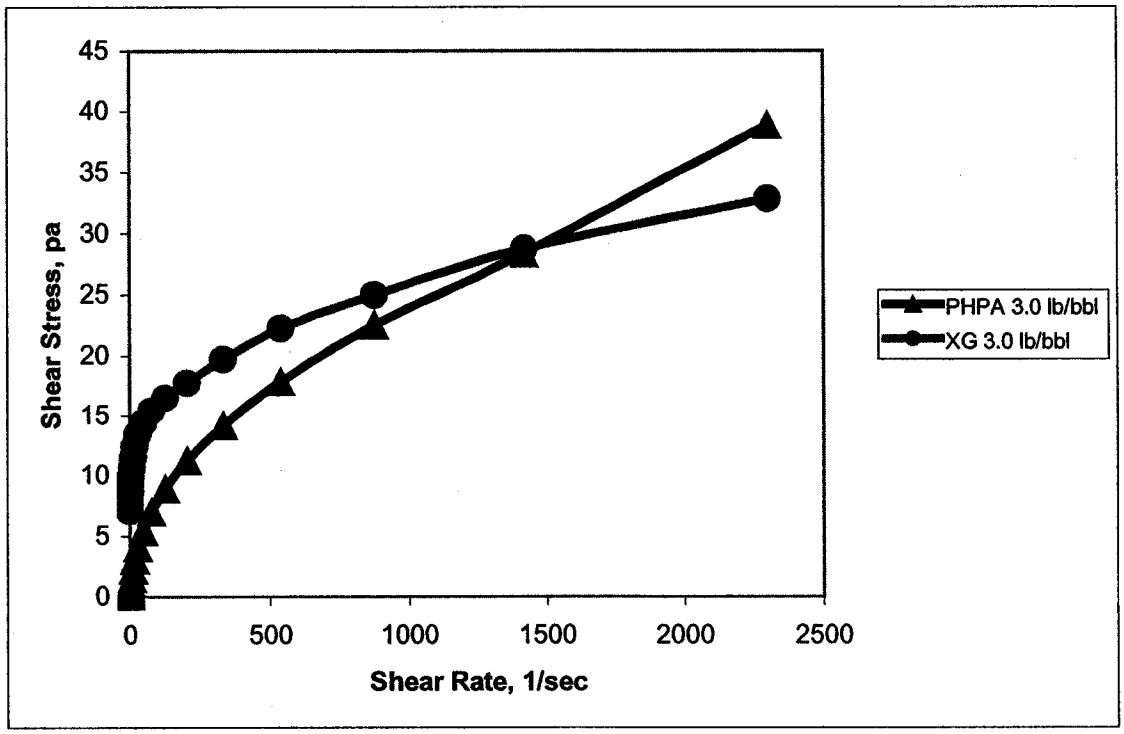

Figure 6.2: Shear Stress vs. Shear Rate of 3.0 lb/bbl PHPA and Xanthan Gum Solutions

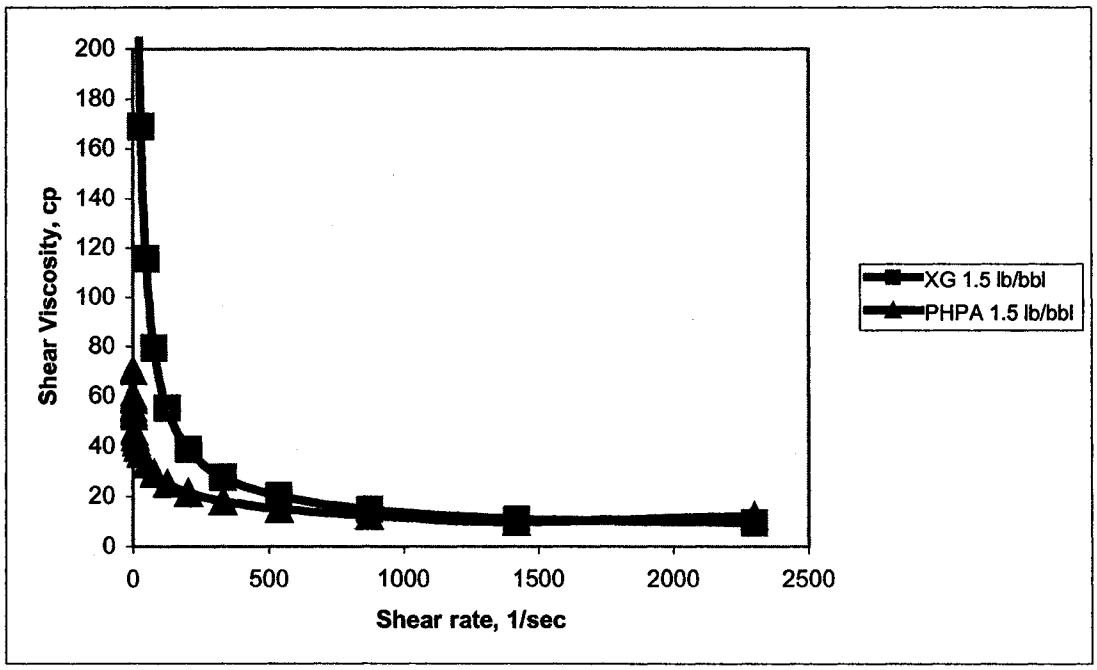

Figure 6.3: Shear Viscosity vs. Shear Rate of 1.5 lb/bbl PHPA and Xanthan Gum Solutions

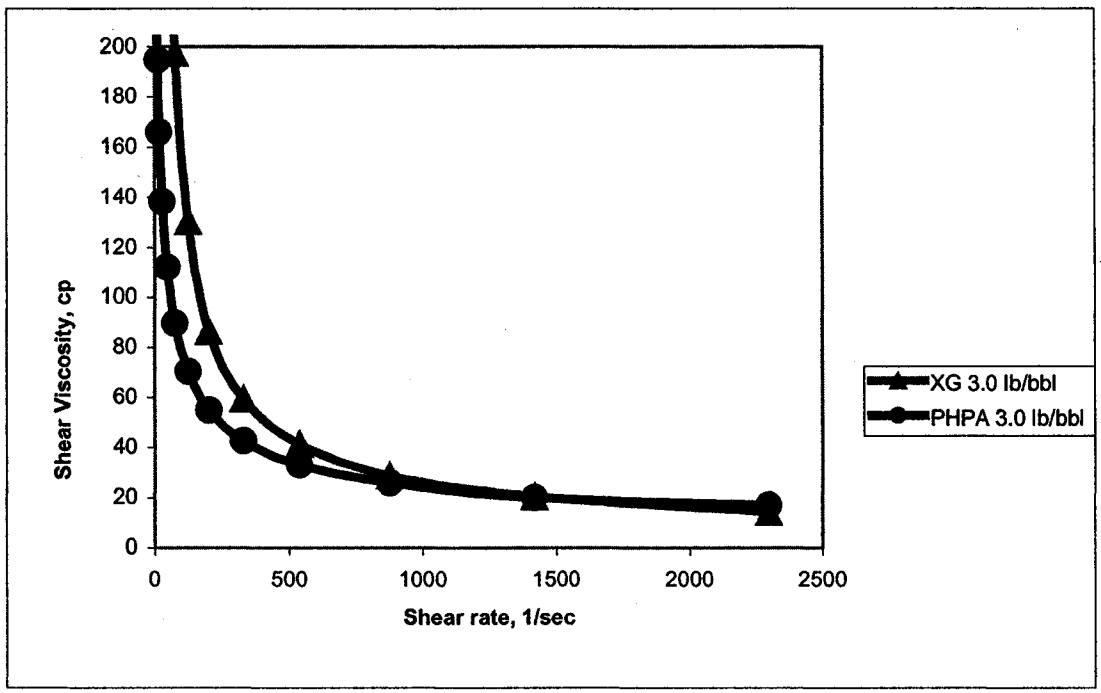

Figure 6.4: Shear Viscosity vs. Shear Rate of 3.0 lb/bbl PHPA and Xanthan Gum Solutions

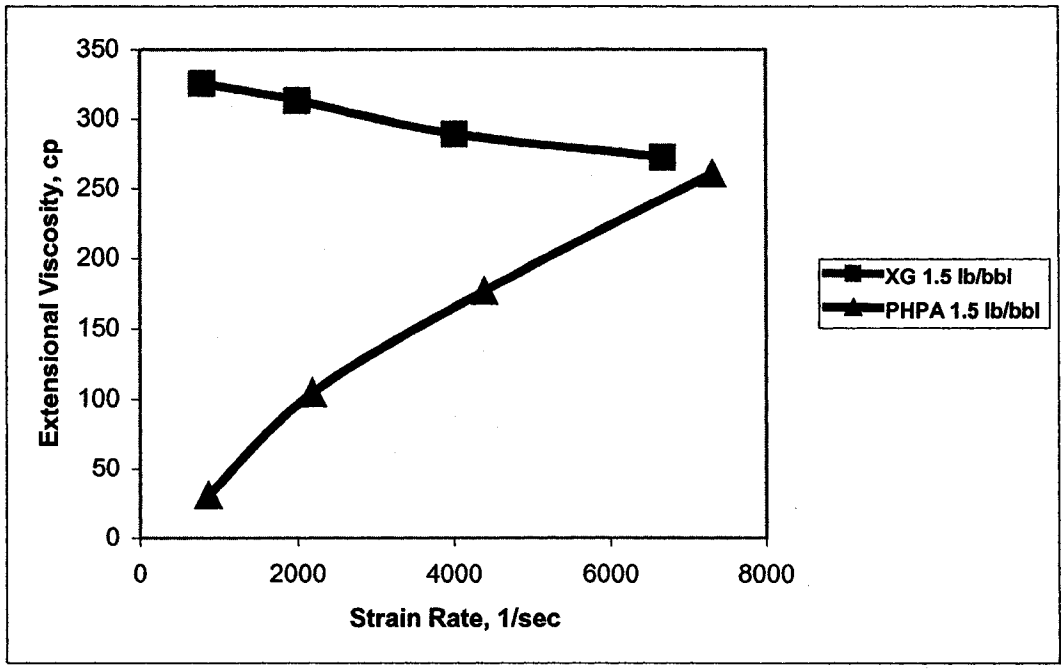

Figure 6.5: Comparison of Extensional Viscosities of 1.5 lb/bbl PHPA and Xanthan Gum Solutions

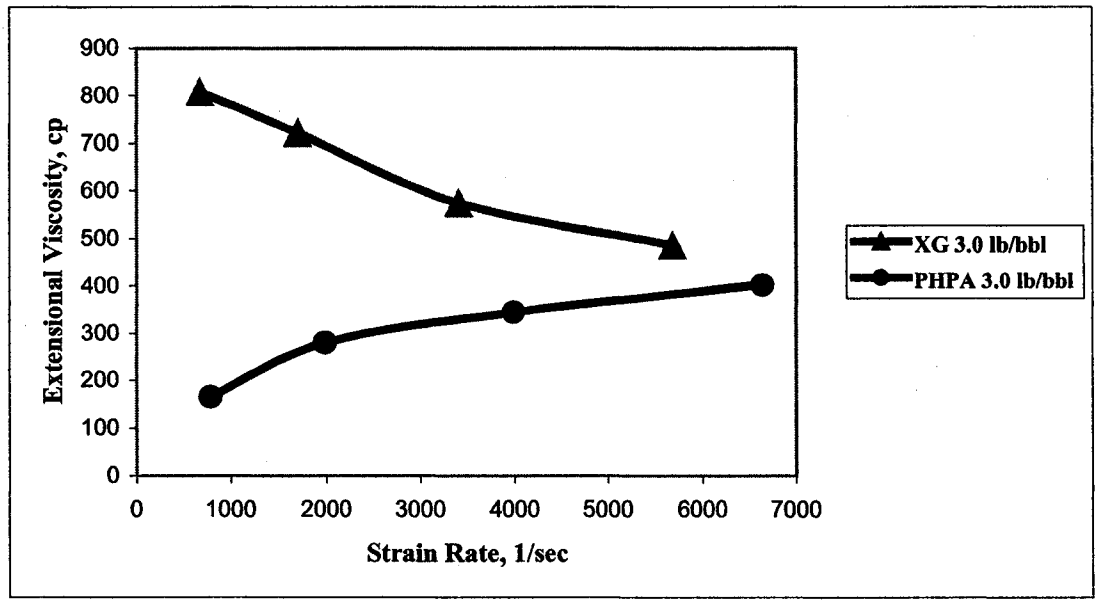

Figure 6.6: Comparison of Extensional Viscosities of 3.0 lb/bbl PHPA and Xanthan Gum Solutions

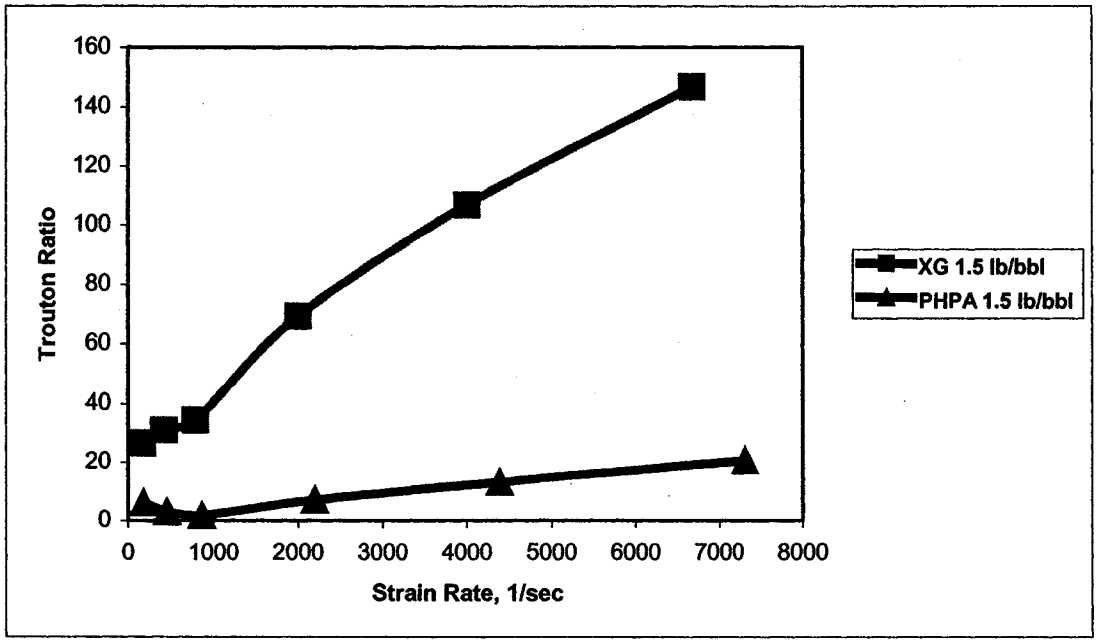

Figure 6.7: Comparison of Trouton Ratio of 1.5 lb/bbl PHPA and Xanthan Gum Solutions

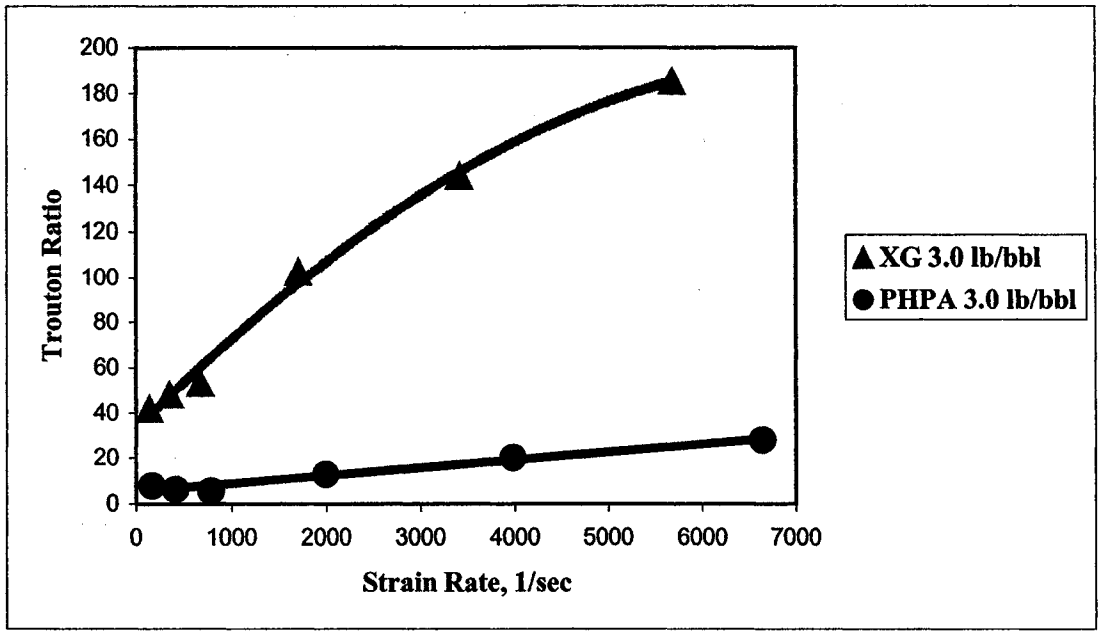

Figure 6.8: Comparison of Trouton Ratio of 3.0 lb/bbl PHPA and Xanthan Gum Solutions

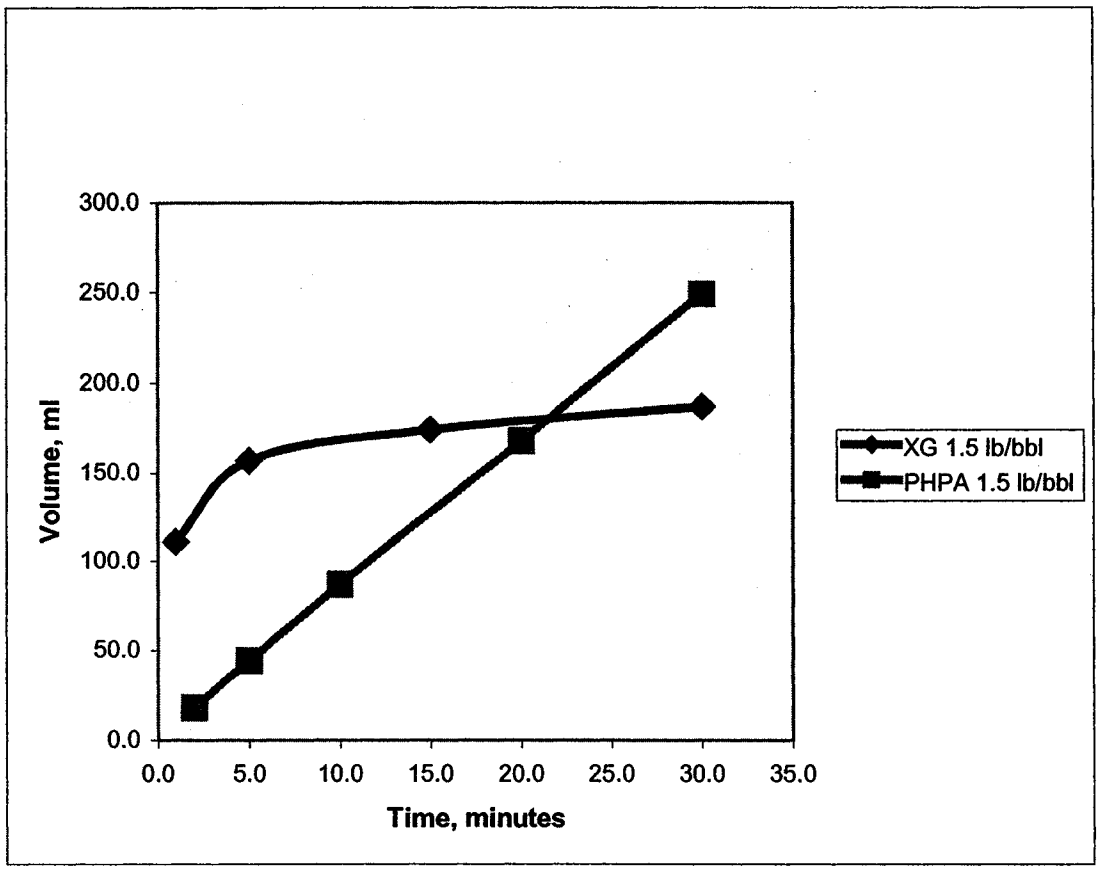

Figure 6.9: Effect of Polymer Concentration on the Filtration Loss of 1.5lb/bbl Xanthan Gum and PHPA Solutions

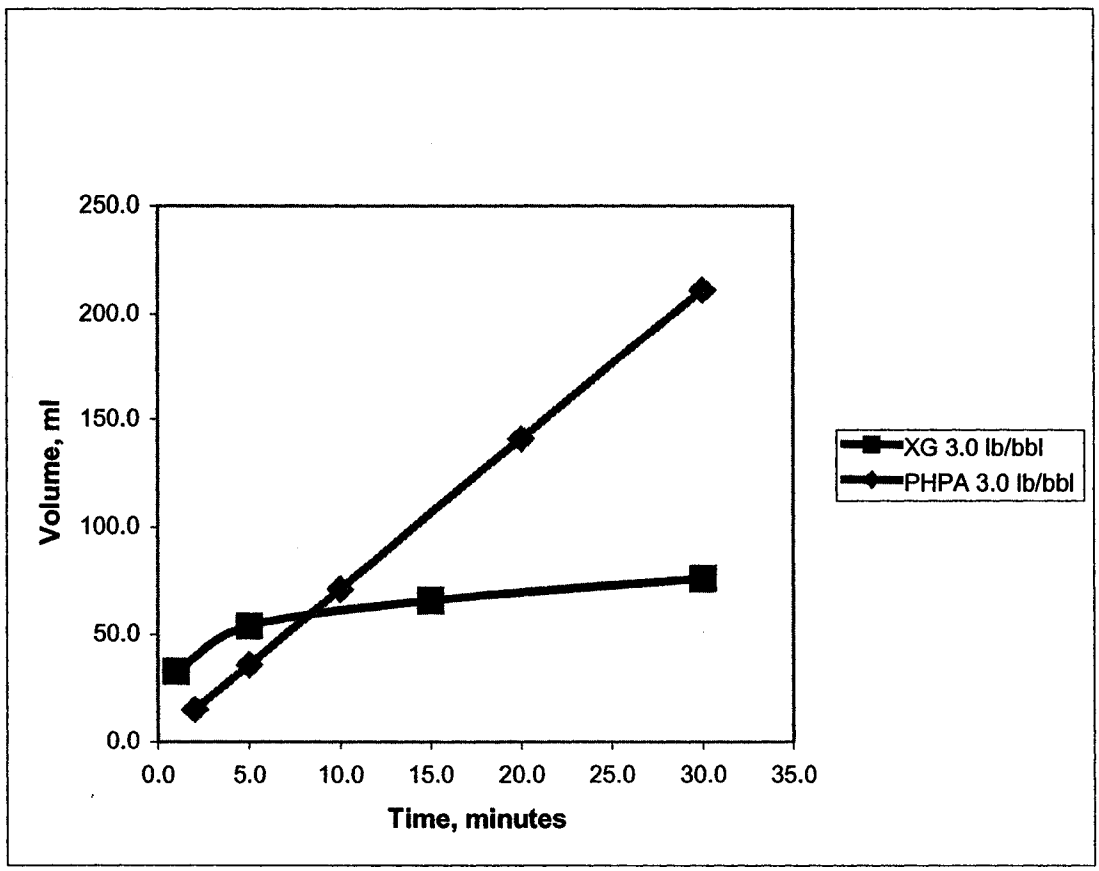

Figure 6.10: Effect of Polymer Concentration on the Filtration Loss of 3.0lb/bbl Xanthan Gum and PHPA Solutions

CHAPTER 7

CONCLUSIONS AND RECOMMENDATIONS

7.1 Conclusions

Based on the experimental work conducted, the following conclusions can be drawn:

1. Flow of polymer-based solutions through a porous media, particularly, in the case of xanthan gum, may cause significant reduction in the original permeability of the porous media.

2. Adsorption and retention of polymer molecules on the rock surface might be one of the primary reasons of permeability reduction (formation damage) when XG solutions flow through the porous media. However, this effect is not significant when flow of partially hydrolyzed polyacrylamide (PHPA) solutions is considered.

3. PHPA solutions can be considered as fluids with extensional thickening whereas xanthan gum solutions can be considered as fluid with extensional thinning characteristics.

4. PHPA solutions have lower shear and extensional viscosity values than XG solutions at the same polymer concentration.

5. PHPA solutions have relatively low shear viscosities. The differences between measured and calculated pressures, however, were high. Significant

differences in measured and calculated pressure losses suggest that flow might have been dominated by extensional viscosity for PHPA.

6. API filtration values of XG solutions are less than that of the PHPA solutions. Considering the fact that the differences in extensional viscosities of XG and PHPA solutions are much higher than the differences in shear viscosities of both fluids. It can be suggested that filtration loss is mostly controlled by extensional viscosity.

7. Efforts for modelling the effect of extensional viscosity on the pressure losses observed during flow of XG and PHPA solutions through porous media were inconclusive.

7.2 Recommendations For Future Research

Based on the experimental work conducted and the results obtained, the following recommendations are suggested for future research in this area.

1. Extensional Viscometer should be modified to measure the extensional viscosities of the polymer-based solutions at very low shear rate (0 to 200 sec^{-1}) to confirm the biaxial extensional viscosity effect at small elongation rates when it becomes three times the zero shear rate viscosity (Trouton ratio =3).

2. A consolidated sand pack or core samples should be considered instead of glass beads to run core flow tests.

3. Core packs with different absolute permeability values (0.5 to 5 darcy) can be used to run the core flow tests. This will be useful to see the effect of original permeability on the extent of the productivity reduction after flow.

4. A temperature and pressure control during core flow tests and viscosity measurements will be helpful to simulate the more realistic subsurface conditions.

5. Experiments can also be conducted using cross-linking agents (to magnify the viscosifying ability of the polymer solutions) with the polymer-based solutions.

6. Polyacrylamide solutions prepared by using very high molecular weight polymers can be used to magnify the effect of extensional viscosity on the pressure loss.

7. More work needs to be conducted to determine the relationship between the extensional viscosity of the polymer based fluids and the pressure losses observed during flow of these fluids through the porous media.

REFERENCES

1. Krueger, R.F., " An Overview of Formation Damage and Well Productivity in Oilfield Operations: An Update", paper SPE 17459, Long Beach, California, March 23-25, 1988.

2. Civan, F., "Reservoir Formation Damage: Fundamentals, Modelling, Assessment, and Mitigation," University of Oklahoma, Gulf Publishing Company, Book Division, P.O.Box 2608, Houston, Texas, pages 1-9, 456-460, 2000.

3. Pitoni, E., ENI-AGIP and Ballard, D.A., Kelly, R.M.: "Changes in Solids Composition of Reservoir Drill in Fluids During Drilling and the Impact on Filter Cake Properties," SPE 54753, SPE European Formation Damage Conference, Hague, Netherlands, 31 May-1 June, 1999.

4. Cobianco, S., Bartosek, M., Lezzi, A., Guameri, A.: "How To Manage Drill-in Fluid Composition to Minimize Fluid losses During Drilling", SPE/IADC 57581, Middle East Drilling Technology, Conf., Abu Dhabi, UAE, 8-10 November, 1999.

5. Navarrete, R.C., Mitchell, J.P., " Fluid-Loss Control for High-Permeability Rocks in Hydraulic Fracturing Under Realistic Shear Conditions," SPE 29504, SPE Production Operations Symposium, Oklahoma City, U.S.A, 2-4 April 1995.

6. Parlar, M., Nelson, E.B., Walton, I.C., Park, E., DeBonis, V.,: " An Experimental Study on Fluid Loss Behavior of Fracturing Fluids and Formation Damage in High Permeability Porous Media," SPE 30458. SPE ATCE, Dallas, U.S.A., 22-25, October 1995.

7. Penny, G.S. and Conway, M.W.: "Fluid Leak-off" Recent Advances in Hydraulic Fracturing, SPE Monograph, Vol.12, Richardson, TX, 1989, pp.147-176.

8. Khan, R. and Kuru, E., Trembley, B., Saasen, A.: "An Investigation of Formation Damage Characteristics of Xanthan Gum Solutions Used for Drilling, Drill-In, Spacer Fluids, and Coiled Tubing Applications", 2003 Annual Canadian International Petroleum Conference, Calgary, Canada, June 10-12.

9. James, D.F. and McLaren D.J.: "The Laminar Flow of Dilute Polymer Solutions Through Porous Media", Journal of Fluid Mech., and Vol.70, p.733-752, 1975.

10. Gupta, R.K. and Sridhar T.: "Viscoelastic effects in Non-Newtonian Flows Through Porous Media", Rheol. Acta, Vol.24, p.148-151, 1985.

11. Durst, F., Haas, R., Interthal, W., " The Nature of Flows Through Porous Media," J.of Non-Newtonian Fluid Mechanics., Vol. 22, p.169-189, 1987.

12. Jones, D.M. and Walters, K.; "The Behavior of Polymer Solutions In Extension-Dominated Flows, with Applications to Enhanced Oil Recovery", Rheologica Acta, Vol. 28, p.482-489, 1989

13. Saasen, A., Tengbreg-Hansen, H., Marken C., and Stavland A.: "Influence of linear Viscoelastic Properties on Invasion of Drilling Fluid Filtrate into a Porous Formation", Oil Gas European Magazine, Vol.4, 1990.

14. Vowerk, J. and Brunn, P.O.: "Porous Medium Flow of the Fluid A1: Effects of Shear and Elongation", Journal of non-Newtonian Fluid Mech., Vol.41, p.119-131, 1991.

15. Koshiba, T., Mori, N. and Nakamura, K.: "Measuement of Pressure Loss in the flow of Polymer Solution Through packed Beds of Particles", Nihon Reoroji Gakkaishi (J. Soc. Rheol. Japan), Vol.21, p.163-169, 1993.

16. Young, N.W.G., Williams, P.A., Meadows, J., Allen, E.: " A Promising Hydrophobically-Modiefied Guar for Completion Applications", paper SPE 39700, Tulsa, Oklahoma, April 19-22, 1998.

17. Naverrete, R.C., Himes, R.E., and Seheult, J.M: "Application of Xanthan Gum in Fluid-Loss Control and related Formation Damage," SPE 59535, SPE Permian Basin Oil and Gas Recovery Conference, Midland, TX, 21-23 March, 2000.

18. Patrice, C.J.S.: "Elongational Flows", Pitman Publishing Co., Biddles of Guildford, U.K., 1977, pp.35-38.

19. Amaefule, J. O., Ajufo, A., Peterson, E., & Durst, K.: "Understanding Formation Damage Processes," SPE 16232 paper, Proceedings of the SPE Production Operations Symposium, Oklahoma City, Oklahoma, 1987.

20. Bennion, D. B., Thomas, F.B., & Bennion, D. W.: "Effective Laboratory Coreflood Tests to Evaluate and Minimize Formation Damage in Horizontal Wells," presented at the Third International Conference on Horizontal Well Technology, Houston, Texas, November 1991.

21. Energy Highlights, "Formation Damage Control in Petroleum Reservoirs," article provided by F. Cavin, the University of Oklahoma Energy Centre, Vol. 1, No. 2 p. 5, Summer 1990.

22. Porter, K. E.: "An Overview of Formation Damage," JPT, Vol. 41, No. 8, pp. 780-786, 1989.

23. Bishop, S. R.: "The Experimental Investigation of Formation Damage Due to the Induced Flocculation of Clays Within a Sandstone Pore Structure by a High salinity Brine," SPE 38156 paper, presented at the SPE European Formation Damage Conference, The Hague, Netherlands, 2-3 June, 1997.

24. Bennion, D. B., & Thomas, F. B.: "Underbalanced Drilling of Horizontal Wells: Does It really Eliminate Formation Damage?," SPE 27352 paper, SPE Formation Damage Control Symposium, Lafayette, Louisiana, February, 1994.

25. Lie Vert, L., and Davis, D .R.: "The Role of Fines During Acidizing treatments," Marine and Petroleum Geology, May, 1987.

26. Dalrymple, E.D., McFatridge, D.G., and Zeltman, T.A.: "Field Evaluation of New Treatment Technique to Remove Permeability Damaged by Polymeric materials," SPE 20117, The Permian Basin Oil & Gas recovery Symposium, Midland, TX, 8-9 March, 1990.

27. Arulahandan, K., Loganathan, P. and Krone, R.B.: "Pore and Eroding Fluid Influences on Surface Erosion of Soil," J. Geotech. Engr., ASCE., 101(2)51, 1975.

28. Gruesbeck, C. and Collins, R. E.: " Entrapment and Deposition of Fines Particles in Porous Media," Soc, Pet. Eng. J., 22(6), 874, 1982.

29. Khilar, K.C. and Fogler, H.S.: "Water Sensitivity of Berea Sandstone's," Soc. Pet. Engr. J., 23(1), 55, 1983.

30. Gary, D.H. and rex, R.W.: "Damage in Berea sandstone Caused by Clay Dispersion and Migration," Proceedings of 14th National Conference on Clays and Clay Minerals, Berkeley, 335, 1966.

31. Nowak, T. J., and Krueger, R.F.: "The effect of Mud Particles and Mud Filtrates Upon the Permeabilities of Cores," API Drilling and production, 164, 1951.

32. Xinghui, L., Indiana, U., and Cavin, F.: "Formation Damage by Fines Migration Including Effects of Filter Cake, Pore Compressibility, and Non-Darcy Flow-A Modelling Approach to Scaling From Core to Field," SPE 28980 paper, The SPE International Symposium on Oilfield Chemistry, San Antonio, TX, USA, 14-17 February, 1995.

33. Jilani, S.Z., Menouar, H., Al-Majed, A.A., Khan, M.A.: "Effect of Overbalance Pressure on Formation Damage", Journal of Petroleum Science and Engineering, Vol. 36, 97-109, 2002.

34. Vitthal, S., McGowen, J.M.,: " Fracturing Fluid Leak-off Under Dynamic Conditions, Part 2: Effect of Shear Rate, Permeability, and Pressure," SPE 36493, SPE ATCE, Denver, U.S.A., 6-9, October 1996.

35. Thomas, R.L., Saxon, A., & Miline, A.W: "The Use of Coiled Tubing During Matrix Acidizing of Carbonate reservoirs Completed in Horizontal Deviated, and Vertical Wells," SPE Production and Facilities, pp. 147-162, August, 1998.

36. Masikevich, J., & Bennion, D.B.: "Fluid Design to Meet Reservoir Isuues-A Process," J. Canadian Petroleum technology, Vol. 38, No. 5, pp. 61-71, My, 1999.

37. Doane, R.D., Bennion, D.B., Thomas, F.B, Bietz, R., & Bennion, D.: "Special Core Analysis Designed to Minimize Formation Damage Associated with Vertical/Horizontal Drilling Applications," JCPT, Vol. 38, No. 5, pp. 35-45, May, 1999.

38. Martins, A.L., Massarani, G., Waldmann, A.T.A., and Costa, F.G: "On the Rheological Mechanism Governing Drill-in Fluid Invasion into reservoir rocks," SPE 82275 paper, The SPE European Formation Damage Conference, The Hague, The Netherlands, 13-14 may, 2003.

39. Dauben, D.L., and Menzie, D.E: "Flow of Polymer Solutions Through porous Media," J. of Petroleum technology, p. 1065-1073, August, 1997.

40. Cakl, J., Machac, I., e Lecjaka, Z.,: "Flow of Viscoelastic Liquids Through Fixed Beds," Progress and Trends in Rheology II, p. 266-268, 1988.

41. Marshall, R.J., & Metzner, A.B.: "Flow of Viscoelastic Fluids Through Porous Media," I & EC Fundamentals, 393-400, August, 1967.

42. Jones, D. and Walters, K.: "Extensional Viscosity in EOR," SPE 18070, SPE ATCE, Houston, TX, U.S.A., 2-5 October, 1988.

43. Svendsen, O., Saasen, A., Vassoy, Skogen, E., Mackin, F., Normann, S.H.: " Optimum Fluid Design for Drilling and Cementing a Well Drilled with Coil Tubing Technology, " SPE 50405, SPE International Conference on Horizontal Well Technology, Calgary, Canada, 1-4, November, 1998.

44. Bird, R.B., Armstrong, R.C., e Hassager, O., Dynamics of Polymer Liquids, Vol. 1. John Wiley & Sons, 1977.

45. Teeuw, D., and Hesselink, F.T.: "Power-Law Flow and Hydrodynamic Behaviour of Biopolymer Solutions in Porous Media", SPE 8982, Fifth International Symposium on Oilfield and Geothermal Chemistry, Stanford, California, May. 28-30, 1980.

46. Gogarty, W.B.: "Rheological Properties of Pseudo-Plastic Fluids in Porous Media," SPE Journal, 149-160, Janue, 1967.

47. Harvey, A.H. & Menzie, D.E.: "Polymer Solution Flow in Porous Media," SPE Journal, 118-118, June, 1970.

48. Wang, F.H.L., Duda, J.L & Klaus, E.E: "Influence of Polymer Solution Properties on Flow in Porous Media," SPE 8414 paper, SPE 54th Annual Fall Tech. Conf. And Exh., Las vagas, Neveda, 23-26 September, 1979.

49. Hill, H.J., Brew, J.R., Claridge, E.L., Hite, J.R., & Pope, G.A.: "The Behaviour of Polymers in Porous Media," SPE 4748 paper, SPE Improved Oil Recovery Symposium, Tulsa, okia., 22-24 April, 1974.

50. Strickland, P.H., Wilson, J.T & Warnock, W.E.: "The Feasibility of Converting an Existing Waterflood to a Polymer Flood: A Case History of West yellow Creek," SPE 7462 paper, SPE 53rd Annual Fall Techn. Conf. And Exh., Houston, Texas, 1-3 October, 1978.

51. Maerker, J.M.: "Shear Degradation of partially Hydrolized Polyacrylamide Solutions," SPE Journal, 311-322, August, 1975.

52. Chauveteau, G., & Kohler, N.: "Polymer Flooding: The essential Elements for Laboratory Evaluation," SPE 4745 paper, SPE Improved Oil recovery, Tulsa, Okla., 22-24 April, 1974.

53. Szabo, M.T.: "A Comparative Evaluation of Polymers for oil recovery-Flow and retention in Porous Media," SPE 6601-B paper, SPE Int. Symposium on Oilfield and Geothermal Chemistry, La Jolla, cal., 27-28 June, 1977.

54. Dawson, R., & Lantz, R.B.: "Inaccessible Pore Volume in Polymer Flooding," SPE Journal, 448-452, October, 1972.

55. Shah, B.N., Willhite, G.P., & Green, D.W.: "The effect of Inaccessible Pore volume on the Flow of Polymer and Solvent Through Porous Media," SPE 7586 paper, SPE 53rd Annual Fall tech. Conf. And Exech., Houston, texas, 1-3 October, 1978.

56. Robert H., C., and Middleman's.: "Power-Law Flow Through a Packed Tube", EC Fundamentals, Vol.4, NO. 4., Nov. 1965 & I.

57. Colby, M.R., and Todd, B.L: "Current Materials and Devices for Control of Fluid Loss," SPE 39593 paper, SPE International Symposium on Formation Damage Control, Lafayette, LA, 18-19 February, 1998.

58. Wojtanowicz, A.K., Krilov, Z. and Langlinais, J.P: "Experimental Determination of Formation Damage Pore Blocking Mechanism," J. Energy Res. Tech., 110,34, 1988.

59. Sharma, M. M., and Yortsos, Y.C.: "Fines Migration in Porous Media," AIChEJ., Vol. 33, No, 10, 1654, 1987.

60. Ford, W.G.F., and Penny, G.S.: "The Influence of Down Hole Conditions on the Leakoff Properties of Fracturing Fluids," SPE Prod. Eng., 43-51, February, 1988.

61. Gulbis, J.: "Dynamic Fluid Loss Study of Fracturing Fluids," paper CIM 82-33-18, Annual Technical Meeting, Calgary, 6-9 June, 1982.

62. Gulbis, J.: "Dynamic Fluid Loss Study of Fracturing Fluids," paper SPE 12154, Annual Technical Conference and Exhibition, San Francisco, 5-8 October, 1983.

63. Penny, G.S. and Conway, M.W. and Lee, W.S.: "Control and Modelling of Fluid Leak-off During Hydraulic Fracturing," JPT, 1071-81, 1985.

64. Navarrete, R.C., Cawiezel, K.E., and Constien, V.G.: " Dynamic Fluid Loss in Hydraulic Fracturing Under Realistic Shear Conditions in High Permeability

Rocks," SPE 28529, Annual technical Conference and Exhibition, New Orleans, 25-28 September, 1994.

65. McGowen, J.M. and McDaniel, B.W.: "The Effects of Fluid Preconditioning and Test Cell Design on the Measurement of Dynamic Fluid Loss Data," SPE 18212 paper, Annual technical Conference and Exhibition, Houston, 2-5 October, 1988.

66. Roodhart, L.P.: "Fracturing Fluids: Fluid-Loss Measurements Under Dynamic Conditions," SPEJ, 629-36, October, 1985.

67. McMechan, D.E.: "Fracturing Fluid Loss at High DP: Laboratory Tests and Field Applications," SPE 21873, Rockey Mountain Regional Meeting, Denver, 15-17 April, 1991.

68. McGowen, J.M., Vitthal, S., Parker, M.A., Rahimi, A., and March, W.E. Jr.: "Fluid Selection from High Permeability Formations," SPE 26559 paper, Annual Technical Conference and Exhibition, Houston, 3-6 October, 1993.

69. Parker, M.A., Vitthal, S., McGowen, J.M., Rahimi, A., and March, W.E.Jr.: "Fracturing Fluid Damage in High Permeability Formations," SPE 27378 paper, SPE Formation Damage Symposium, Lafayette, Louisiana, 7-9 February, 1994.

70. Mayerhofer, M.J., Economides, M.J., and Nolte, K.G.: "Experimental Study of Fracturing Fluid Loss," paper CIM/AOSTRA 91-92, Technical Conference, Banff, Alberta, 22-24 April, 1991.

71. Zeilinger, S.C., Mayerhofer, M.J., and Economides, M.J.: "A Comparison of The Fluid-Loss Properties of Borate-Zirconate-Crosslinked and Non-Crosslinked Fracturing Fluids," SPE 23435 paper, Eastern Regional Meeting, Lexington, Kentucky, 22-25 October, 1991.

72. Penny, G.S.: "Nondamaging Fluid Loss Additives for Use in Hydraulic Fracturing of Gas Wells," SPE 10659 paper, Formation Damage Symposium, Lafayette, 24-25 march, 1982.

73. Ghofrani, Reza and mazeel, Alaboudi M.A., ITE-TU Clausthal, and Sengupta, Pinaki.: " Damage Caused by Clay Based and Clay Free Inhibitive Fluids in Sandstone Formations," SPE 23815, Symposium on Formation Damage Control, Lafayette, Louisiana, 26-27 February, 1992.

74. Pitoni, E., Ripa, G., Lorefice, R., Formisani, D.: "High Productivity Open Hole Gravel Packs in Depleted Permeable Sands," SPE 38157, European Formation Damage Conference, The Hague, The Netherlands, 2-3 June, 1997.

75. Jiao, Di and Sharma.: "Formation Damage Due to Static and Dynamic Filtration of water-Based Muds," SPE 23823, Symposium on Formation Damage Control, Lafayette, Louisiana, 26-27 February, 1992.

76. Price, P.A., Qui, X.: "Fluid Loss Control Additives for Use with Gravel Pack Placement Fluids," United States Patent 5,415,228, 16 May, 1995.

77. Bailey, L., Meeton, G., Way, P.: "Filtercake Integrity and reservoir Damage," SPE 39429, Symposium on Formation Damage Control, Lafayette, Louisiana, 18-19 February, 1998.

78. Bailey, B., Crabtree, M., Tyrie, J., Eliphick, J., Kuchuk, F., Romano, C., Roodhart, L.: "Water Control, Oilfield Review," Spring, 30-51, 2000.

79. Chiappa, L., Andrei, M., Lockhart, T.P., Maddinelii, G., and Burrafato, G.: "Polymer Design for Relative Permeability Modification at High Temperature, SPE 80202 paper, International Oilfield Chemistry Symposium, Houston, 5-7 February, 2003.

80. Zitha, P., Chauveteau, G., Leger, L.: "Unsteady-State Flow of Flexible Polymers in Porous Media," J. of Colloid and Interface Science, 234,269-283,2001

81. Chauveteau, G., Denys, K., Zaitoun, A.: "New Insight on Polymer Adsorption Under High Flow rates," SPE 75183 paper, Symposium on Improved Oil recovery, Tulsa Oklahoma, 13-17 April, 2002.

82. Zitha, P.L.J.: "In-Depth Filtration of Macromolecules Induced by Bridging Adsorption in Porous Media, SPE 68980 paper, European Formation Damage Conference, The Hague, the Netherlands, 21-22 May, 2001.

83. Xiao, D. and Sharma, M.M.: "Formation Damage Due to Static And Dynamic Flitration of Water-Based Muds," SPE 23823, SPE International Symposium on Formation Damage Control, 1992.

84. Peng, S.J. and Peden, J.M.: "Prediction of Filtration Under Dynamic Conditions," SPE 23824, SPE International Symposium on Formation Damage Control, 1992.

85. Carlson, E.S. et al.: "Predicting the Fluid Loss of Drilling, Workover and Fracturing Fluids into a Formation with and without Filter cake," SPE 35227, SPE Permian Basin Oil and Gas Recovery Conference, Midland, TX, 27-29 March, 1996.

86. Longeron, D.G., Alfenore, J., Poux-Guillaume, G.: "Drilling Fluids and Permeability Impairment; Performance Evaluation of various Mud Formulations," SPE 48988, SPE Annual tech. Conf. And Exhibition, New Orleans, LA, 27-30 September, 1998.

87. Clark, P.E. et al.: "Predicting Fluid Invasion by Polymer-Based Drilling Fluids," AADE Drilling Fluid Conference and Exhibition, Houston, TX, 3-4 April, 1996.

88. Gallino, G. and Maglione, R.: "L'Applicaczione del Modello di Herschel & Bulkley Alle Attuali Teorie per L'Ottimizzazione Della Pulizia del Foro Durante la Perorazione," IV Italian Applied Rheology Conference, Vico Equense, Italy, 12-15 June, 1996.

89. Audibert, A. et al.: "The Role of Polymers on Formation Damage," SPE 54767, SPE European Formation Damage Conference, the hague, the Netherlands, 31 may – 1 June, 1999.

90. Naverrete, R.C., Himes, R.E., and Seheult, J.M: "Application of Xanthan Gum in Fluid-Loss Control and related Formation Damage," SPE 59535, SPE Permian Basin Oil and Gas Recovery Conference, Midland, TX, 21-23 March, 2000.

91. Lomba, R.F.T., et al.: "Drill-in Fluids: Identifying Invasion Mechanism," SPE 73714, SPE International Symposium and Exhibition on Formation Damage Control, Lafayette, Louisiana, LA, 20-21 February, 2002,

92. Young, N.W.G. and Muhrbeck, P.: " Comparision of Shear and extensional Viscosity Characterisitcs of Starch Pastes," Ann. Trans. Nordic. Rheology. Soc., Vol. 5, pp. 40-43, 1997.

93. Barnes, H.A., Hutton, J.F., and Walters, K.: "An Introduction to Rheology," Elsevier, Amsterdam, 1989.

94. Tremblay, B.: "Elongational Viscosity Estimates of Polymer Melts", Handbook of Advanced Materials Testing, Chapter, 51, 971-984, 1992, Marcel Dekker, New York.

95. Gupta, M.: "Effect of Elongational Viscosity on Axisymmetric Entrance Flow of Polymers", Polymer Engineering and Science, Vol. 40, 23-35. January 2000.

96. Bagley, E.B.: "J. Appl. Phys. 28:624, 1957.

97. Piau, J.M., El Kissi, N. and Tremblay, B.: "Influence of Upstream Instabilities and Wall Slip on Melt Fracture and Sharkskin Phenomena During Silicones Extrusion Through orifice Dies," J. Non Newt. Fluid Mech.34: 145, 1990.

98. Cogswell, F.N.: "Polymer Melt Rheology," Halsted Press, John Wiley and Sons, Toronto, p. 50-51, p. 100-101, 1981.

99. Cogswell, F.N.: "Converging Flow of Polymer Melts in Extrusion Dies," Polym. Eng. And Sci. 12(1): 64, 1972.

100. Cogswell, F.N.: "Measuring the extensional Rheology of Polymer melts," Trans. Soc. Rheol. 16(3):383, 1972.

101. Gibson, A.G.: "Converging Dies," Rheological Measurements, (A.A. Collyer and D.W. Clegged.), Elsevier Applied Science, New York, p. 49, 1988.

102. Gibson, A.G.: "Die Entry Flow of reinforced Polymers ," Composites 2091):57, 1989.

103. Binding, D.M.: "An Approximate Analysis for Contraction and Converging Flows," J. Non-Newt. Fluid Mech. 27: 173, 1988.

104. Laun, H.M. and Schuch, H.: "Transient Elongational Viscosity and Drawbility of Polymer Melts," J. Rheol. 33(1): 119, 1989

105. Fischer, C.C. Navarrete, Constien, V.G., Coffey, Aasadi, M.: "Novel Application of Synergistic Guar/Non-Acetylated Xanthan Gum Mixtures in Hydraulic Fracturing," paper SPE 65037 presented at the 2001 SPE International Symposium on Oilfield Chemistry, Houston, Texas, Feb. 13-16.).

106. Salamone, J.C., Clough, S.B., Salamone, A. Beal, Reid, K.I.G., Jamison, D.E.: "Xanthan Gum- A Lyotropic Crystalline Polymer and its Properties as a Suspending Agent," SPE 9097 SPEJ Forum Article, 1982.

107. Li, H., and Tian, J. Liu, Y.Z.: "Pilot Test of Xanthan Gum Flooding in Shengli Oilfield," paper SPE 57294, SPE Asia Pacific Improved Oil recovery Conference, Kuala Lumpur, Malaysia, Oct. 25-26, 1999.

108. Saasen, A. and Loklingholm, G.: " The Effect of Drilling Fluid Rheological Properties on Hole Cleaning," SPE 74558, IADC/SPE Drilling Conference, Dallas, TX, U.S.A, Feb. 26-28, 2002.

109. Ibrahim Nashawi, S.: "Laboratory Investigation of the Effect of Brine Composition on Polymer Solutions-Part-1 Partially Hydrolyzed Polyacrylamide (HPAM) Case", paper SPE 23533, 1991.

110. Foshee, W.C., Jennings, R.R., and West, T.J., "Preparation and Testing of Partially Hydrolyzed Polyacrylamide Solutions", paper SPE 6202, New Orleans, Oct. 3-6, 1976.

111. Enevoldsen, J., Rasmussen, H.K. and Saasen, A., "Pressure Drop Through Gravel Packs", Ann. Trans. Nordic Rheol. Soc., vol. 3, pp. 45-47, 1995.

112. Powell, J.W, Stephens, M.P., Seheult, L.L.C.J.M., Sifferman, T., and Swazey, J. : " Minimization of Formation Damage, Filter Cake Deposition and Stuck Pipe Potential in Horizontal Wells Through the Use Of Time-Dependent Viscoelastic Yield Stress Fluids and Filtrates," IADC/SPE 29408, IADC/SPE Drilling Conference, Amsterdam, 28 February-March2, 1995.

113. Born, K., Langendorff, V., Boulenguer, P.: "Xanthan", DEGUSSA Texturant Systems France SAS, Research Centre, Baupte, France, 11, p.261-291.

APPENDIX A: GIBSON MODEL

$$P_s = 2K (\sin(\alpha))^{3n} / 3n\alpha^{(1+3n)})^* ((1+3n)/(4n))^n * (1- R_0 / R_b)^{3n}) \gamma_A^n \ldots\ldots\ldots (A.1)$$

$$P_e = l\gamma_A^t [(2 / (3t)(\sin(\alpha)(1+\cos(\alpha)) / 4)^t (1 - R_o / R_l)^{(3t)}) + \phi (t, \alpha) / 4^t] \ldots (A.2)$$

$$P_o = P_e + P_s \ldots (A.3)$$

where,

P_o = entrance pressure P_e = elongational contribution of the pressure

P_s = shear contribution of the pressure R_o = orifice radius R_b = radius of barrel

Newtonian Fluid:

$$K = \mu_N \qquad n = 1$$

$$l = 3\mu_N \qquad t = 1$$

where,

μ_N = viscosity of oil measured in shear rheometer

l = Trouton Viscosity

Sudden Contraction:

$\alpha = \pi / 2$ where, α = converging angle of die (half angle)

P_o = pressure drop measured in test therefore

$$P_s = 2\mu_N / (3 (\pi / 2))^4 (1 - R_o / R_l)^3) \gamma A$$

$$P_e = 3\mu_N \gamma_A [(2 / 3 * 1 / 2)(1- (R_o / R_l)^3) + \pi / 2 \text{ lnt zero } (\sin(\beta))^2 db / 4$$

where,

$\pi / 2$ lnt zero $\sin^2 x\, dx = \pi / 4$

Assume = $R_o / R_1 = 0$

$P_s = 32 / (3\pi)^4 \mu_N \gamma_A$

$P_e = 3[1 / 3 + \pi / 16] \mu_N \gamma_A$

$$Po = \{32 / (3\pi)^4 + 1 / 2 + 3\pi / 16\} \mu_N \gamma_A \ldots (A.4)$$

$$\gamma_A = 4Q / (\pi R_o^3) \ldots (A.5)$$

$$Q = V_p * \pi R_b^2 \ldots . (A.6)$$

where,

R_o = capillary radius n = power law index γA = apparent shear rate

Q = flow rate V_p = piston velocity R_1 = radius of upstream conduit / radius of rheometer barrel

Steps:

1. Using equation A.4, A.5 and A.6 calculate Po versus γ_A curve for oil (only) and compare to measurement. Since the flow through the orifice in the piston head is more complicated than assumed in driving the equation for entry flow. R_o in equation A.5 will be back calculated from the measurement entrance pressure P_o,

$$R_o = [\{(4Q / \pi) (32 / 3\pi^4) + 1 / 2 + 3\pi / 16) \mu_N\} / P_o]^{1/3} \ldots . (A.7)$$

In other words equation A.7 is used to "calibrate" the radius of the orifice. By calculating an "equivalent" radius for the orifice we will hopefully correct for non-ideal flow into the orifice.

The next step is to use equations A.1, A.2 and A.3 to calculate the elongational viscosities.

Note that we will use the equivalent radius in equation A.7 in the elongational viscosity calculations.

2. Substitute K and n (consistency index and power law index measured in the shear rheometer) and apparent shear rate γ_A into equation A.1.

3. Calculate P_e from equation A.3.

$$P_e = P_o - P_s$$

where, P_o = pressure drop across the orifice measured in test

4. Plot P_e versus γ_A on a log-log scale.

5. Calculate the slope of the line. This slope is the power law index t in the expression for the elongational viscosity.

$$\mu_E = 1\, \varepsilon^{t-1}$$

$$1 = \text{constant}$$

$$\varepsilon = \gamma_A \sin(\alpha)\,(1 + \cos(\alpha))\,/\,4$$

$$\varepsilon = \text{average extensional rate}$$

6. Calculate ϕ in equation A.2, where;

$$\phi = \pi / 2 \text{ lnt zero } (\sin x)^{(t+1)}\,(1 + \cos x)^{(t-1)}\,dx$$

This integral will be calculated numerically on a spreadsheet.

7. Calculate l from equation A.2.

APPENDIX B: ORIFICE SIZE CALIBRATION USING PUMP OIL

Calculation for P_o versus γ_A plot for oil:

$$P_o = \{32 / (3\pi)^4 + 1 / 2 + 3\pi / 16\} \mu_N \gamma_A \ldots. \text{(B.1)}$$

$$\gamma_A = 4Q / (\pi R_o^3) \ldots \text{(B.2)}$$

$$Q = V_p * \pi R_b^2 \ldots \text{(B.3)}$$

where,

R_o = capillary radius

γ_A = apparent shear rate

Q = flow rate

n = power law index

K = power law coefficient

V_p = piston velocity

R_1 = radius of upstream conduit / radius of rheometer barrel

μ_N = viscosity of oil measured in shear rheometer

R_o = 1.172821 mm = 0.00117282 m

R_b = 2.615 mm = 0.02615 m

μ_N = 0.0798 Pa.sec

Table B.1: Entrance Pressure P_o Calculation for pump oil

Vp	Vp	Vp	Q	γ_A	P_o,from eq	P_o, from test
rev / sec	cm / s	m / s	M^3 / s	1 / s	Pa	Pa
0.983	0.5000	0.00500	1.0741E-05	8477	811	807.844354
0.590	0.3000	0.00300	6.4447E-06	5086	487	398.676675
0.295	0.1500	0.00150	3.2223E-06	2543	243	169.699085
0.116	0.0590	0.00059	1.2675E-06	1000	96	80.6882876
0.061	0.0313	0.00031	6.7132E-07	530	51	57.3930347
0.025	0.0125	0.00013	2.6853E-07	212	20	41.9360566

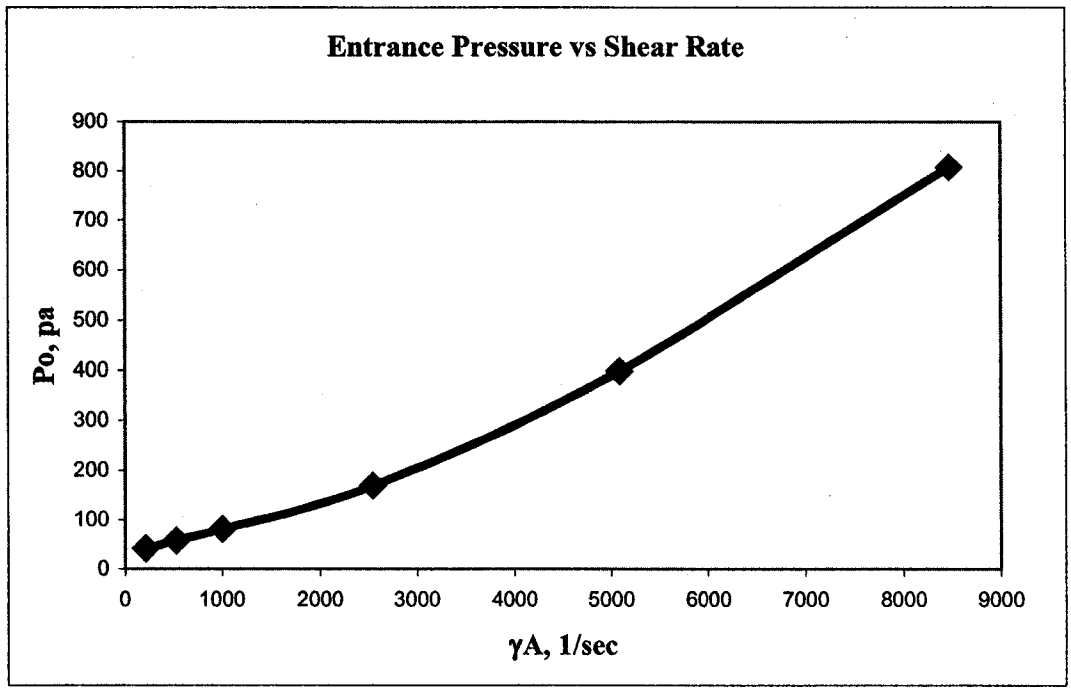

Figure B.1: Entrance pressure versus apparent shear rate plot for pump oil

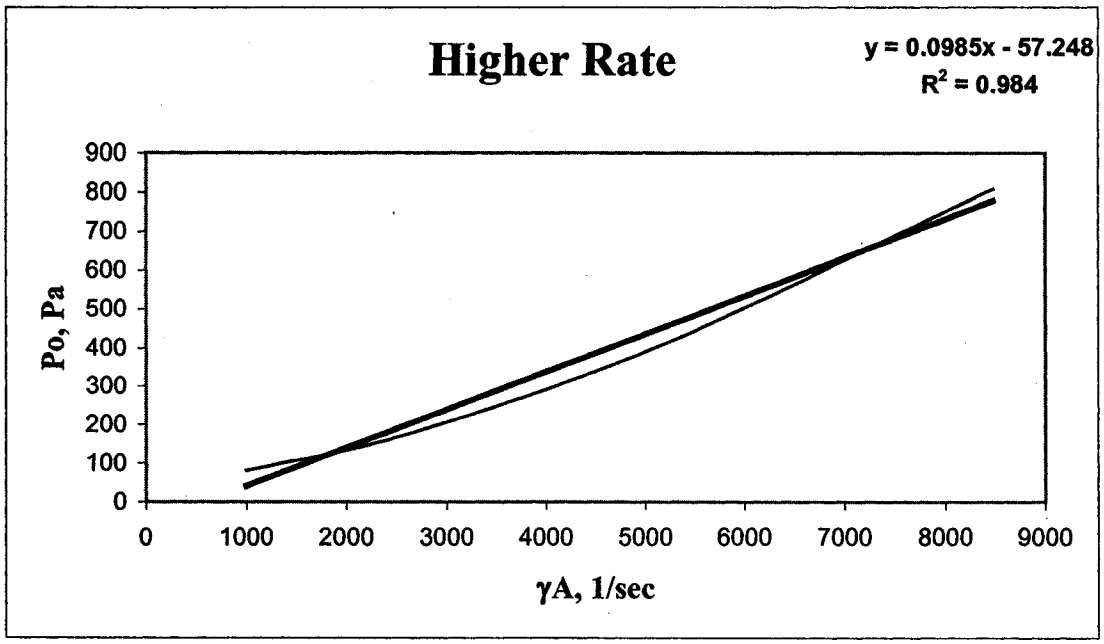

Figure B.2: Entrance pressure versus apparent shear rate plot for pump oil (at higher apparent shear rate)

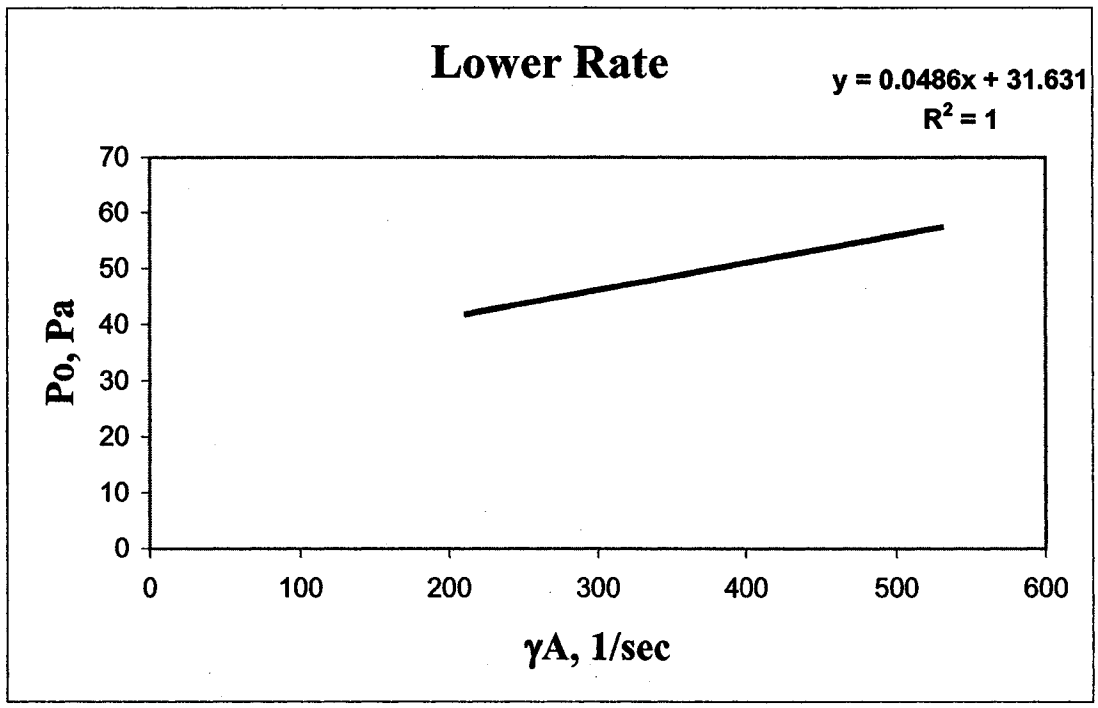

Figure B.3: Entrance pressure versus apparent shear rate plot for pump oil (at lower apparent shear rate)

Higher rate = 0.0985 Pa.sec

Lower rate = 0.486 Pa.sec

Back calculation of R_o from measurement entrance pressure P_o:

$$R_o = [\{(4Q / \pi) (32 / 3\pi^4) + 1 / 2 + 3\pi / 16) \mu_N\} / P_o]^{1/3}$$

K = 0.0823 Pa.sec

n = 1.02

γ_T = true shear rate $(3n + 1) / (4n) \gamma_A$

μ_N = apparent shear viscosity = $K \gamma_A^{n-1}$

μ_T = true shear viscosity = $\mu_N \gamma_A / \gamma_T$

Trouton ratio = μ_E / μ_T

Table B.2: Calibration of orifice size using pump oil

Calibration				True Shear	APPARENT	TRUE	Reynolds
				Rate	Shear Visc	Shear Visc	Number
Q	R_o	R_o	γ_A	γT	μ_N	μ_T	N_{RE}
m^3 / sec	m	mm	1 / s	1/s	Pa-s	Pa-s	
1.0741E-05	**0.00125964**	**1.2596381**	5702.44316	5674.49	0.09784104	0.09832301	69.58179
6.4447E-06	**0.00134441**	**1.3444103**	3421.4659	3404.694	0.09684653	0.09732361	42.17779
3.2223E-06	**0.00141852**	**1.4185204**	1710.73295	1702.347	0.09551322	0.09598373	21.38329
1.2675E-06	**0.00133162**	**1.3316155**	672.888293	669.58982	0.09374728	0.09420909	8.569194
6.7132E-07	**0.00095374**	**0.953737**	1311.68983	1305.26	0.09500719	0.0954752	4.478579
2.6853E-07	**0.0007802**	**0.7801998**	524.675932	522.10399	0.09328196	0.09374148	1.824564
Average	**0.00133855**	**1.3385461**					
Average	**0.00086697**	**0.8669684**					

APPENDIX C: RESULTS OF ORIFICE SIZE CALIBRATION USING DIFFERENT VISCOSITY PUMP OILS

Radius:

Table C.1: Results of orifice size calibration using different viscosity pump oils

Pump Oil	Higher Rate	Lower Rate	Avg
	Ro, mm	Ro, mm	Ro, mm
90 cp	1.3596	0.9485	1.1540750
80 cp	1.3385	0.8670	1.1027572
10 cp	1.2356	0.6423	0.9389945
Average	1.3113	0.8193	1.0652756

Table C.2: Pump oil (90 cp) and its shear viscosity at different flow rates

Pump Oil	TRUE	Reynolds
90 cp	Shear Viscosity	Number
Q	μ_T	N_{RE}
m^3 / sec	Pa-s	
1.07411E-05	0.105614842	64.77774816
6.44469E-06	0.104562683	39.25774345
3.22234E-06	0.103151734	19.89736308
1.26745E-06	0.101282367	7.970745942
6.71321E-07	0.102168895	4.185160555
2.68529E-07	0.100350392	1.704400837

Table C.3: Pump oil (80 cp) and its shear viscosity at different flow rates

Pump Oil	TRUE	Reynolds
80 cp	Shear Viscosity	Number
Q	μ_T	N_{RE}
m^3 / sec	Pa-s	
1.07411E-05	0.098323014	69.581793
6.44469E-06	0.09732361	42.177792
3.22234E-06	0.095983727	21.383286
1.26745E-06	0.094209093	8.5691942
6.71321E-07	0.095475202	4.4785789
2.68529E-07	0.093741476	1.8245637

Table C.4: Pump oil (10 cp) and its shear viscosity at different flow rates

Pump Oil	TRUE	Reynolds
10 cp	Shear Viscosity	Number
Q	μ_T	N_{RE}
m^3 / sec	Pa-s	
1.07411E-05	0.017471513	391.57981
6.44469E-06	0.016962328	242.00068
3.22234E-06	0.016295055	125.95524
1.26745E-06	0.015438051	52.292612
6.71321E-07	0.016671148	25.648697
2.68529E-07	0.015809742	10.818474

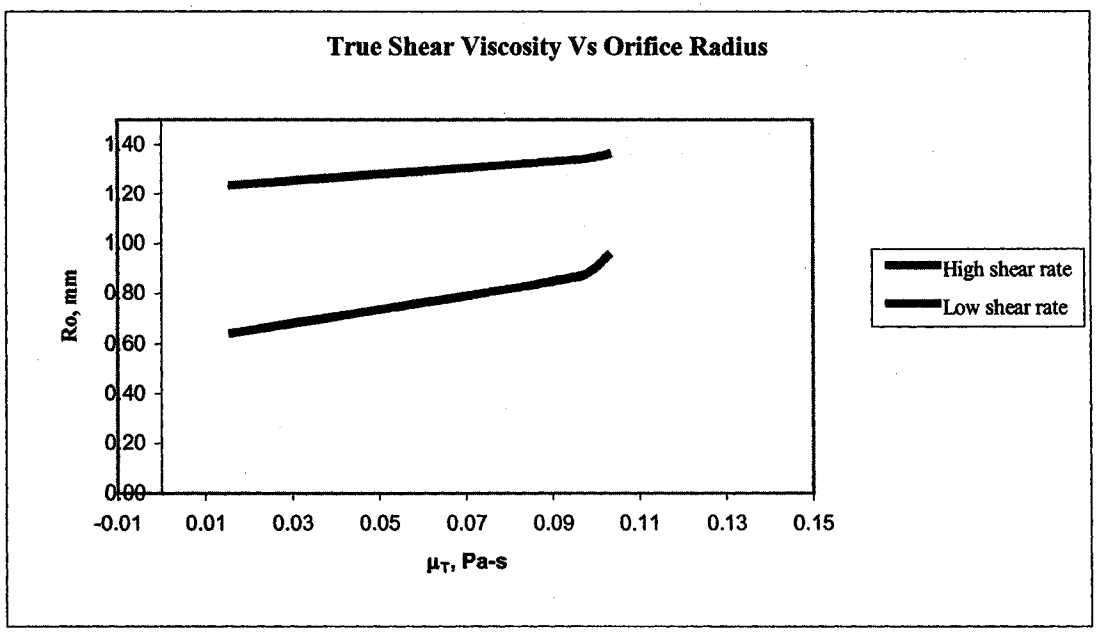

Figure C.1: True shear viscosity versus orifice radius for high and low shear rates

APPENDIX D: ENTRANCE PRESSURE DATA PLOTS AT DIFFERENT PISTON VELOCITY THROUGH EXTENSIONAL VISCOMETER FOR XANTHAN GUM SOLUTIONS

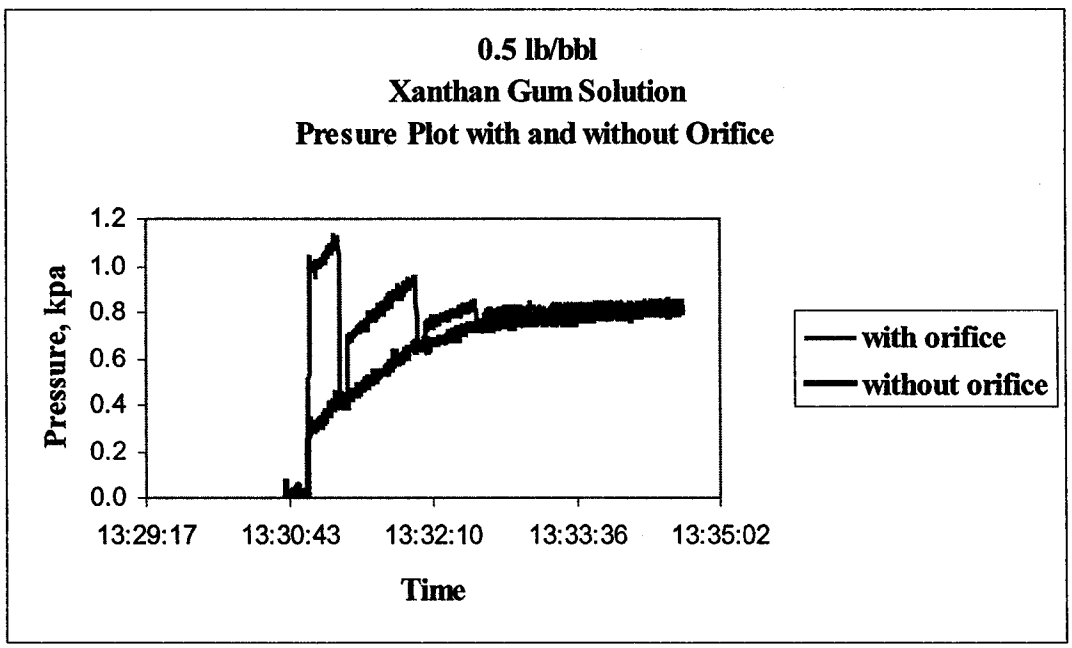

Figure D.1: 0.5 lb/bbl Xanthan Gum solution entrance pressure plot with and without orifice presence

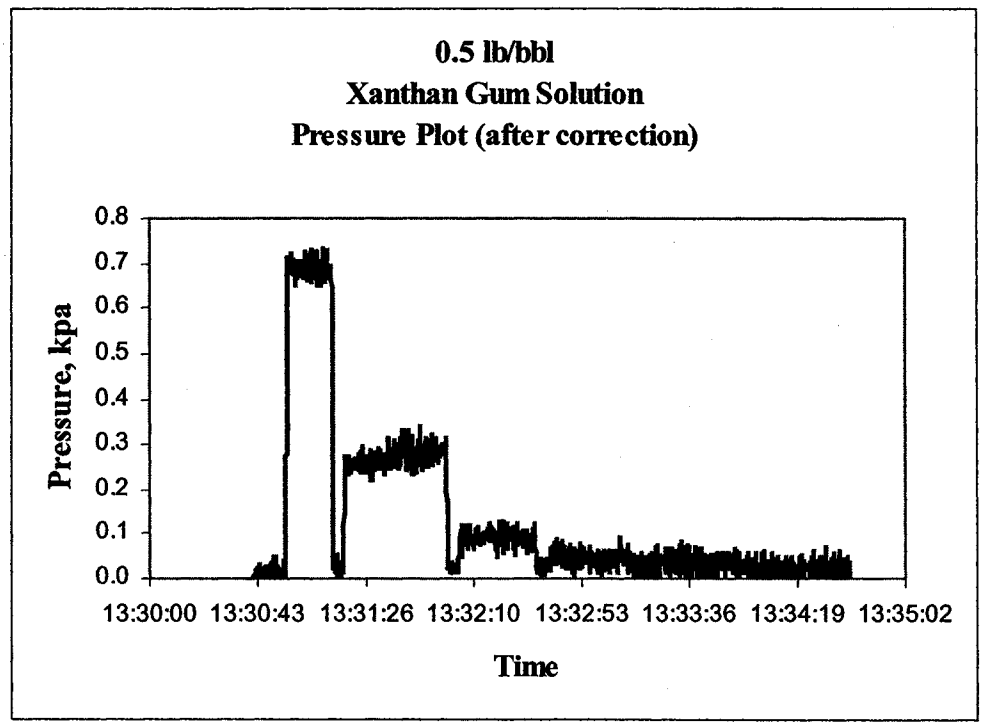

Figure D.2: 0.5 lb/bbl Xanthan Gum solution entrance pressure plot after the hydrostatic column pressure correction

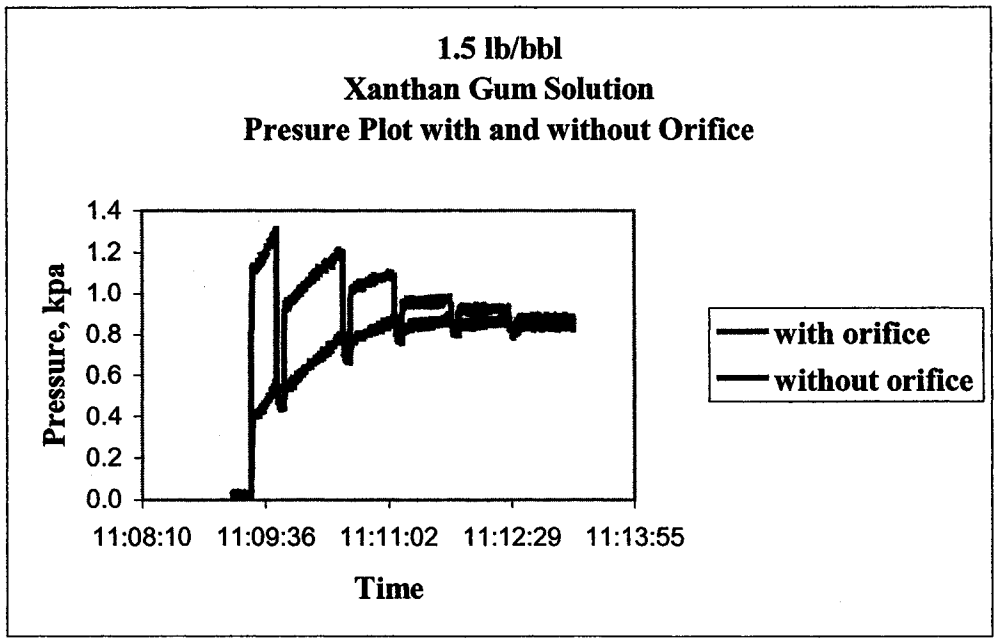

Figure D.3: 1.5 lb/bbl Xanthan Gum solution entrance pressure plot with and without orifice presence

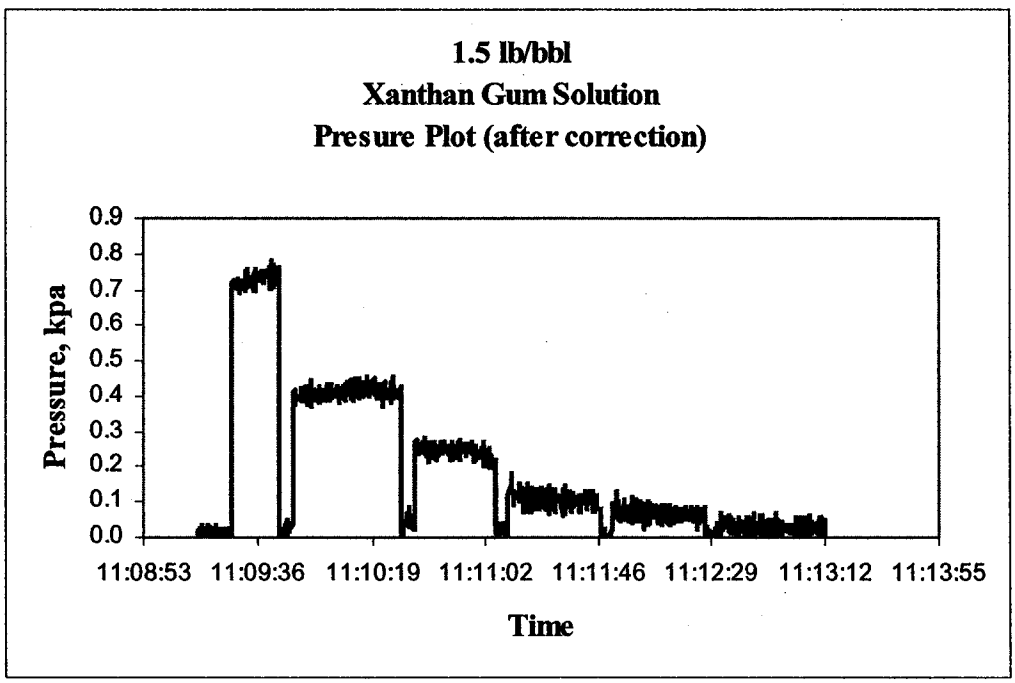

Figure D.4: 1.5 lb/bbl Xanthan Gum solution entrance pressure plot after the hydrostatic column pressure correction

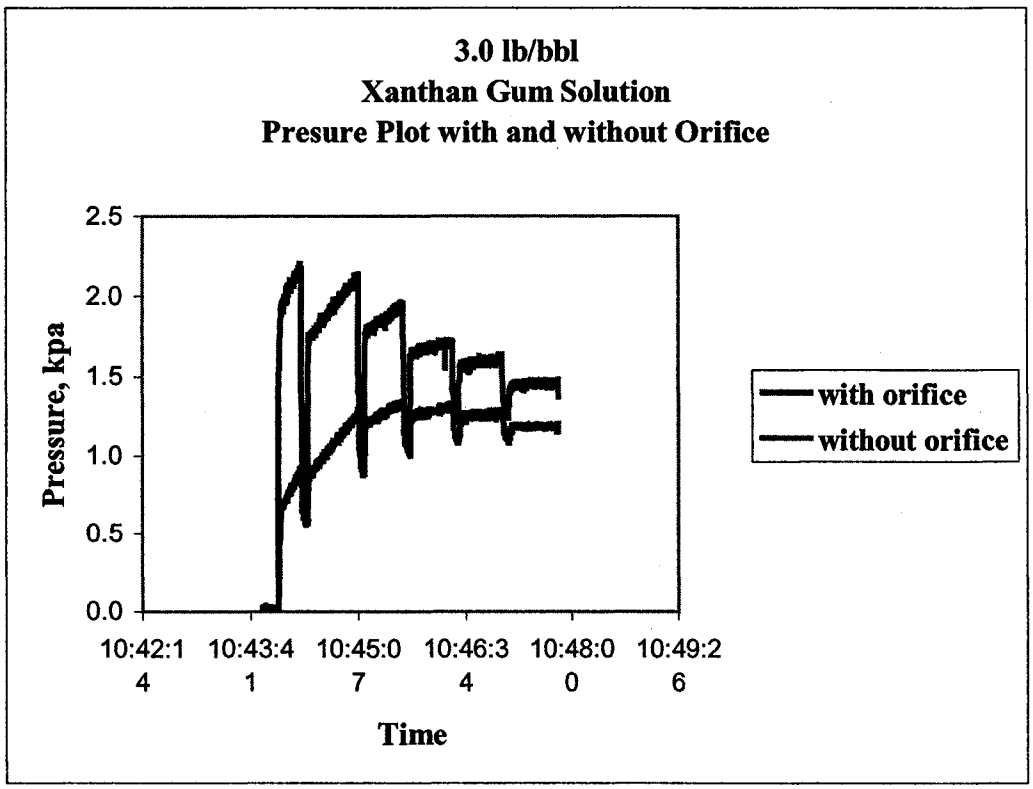

Figure D.5: 3.0 lb/bbl Xanthan Gum solution entrance pressure plot with and without orifice presence

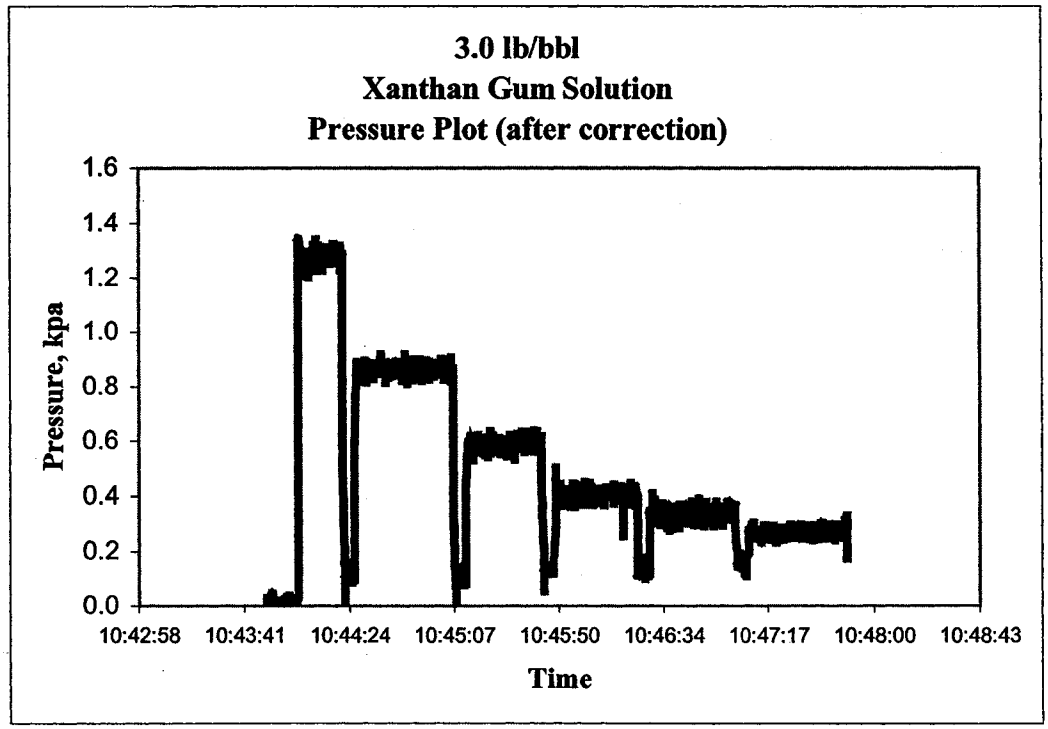

Figure D.6: 3.0 lb/bbl Xanthan Gum solution entrance pressure plot after the hydrostatic column pressure correction

APPENDIX E: REPEATABILITY OF ENTRANCE PRESSURE MEASURED THROUGH EXTENSIONAL VISCOMETER FOR XANTHAN GUM SOLUTIONS

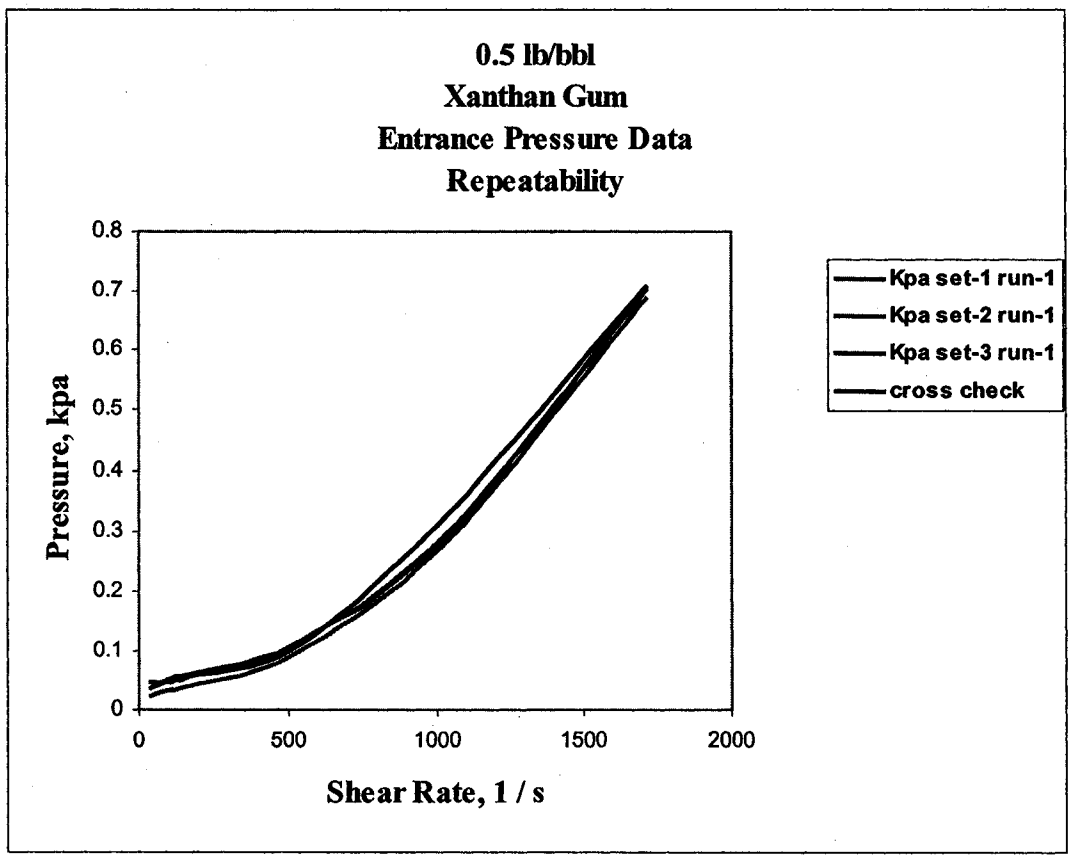

Figure E.1: Repeatability of 0.5 lb/bbl Xanthan Gum solutions entrance pressure plot

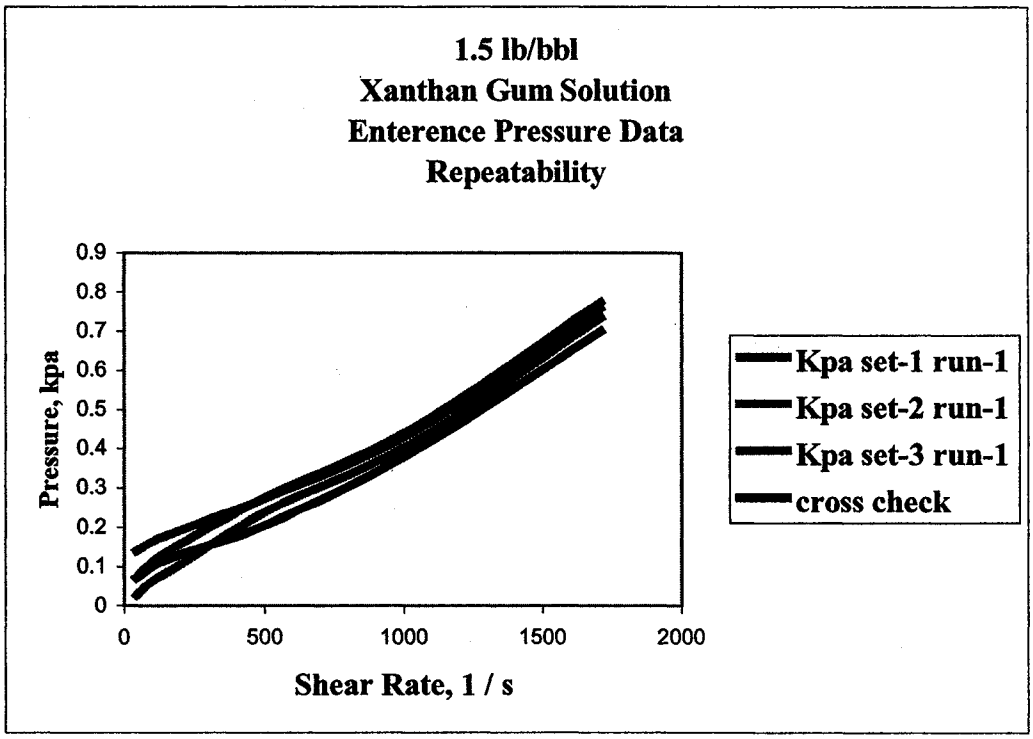

Figure E.2: Repeatability of 1.5 lb/bbl Xanthan Gum solutions entrance pressure plot

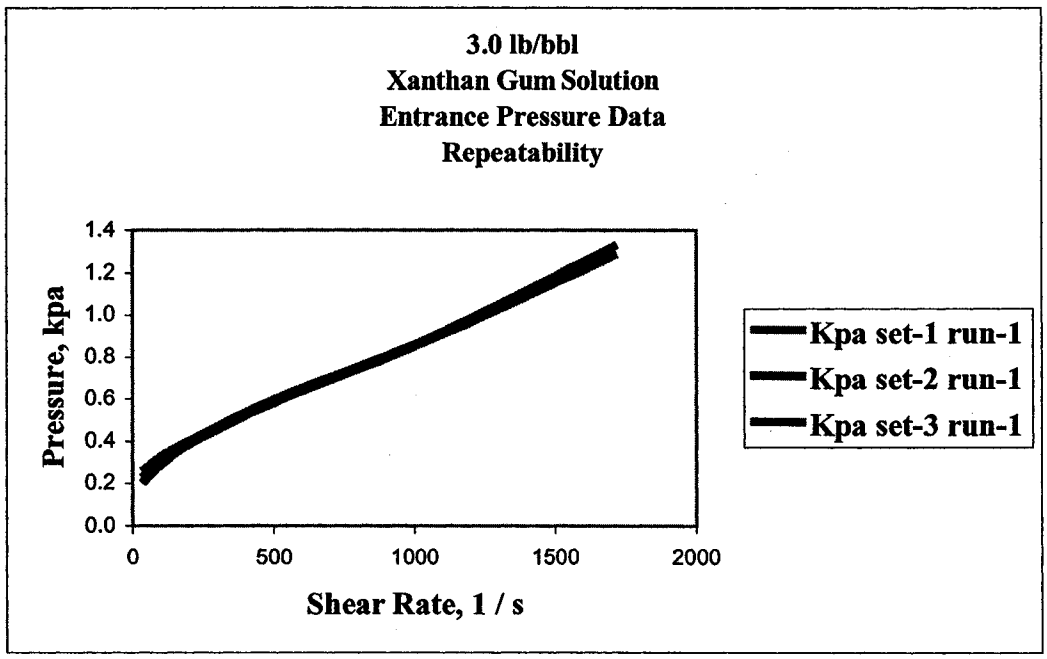

Figure E.3: Repeatability of 3.0 lb/bbl Xanthan Gum solutions entrance pressure plot

APPENDIX F: ENTRANCE PRESSURE DATA PLOTS AT DIFFERENT PISTON VELOCITY THROUGH EXTENSIONAL VISCOMETER FOR PHPA SOLUTIONS

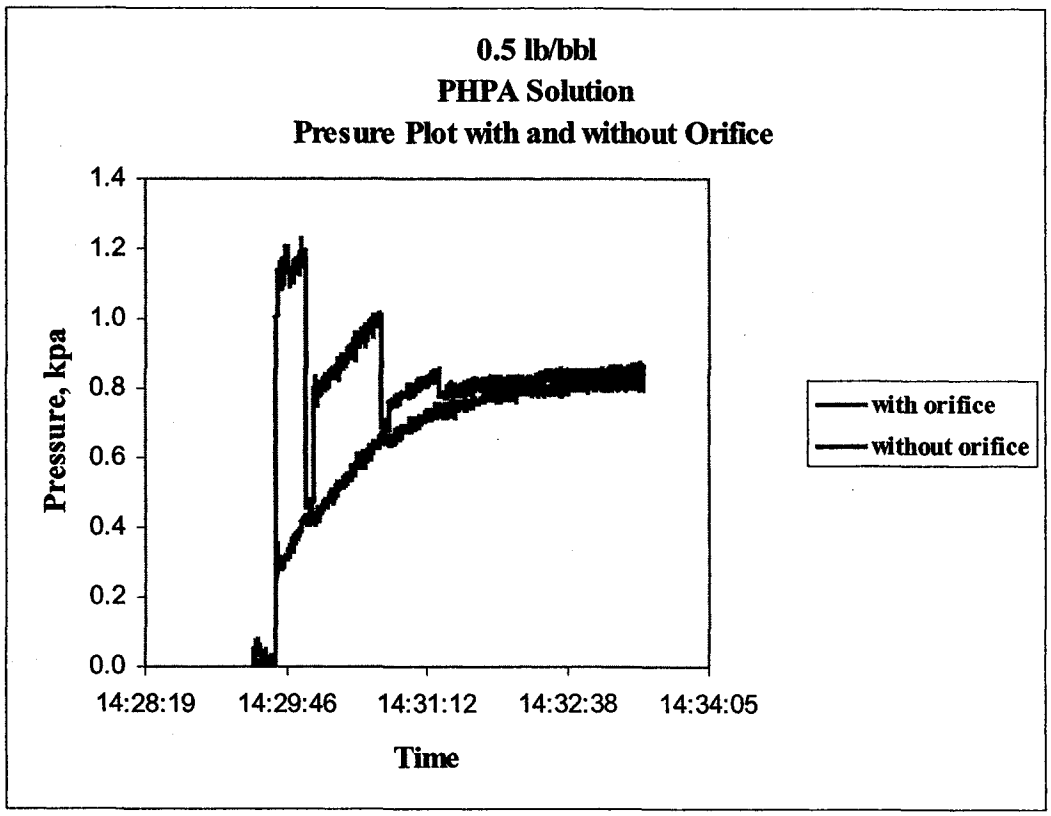

Figure F.1: 0.5 lb/bbl PHPA solution entrance pressure plot with and without orifice presence

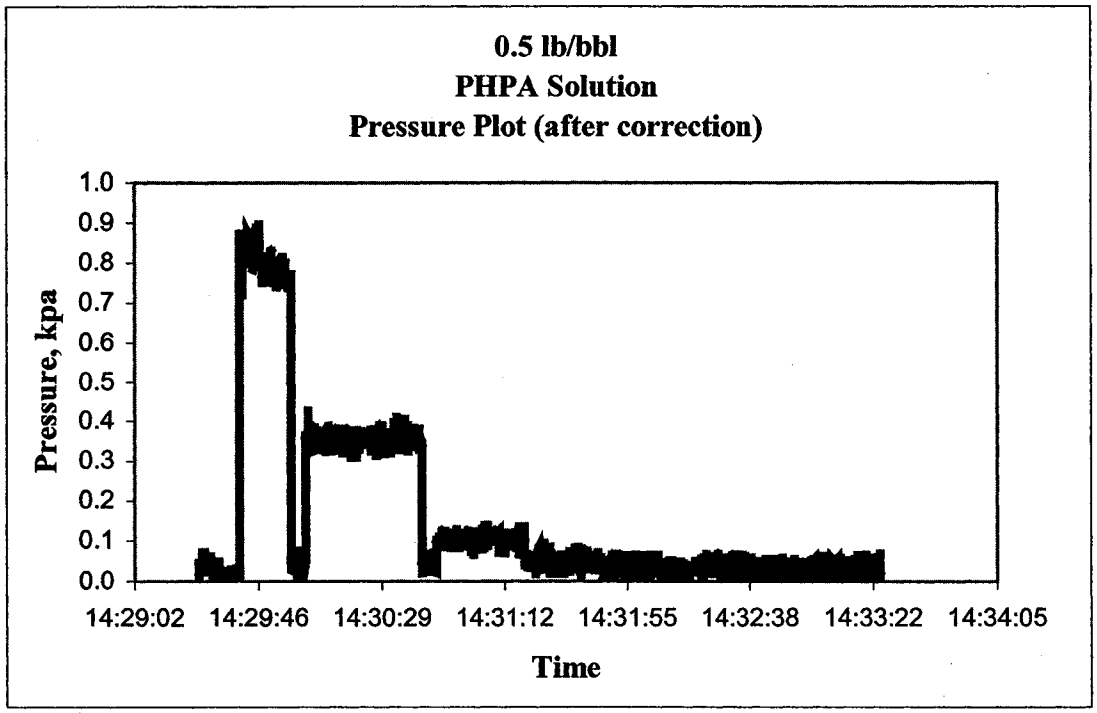

Figure F.2: 0.5 lb/bbl PHPA solution entrance pressure plot after the hydrostatic column pressure correction

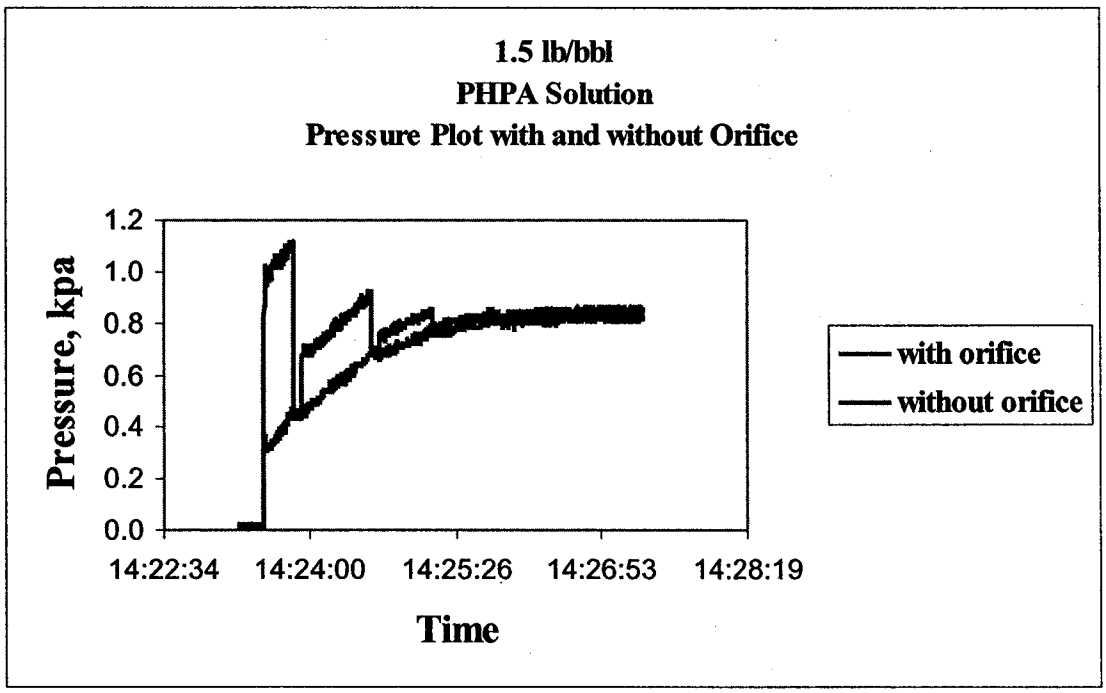

Figure F.3: 1.5 lb/bbl PHPA solution entrance pressure plot with and without orifice presence

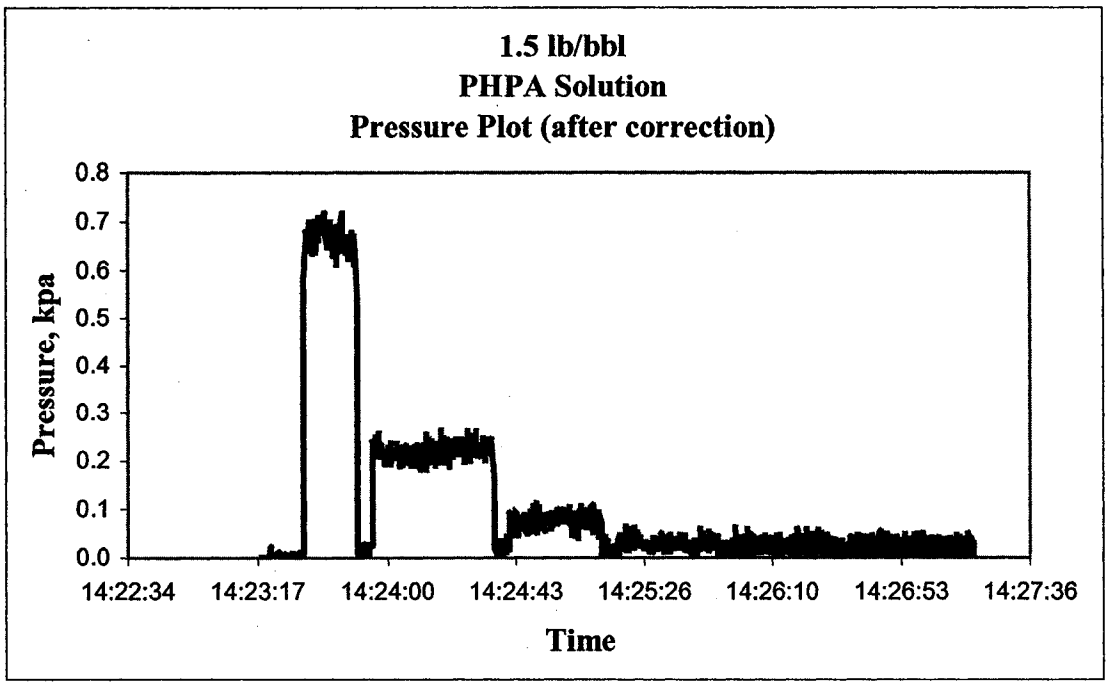

Figure F.4: 1.5 lb/bbl PHPA solution entrance pressure plot after the hydrostatic column pressure correction

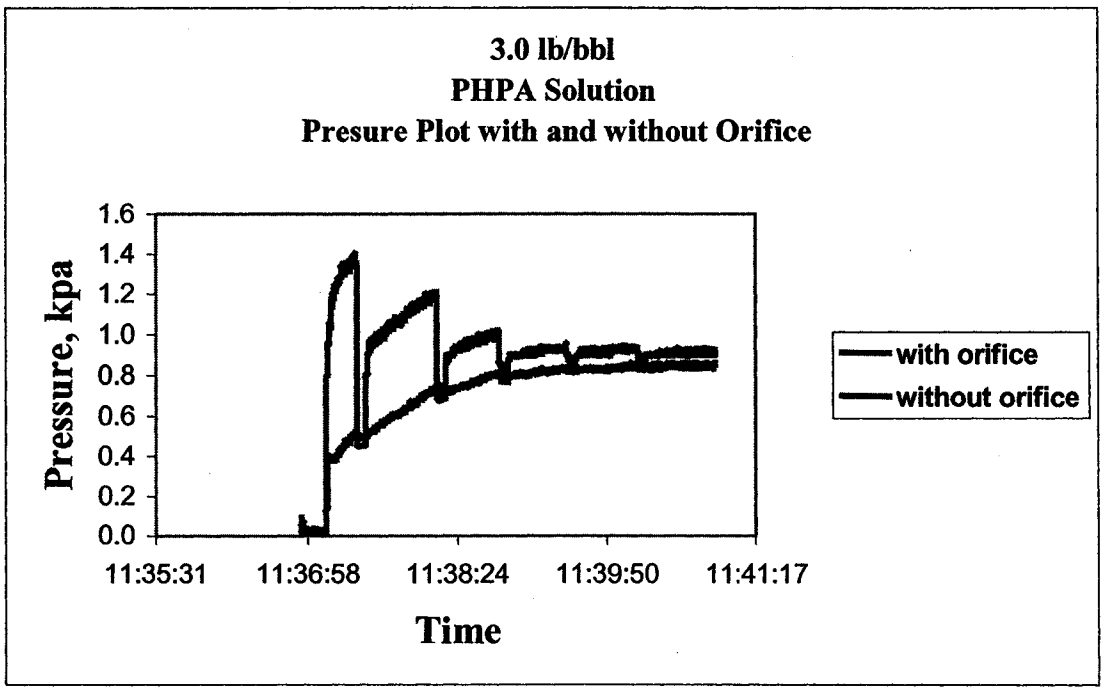

Figure F.5: 3.0 lb/bbl PHPA solution entrance pressure plot with and without orifice presence

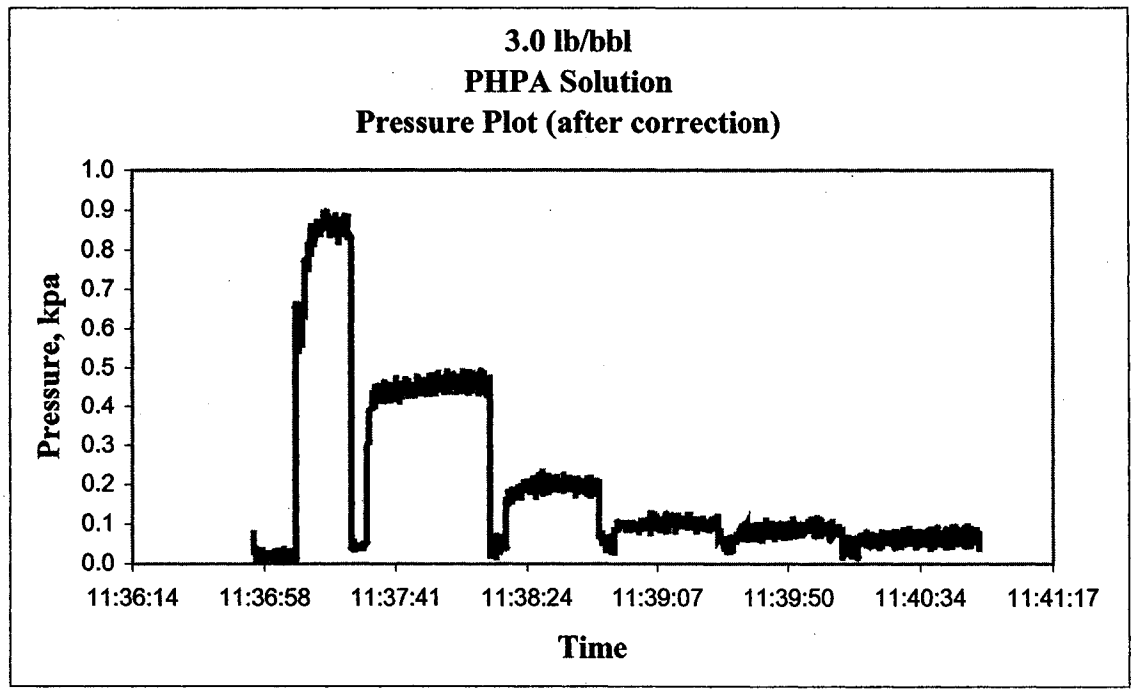

Figure F.6: 3.0 lb/bbl PHPA solution entrance pressure plot after the hydrostatic column pressure correction

APPENDIX G: REPEATABILITY OF ENTRANCE PRESSURE MEASURED THROUGH EXTENSIONAL VISCOMETER FOR PHPA SOLUTIONS

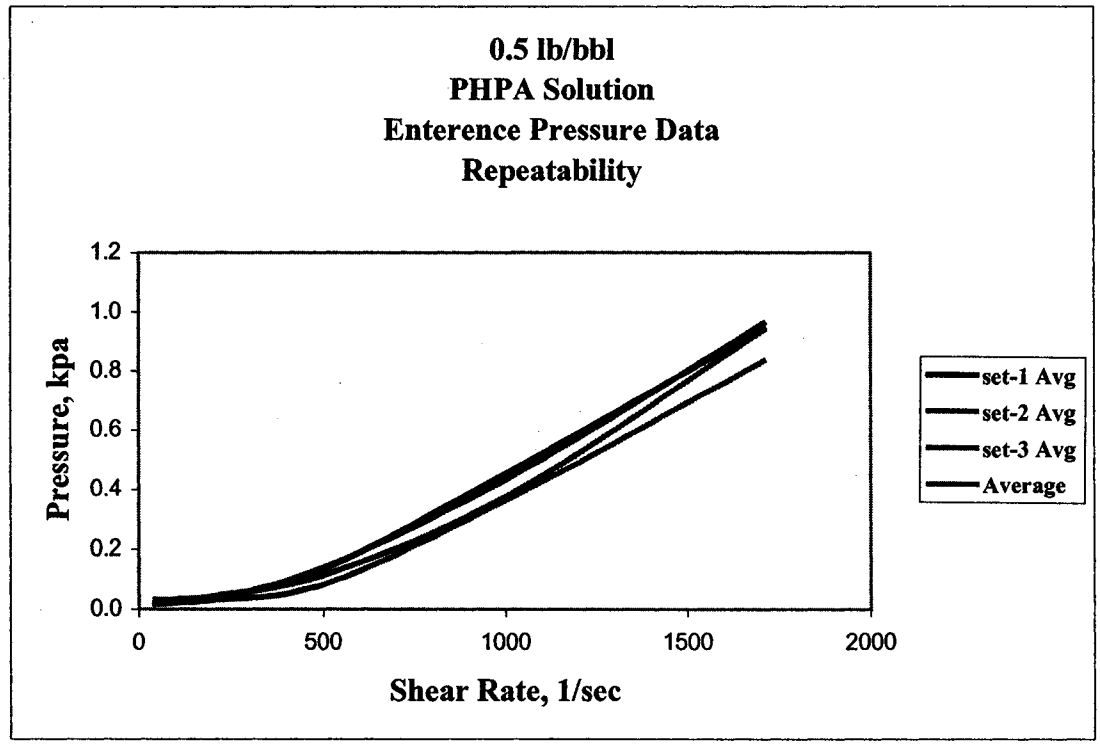

Figure G.1: Repeatability of 0.5 lb/bbl PHPA solutions entrance pressure

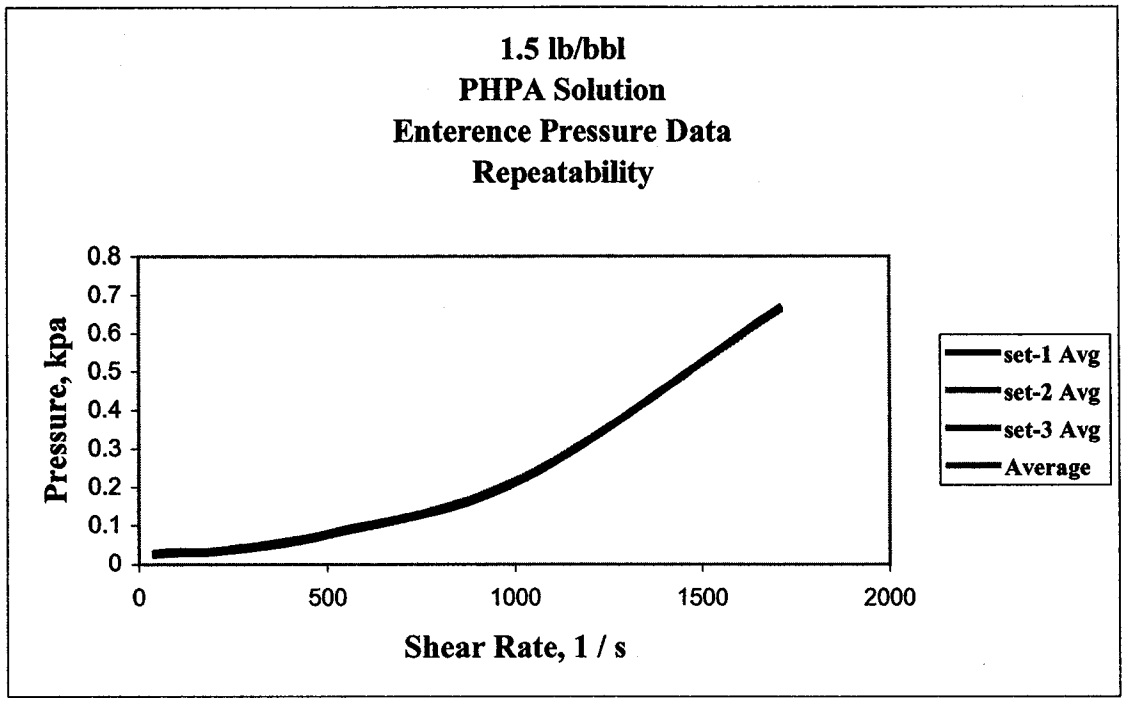

Figure G.2: Repeatability of 1.5 lb/bbl PHPA solutions entrance pressure

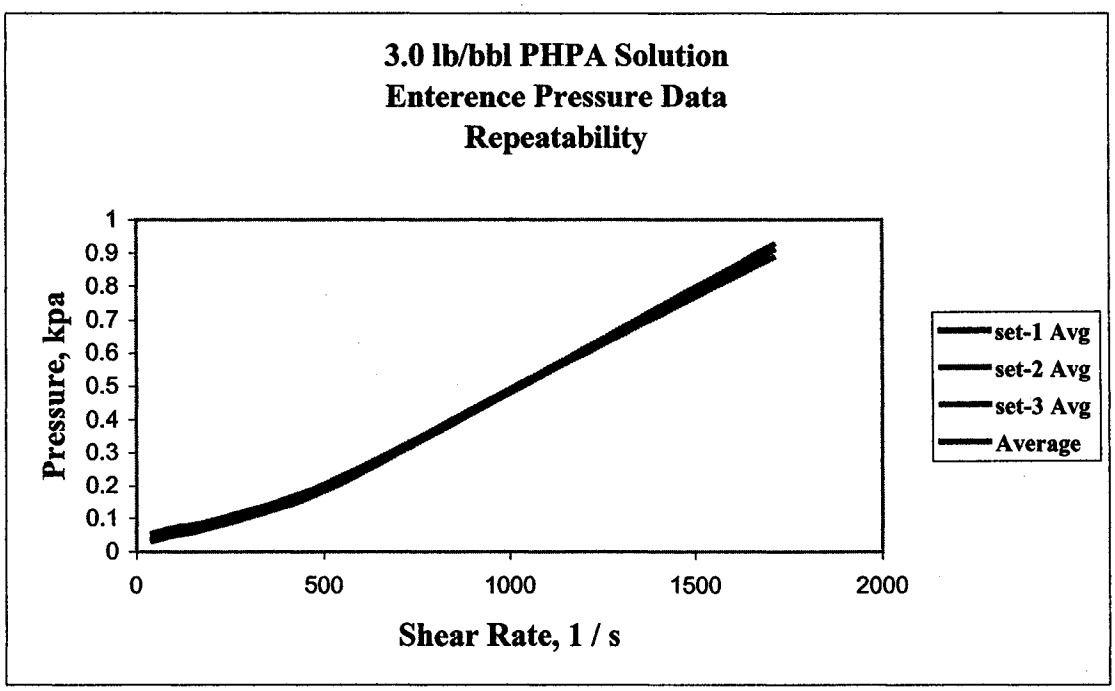

Figure G.3: Repeatability of 3.0 lb/bbl PHPA solutions entrance pressure

APPENDIX H: EXTENSIONAL VISCOSITY DATA OF XANTHAN GUM SOLUTIONS

Table H.1: Extensional viscosity data for 0.5 lb/bbl Xanthan Gum solution

Shear Rate	Elongationa Pressure	Coefficient	Elongation Viscosity	True Shear Rate	APPARENT Shear Visc	TRUE Shear Visc	Reynolds Number	Flow Rate	Trouton Ratio
γ_A	P_e	I	μ_E	γT	μ_N	μ_T	N_{RE}	Q	
1/s	pa	pa.s	pa-s	1/s	Pa-s	Pa-s		m^3 / s	
7349	688.8114	0.003235	0.282	8627.1338	0.00327954	0.0027938	3143.52544	1.4E-05	100.919
4410	276.28055	0.002937	0.208	5176.2803	0.00404404	0.003445	1631.52824	8.8E-06	60.2672
2205	99.538119	0.003205	0.137	2588.1401	0.005374	0.004578	613.878037	4.4E-06	29.9421
867	53.856835	2.959884	0.102	1018.0018	0.00788002	0.0067128	209.325897	2.2E-06	15.1915
459	43.916854	3.056521	0.152	539.19586	0.01022688	0.0087121	40.322454	5.5E-07	17.4512
184	30.364612	2.970560	0.270	215.67835	0.01489286	0.0126869	11.075720	2.2E-07	21.3135
	Average =	0.003125	1 = constant						
	Average =	2.995655	1 = constant						

Table H.2: Extensional viscosity data for 1.5 lb/bbl Xanthan Gum solution

Shear Rate	Elongational Pressure	Coefficient	Elongation Viscosity	True Shear Rate	APPARENT Shear Visc	TRUE Shear Visc	Reynolds Number	Flow Rate	Trouton Ratio
γ_A	P_e	I	μ_E	γT	μ_N	μ_T	N_{RE}	Q	
1/s	pa	pa.s	pa-s	1/s	Pa-s	Pa-s		m^3 / s	
6677	728.75627	0.672728	0.273	11387.846	0.00317029	0.0018587	4725.00737	1.4E-05	146.613
4006	410.84739	0.595733	0.289	6832.7079	0.00462287	0.0027103	2073.81183	8.8E-06	106.682
2003	248.46259	0.664880	0.313	3416.3539	0.00771245	0.0045217	621.525287	4.4E-06	69.2998
788	138.2403	6.310554	0.310	1343.7659	0.01536105	0.0090059	156.027140	2.2E-06	34.3993
417	103.62997	6.219236	0.445	711.7404	0.02455957	0.0143989	24.397217	5.5E-07	30.8981
167	70.757348	6.299939	0.750	284.69616	0.04831251	0.0283249	4.960910	2.2E-07	26.4679
	Average =	0.644447	1 = constant						
	Average =	6.276576	1 = constant						

Table H.3: Extensional viscosity data for 3.0 lb/bbl Xanthan Gum solution

Shear	Elongationa	Coefficient	Elongation	True Shear	APPARENT	TRUE	Reynolds	Flow	Trouton
Rate	Pressure		Viscosity	Rate	Shear Visc	Shear Visc	Number	Rate	Ratio
γ_A	P_e	I	μ_E	γT	μ_N	μ_T	N_{RE}	Q	
1/s	pa	pa.s	pa-s	1/s	Pa-s	Pa-s		m^3/s	
5684	1237.9438	5.455772	0.485	12295.574	0.00565981	0.0026164	3356.67687	1.4E-05	185.319
3410	818.01108	5.076627	0.574	7377.3443	0.00861798	0.0039839	1410.86612	8.8E-06	144.047
1705	548.68598	5.418264	0.721	3688.6722	0.01524696	0.0070482	398.729179	4.4E-06	102.338
671	358.88023	24.779800	0.808	1450.8777	0.03286517	0.0151927	92.490174	2.2E-06	53.153
355	282.59191	24.118742	1.233	768.47337	0.05545147	0.0256337	13.704348	5.5E-07	48.1178
142	213.2326	24.703672	2.272	307.38935	0.11788471	0.0544948	2.578540	2.2E-07	41.6858
	Average =	5.316888	1 = constant						
	Average =	24.534072	1 = constant						

APPENDIX I: EXTENSIONAL VISCOSITY DATA OF PHPA SOLUTIONS

Table I.1: Extensional viscosity data for 0.5 lb/bbl PHPA solution

Shear Rate	Elongational Pressure	Coefficient	Elongation Viscosity	True Shear Rate	APPARENT Shear Visc	TRUE Shear Visc	Reynolds Number	Flow Rate	Trouton Ratio
γ_A	P_e	I	μ_E	γT	μ_N	μ_T	N_{RE}	Q	
1/s	pa	pa.s	pa-s	1/s	Pa-s	Pa-s		m^3/s	
7517	879.25582	0.000811	0.382	7749.9098	0.00567453	0.0055038	1595.68912	1.4E-05	69.495
4510	381.2687	0.000888	0.253	4649.9459	0.00600375	0.0058231	965.24188	8.8E-06	43.3809
2255	100.08386	0.000818	0.144	2324.973	0.00648121	0.0062862	447.066829	4.4E-06	22.8875
887	35.895806	3.156316	0.048	914.48936	0.00718446	0.0069683	201.652699	2.2E-06	6.83479
470	27.469876	2.798437	0.078	484.36937	0.00770664	0.0074747	46.997356	5.5E-07	10.3833
188	24.718505	3.113465	0.157	193.74775	0.00852703	0.0082704	16.990292	2.2E-07	18.9749
	Average =	0.000839	1 = constant						
	Average =	3.022740	1 = constant						

Table I.2: Extensional viscosity data for 1.5 lb/bbl PHPA solution

Shear Rate	Elongational Pressure	Coefficient	Elongation Viscosity	True Shear Rate	APPARENT Shear Visc	TRUE Shear Visc	Reynolds Number	Flow Rate	Trouton Ratio
γ_A	P_e	I	μ_E	γT	μ_N	μ_T	N_{RE}	Q	
1/s	pa	pa.s	pa-s	1/s	Pa-s	Pa-s		m^3/s	
7314	647.849	0.000940	0.261	7575.9531	0.01312793	0.0126732	692.98117	1.4E-05	20.5556
4388	215.8707	0.000769	0.177	4545.5719	0.01399711	0.0135123	415.96749	8.8E-06	13.0896
2194	76.535089	0.000922	0.105	2272.7859	0.01526924	0.0147404	190.655846	4.4E-06	7.09525
863	30.941205	3.821778	0.031	893.96247	0.01716623	0.0165717	84.793509	2.2E-06	1.86642
457	29.678308	3.911534	0.055	473.49707	0.01859145	0.0179475	19.573314	5.5E-07	3.04925
183	26.476954	3.831826	0.125	189.39883	0.02085714	0.0201348	6.978834	2.2E-07	6.18816
	Average =	0.000877	1 = constant						
	Average =	3.855046	1 = constant						

Table I.3: Extensional viscosity data for 3.0 lb/bbl PHPA solution

Shear Rate	Elongational Pressure	Coefficient	Elongation Viscosity	True Shear Rate	APPARENT Shear Visc	TRUE Shear Visc	Reynolds Number	Flow Rate	Trouton Ratio
γ_A	P_e	I	μ_E	γT	μ_N	μ_T	N_{RE}	Q	
1/s	pa	pa.s	pa-s	1/s	Pa-s	Pa-s		m^3/s	
6645	876.338427	0.041647	0.402	7494.788	0.01634978	0.0144961	605.83857	1.4E-05	27.7283
3987	477.621143	0.044159	0.344	4496.8728	0.01943505	0.0172316	326.18447	8.8E-06	19.9836
1994	183.613719	0.041881	0.279	2248.4364	0.02457277	0.0217868	128.992580	4.4E-06	12.8131
784	73.9662272	3.460245	0.165	884.38499	0.03369668	0.0298763	47.032902	2.2E-06	5.51804
415	55.3446974	3.391309	0.238	468.42425	0.04178171	0.0370447	9.482934	5.5E-07	6.41461
166	38.179646	3.452458	0.403	187.3697	0.05697038	0.0505114	2.781889	2.2E-07	7.9697
	Average =	0.042562	1 = constant						
	Average =	3.434671	1 = constant						

APPENDIX J: PRESSURE DATA PROFILE OF XANTHAN GUM CORE FLOW TESTS

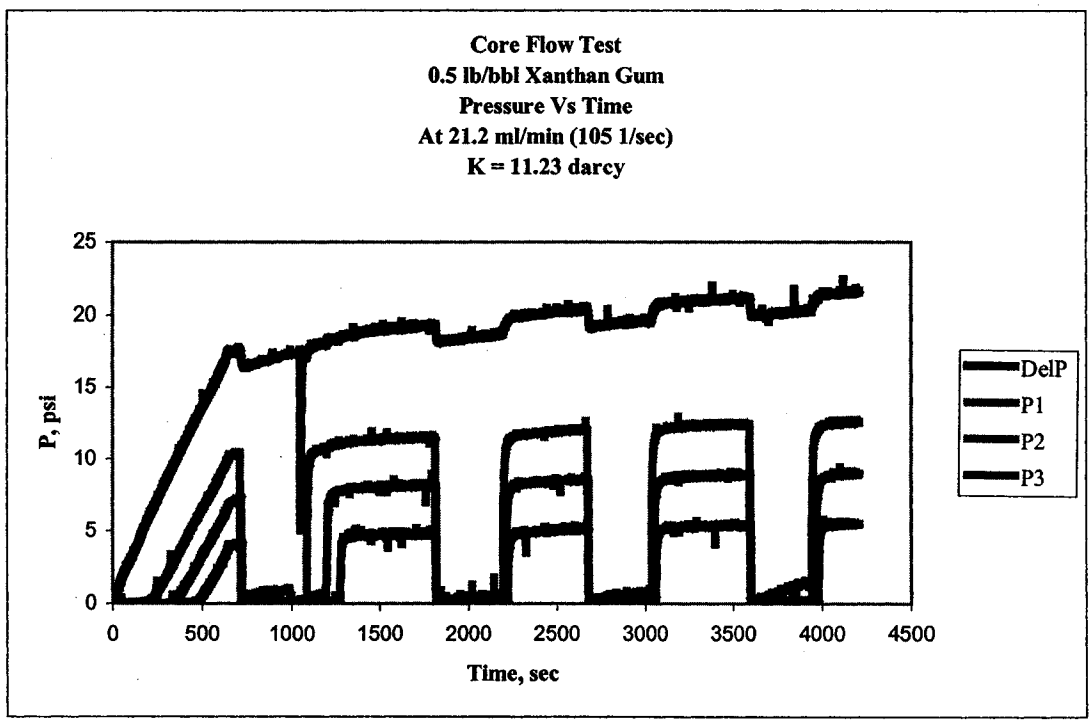

Figure J.1: 0.5 lb/bbl Xanthan Gum solution pressure profile during core flow test

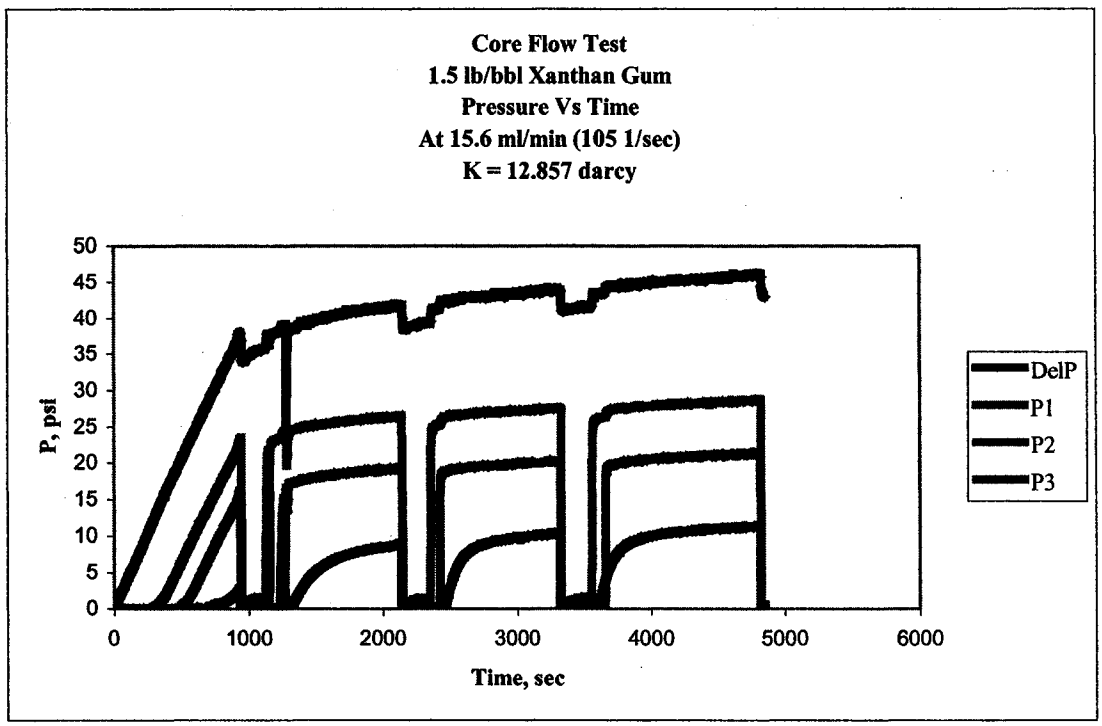

Figure J.2: 1.5 lb/bbl Xanthan Gum solution pressure profile during core flow test

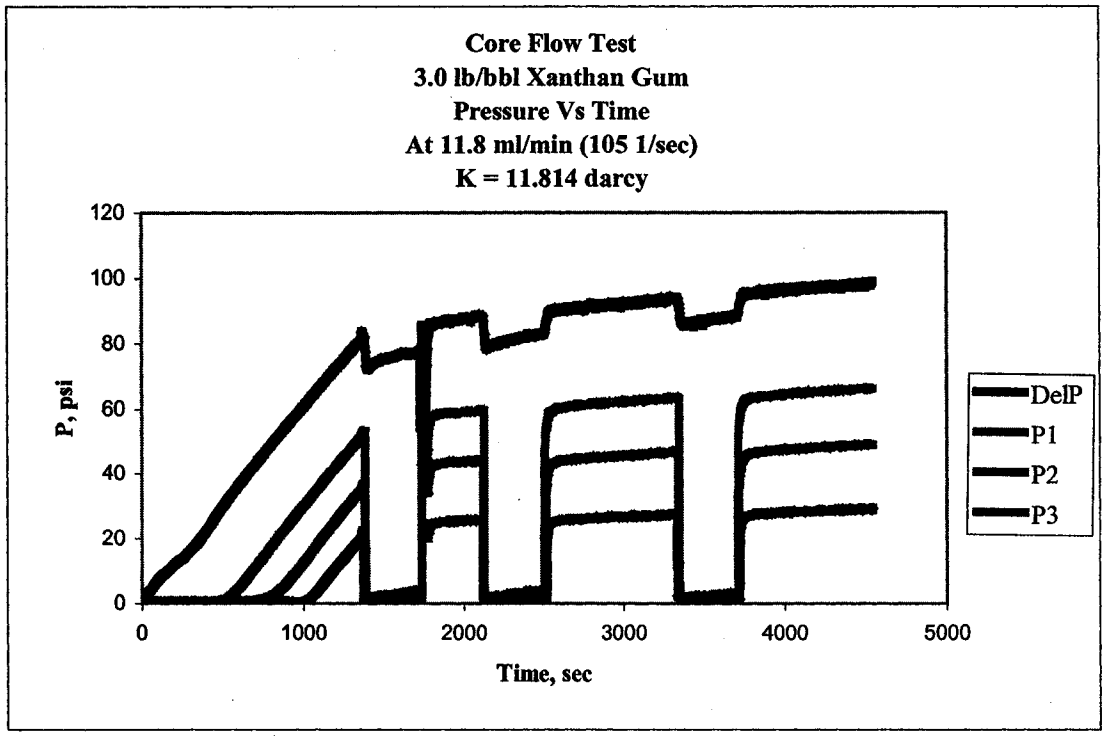

Figure J.3: 3.0 lb/bbl Xanthan Gum solution pressure profile during core flow test

APPENDIX K: PRESSURE DATA PROFILE OF PHPA CORE FLOW TESTS

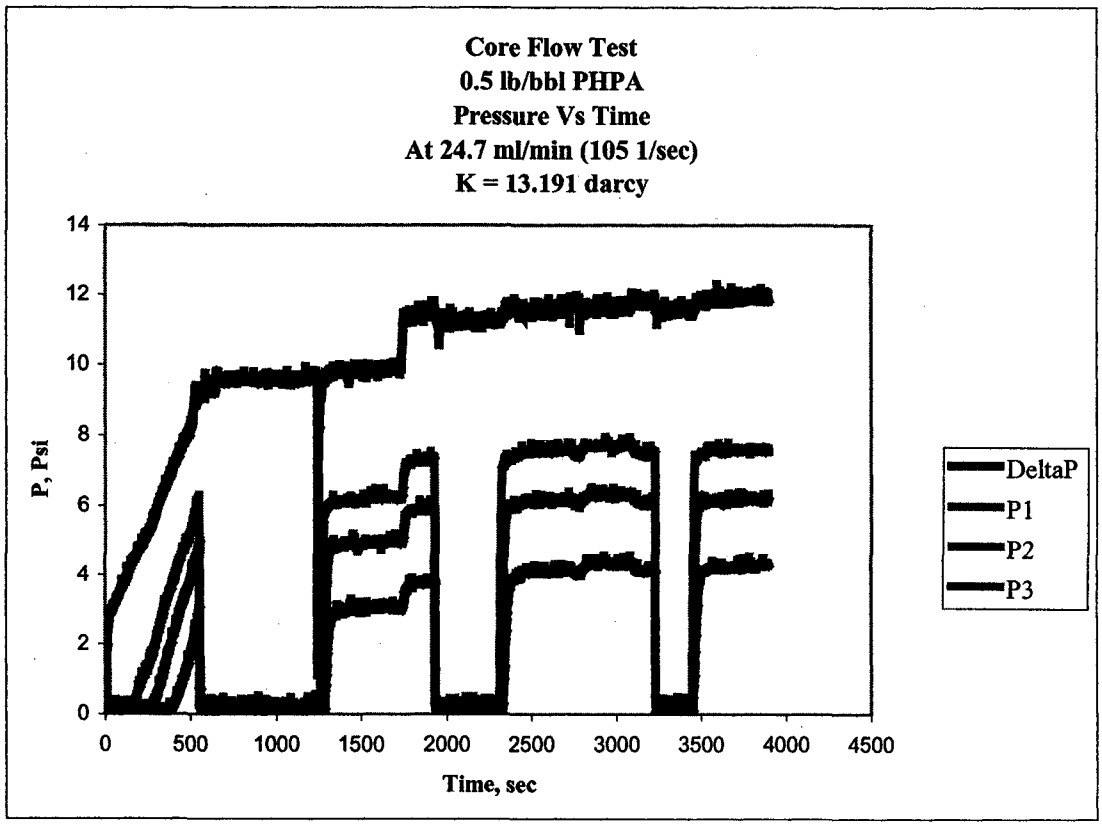

Figure K.1: 0.5 lb/bbl PHPA solution pressure profile during core flow test

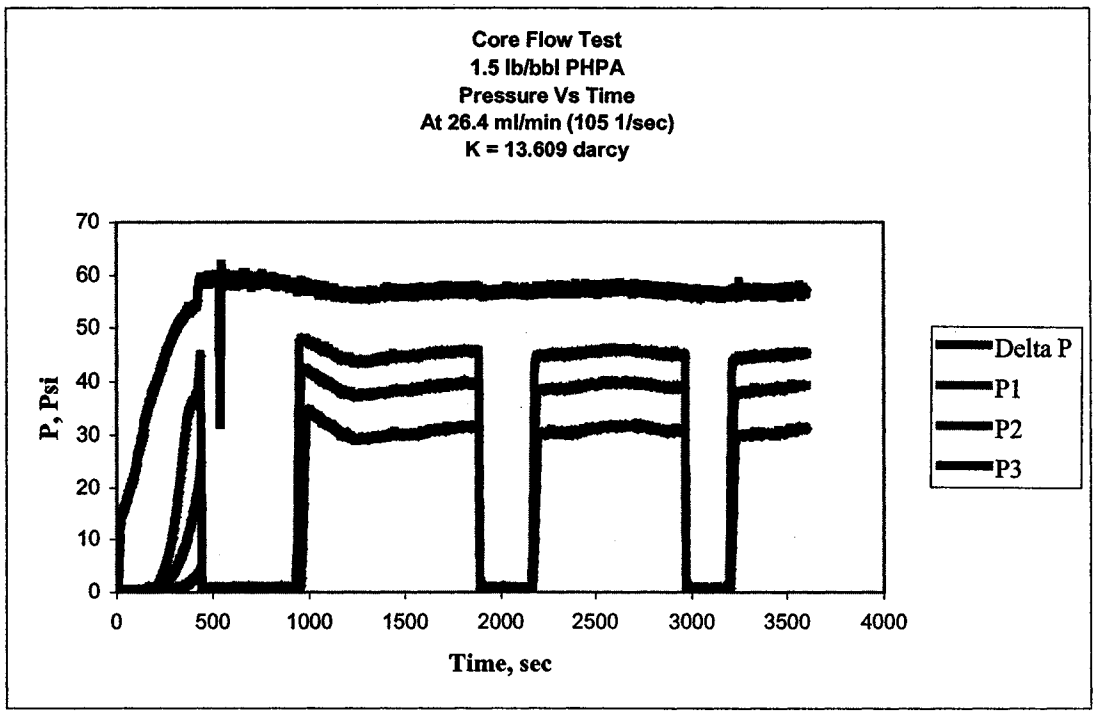

Figure K.2: 1.5 lb/bbl PHPA solution pressure profile during core flow test

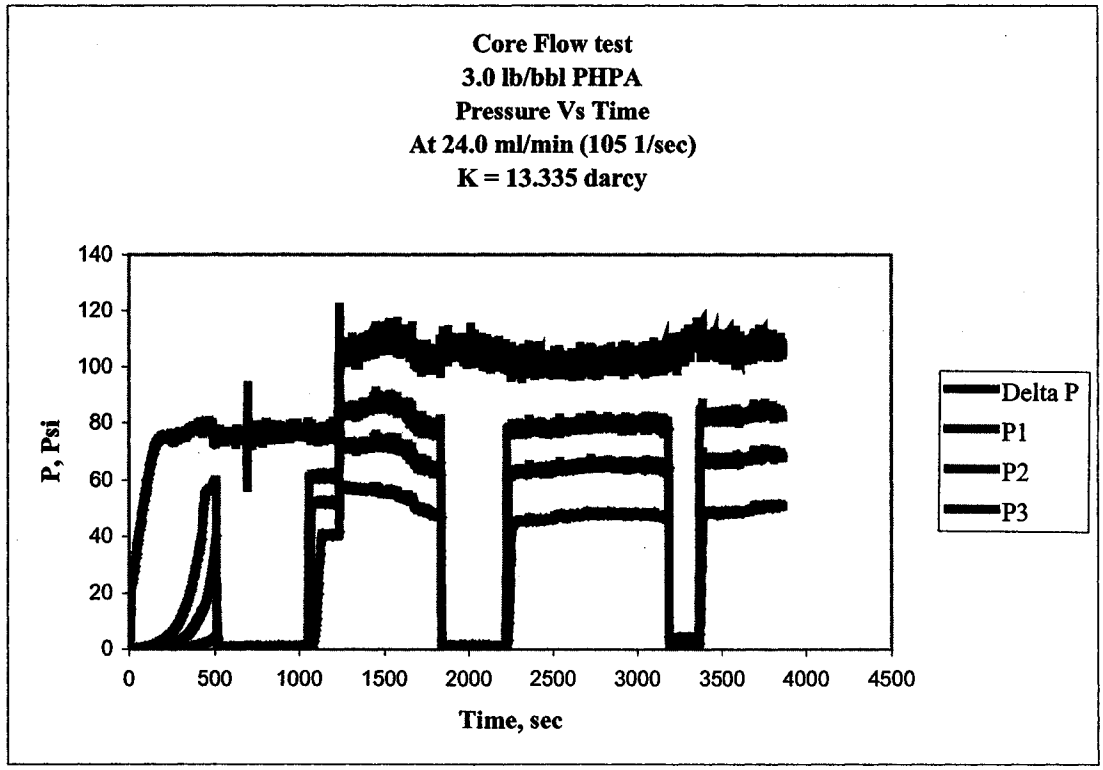

Figure K.3: 3.0 lb/bbl PHPA solution pressure profile during core flow test

APPENDIX L: FORMATION DAMAGE AFTER XANTHAN GUM CORE FLOW TESTS

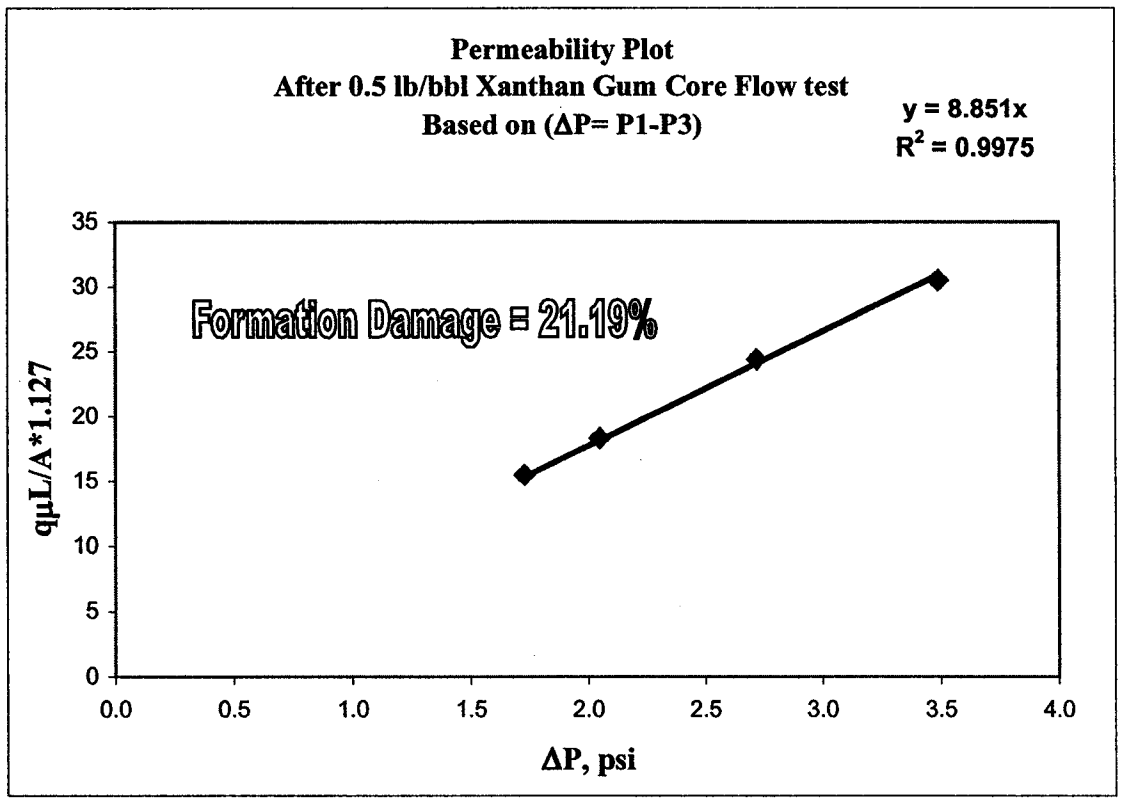

Figure L.1: Permeability plot to calculate the formation damage after 0.5 lb/bbl Xanthan Gum solution core flow test

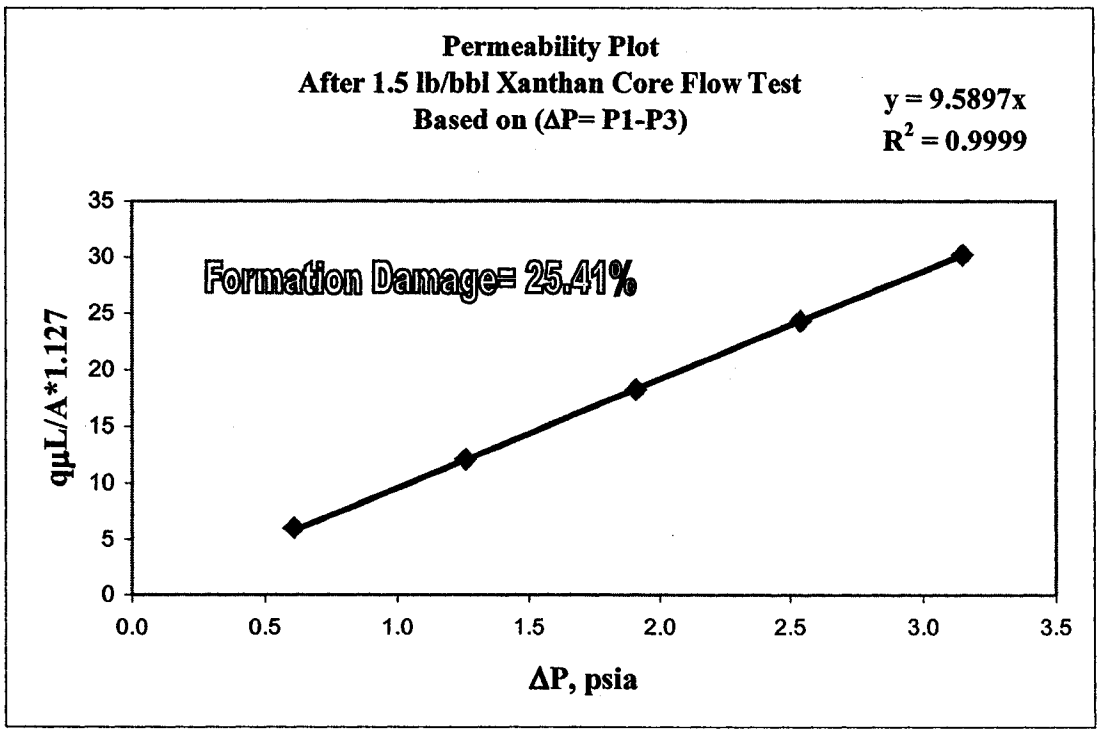

Figure L.2: Permeability plot to calculate the formation damage after 1.5 lb/bbl Xanthan Gum solution core flow test

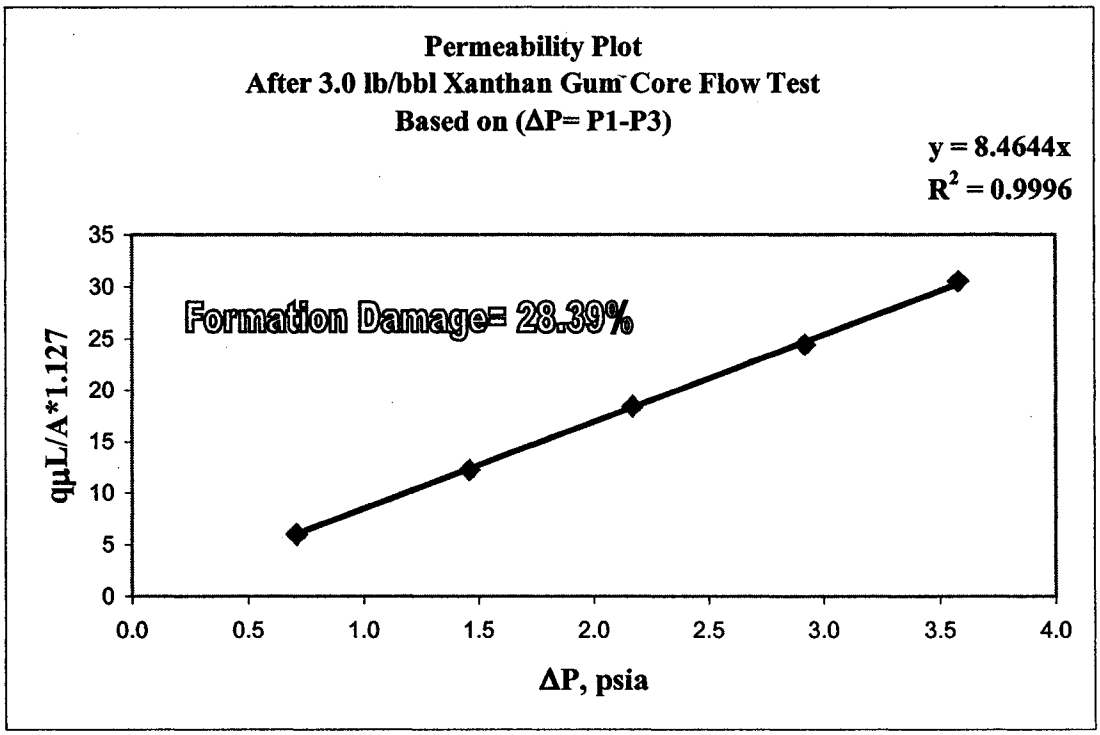

Figure L.3: Permeability plot to calculate the formation damage after 3.0 lb/bbl Xanthan Gum solution core flow test

APPENDIX M: FORMATION DAMAGE AFTER PHPA CORE FLOW TESTS

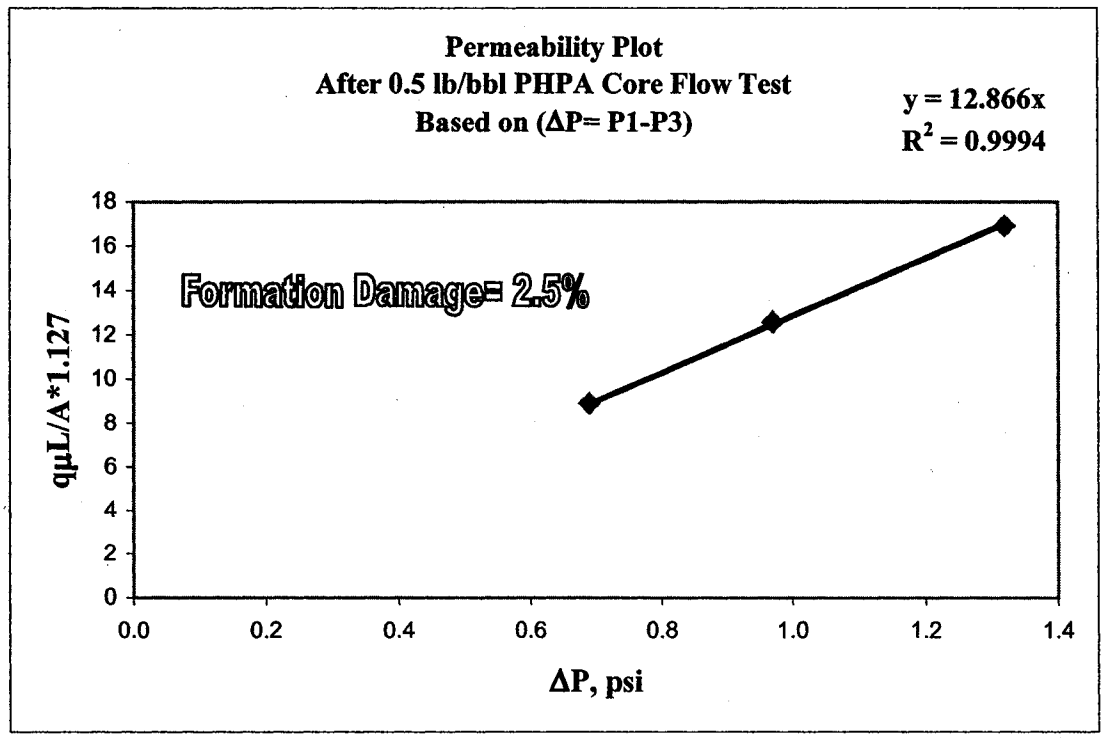

Figure M.1: Permeability plot to calculate the formation damage after 0.5 lb/bbl PHPA solution core flow test

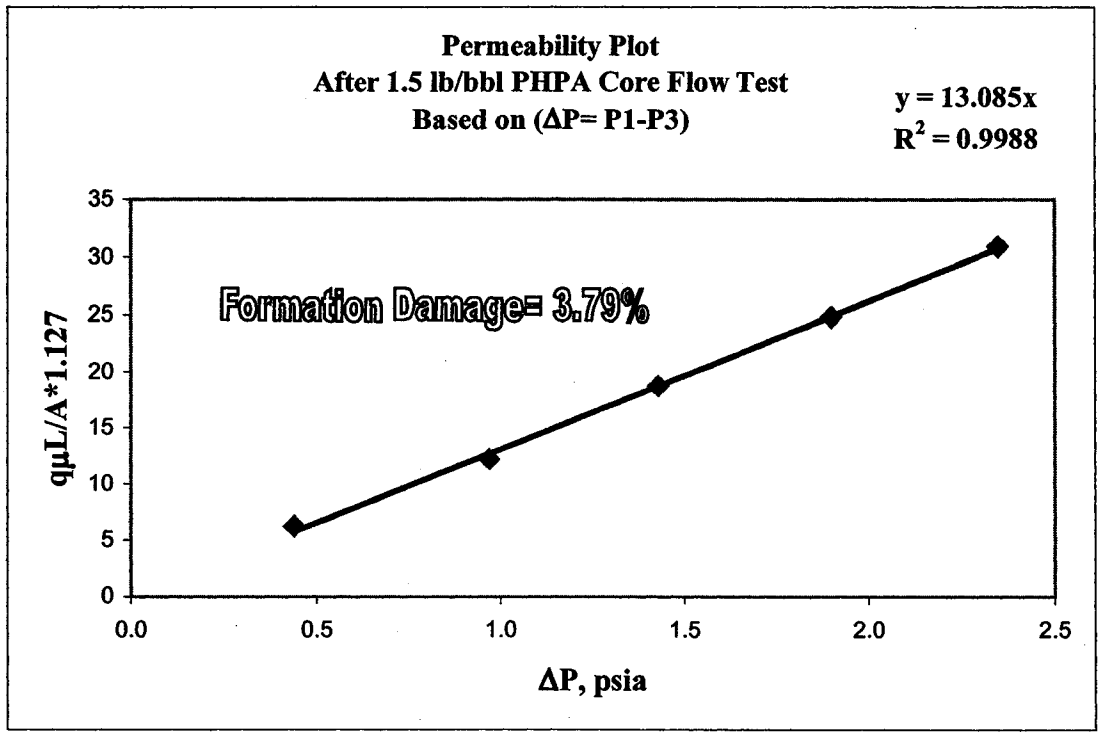

Figure M.2: Permeability plot to calculate the formation damage after 1.5 lb/bbl PHPA solution core flow test

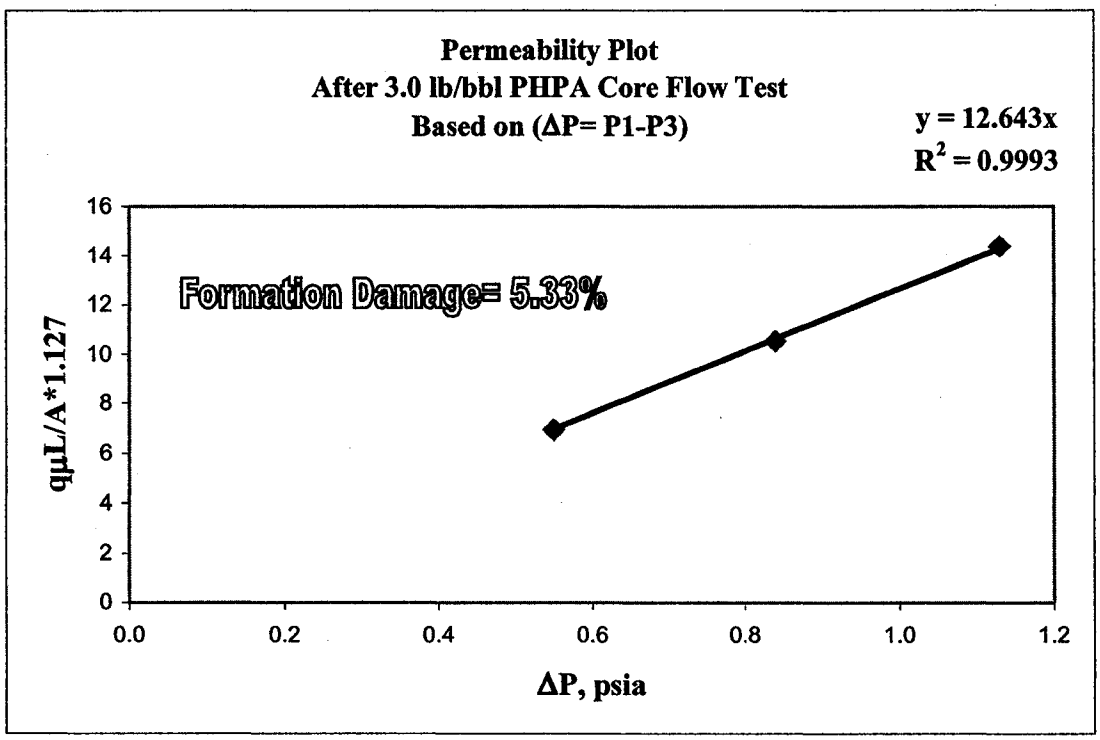

Figure M.3: Permeability plot to calculate the formation damage after 3.0 lb/bbl PHPA solution core flow test

APPENDIX N: HAAKE VISCOMETER SHEAR VISCOSITY DATA (XANTHAN GUM)

Table N.1: Shear viscosity data for 0.5 lb/bbl Xanthan Gum solution

Nr-Seg	t [s]	t_seg [s]	τ [Pa]	γ [1/s]	T [°C]
1|1	32.66	31.52	0.02449	0.211	21.6
1|2	64.93	63.79	0.05113	0.348	21.6
1|3	97.05	95.91	0.08259	0.583	21.6
1|4	129.2	128	0.133	0.968	21.6
1|5	161.3	160.1	0.17	1.625	21.6
1|6	193.3	192.1	0.246	2.621	21.6
1|7	225.9	224.7	0.348	4.256	21.6
1|8	257.9	256.8	0.458	6.92	21.6
1|9	290.1	288.9	0.612	11.2	21.6
1|10	322.1	321	0.776	18.2	21.6
1|11	354.1	353	0.998	29.58	21.6
1|12	386.3	385.1	1.272	47.99	21.6
1|13	418.4	417.2	1.617	77.87	21.6
1|14	450.4	449.2	2.028	126.3	21.6
1|15	482.5	481.4	2.598	204.9	21.6
1|16	514.7	513.5	3.324	332.3	21.6
1|17	546.7	545.5	4.335	539	21.6
1|18	578.7	577.6	5.675	874.2	21.6
1|19	611.2	610.1	10.15	1418	21.6
1|20	643.5	642.4	16.7	2300	21.6
2|1	675.5	30.94	16.77	2300	21.6
2|2	706.7	62.21	10.05	1418	21.6
2|3	737.9	93.33	5.437	874.2	21.6
2|4	769	124.5	4.159	539	21.6
2|5	800.2	155.7	3.225	332.3	21.6

2|6	831.4	186.8	2.522	204.9	21.6
2|7	862.5	218	1.986	126.3	21.6
2|8	893.8	249.3	1.584	77.86	21.6
2|9	924.9	280.4	1.273	47.97	21.6
2|10	956.2	311.6	0.997	29.6	21.6
2|11	987.4	342.8	0.793	18.19	21.6
2|12	1019	374.1	0.615	11.18	21.6
2|13	1050	405.5	0.46	6.924	21.6
2|14	1081	436.8	0.349	4.247	21.6
2|15	1112	467.9	0.263	2.612	21.6
2|16	1144	499.2	0.183	1.625	21.6
2|17	1175	530.6	0.125	0.977	21.6
2|18	1206	561.9	0.07367	0.592	21.6
2|19	1238	593.3	0.04793	0.357	21.6
2|20	1269	624.8	0.03052	0.197	21.6
3|1	1301	31.24	0.04069	0.207	21.6
3|2	1333	63.37	0.05734	0.362	21.6
3|3	1365	95.47	0.08177	0.583	21.6
3|4	1398	127.6	0.126	0.968	21.6
3|5	1430	159.6	0.198	1.621	21.6
3|6	1462	191.6	0.26	2.607	21.6
3|7	1494	223.7	0.339	4.247	21.6
3|8	1526	255.8	0.481	6.929	21.6
3|9	1558	287.8	0.616	11.2	21.6
3|10	1590	319.8	0.795	18.21	21.6
3|11	1622	352	0.991	29.57	21.6
3|12	1654	384	1.265	47.99	21.6
3|13	1686	416	1.596	77.86	21.6
3|14	1718	448.1	1.98	126.3	21.6
3|15	1750	480.1	2.528	204.8	21.6
3|16	1782	512.2	3.224	332.3	21.6
3|17	1814	544.4	4.169	538.9	21.6

3|18	1846	576.4	5.43	874.2	21.6
3|19	1878	608.4	9.949	1418	21.6
3|20	1911	640.5	16.51	2300	21.6
4|1	1942	30.86	16.49	2300	21.6
4|2	1974	62.19	9.948	1418	21.6
4|3	2005	93.66	5.357	874.2	21.6
4|4	2037	125	4.126	538.9	21.6
4|5	2068	156.3	3.187	332.3	21.6
4|6	2099	187.7	2.49	204.9	21.6
4|7	2131	219.1	1.967	126.3	21.6
4|8	2162	250.5	1.571	77.85	21.6
4|9	2193	282	1.246	48	21.6
4|10	2225	313.4	1.02	29.58	21.6
4|11	2256	344.8	0.775	18.21	21.6
4|12	2287	376	0.599	11.21	21.6
4|13	2319	407.4	0.469	6.953	21.6
4|14	2350	438.9	0.355	4.256	21.6
4|15	2382	470.1	0.254	2.593	21.6
4|16	2413	501.5	0.172	1.635	21.6
4|17	2444	532.8	0.117	0.968	21.6
4|18	2476	564.1	0.07174	0.592	21.6
4|19	2507	595.5	0.02935	0.348	21.6
4|20	2538	626.9	0.01835	0.216	21.6

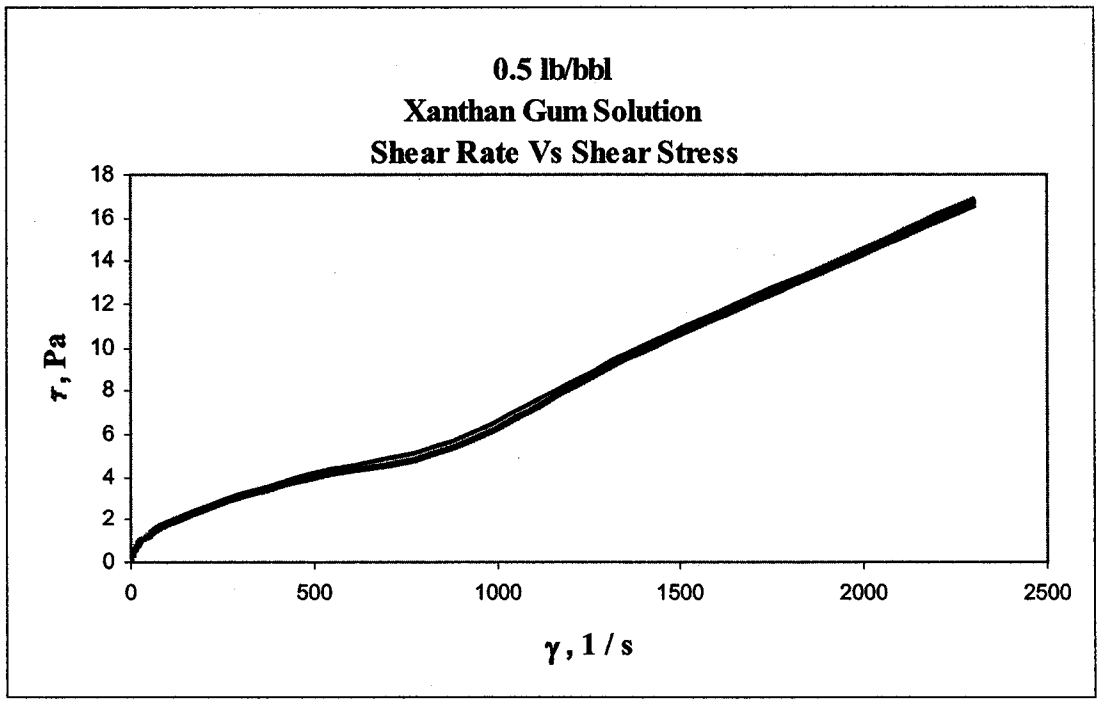

Figure N.1: Shear rate versus shear stress plot for 0.5 lb/bbl Xanthan Gum solution

Table N.2: Shear viscosity data for 1.5 lb/bbl Xanthan Gum solution

Nr-Seg	t [s]	t_seg [s]	τ [Pa]	γ [1/s]	T [°C]
1|1	32.52	31.31	1.609	0.216	21.9
1|2	64.93	63.72	1.802	0.352	21.9
1|3	97.17	95.97	2.057	0.597	21.9
1|4	129.3	128.1	2.315	0.972	21.9
1|5	161.4	160.2	2.653	1.63	21.9
1|6	193.8	192.6	2.938	2.598	21.9
1|7	226.1	224.9	3.29	4.256	21.9
1|8	258.3	257.1	3.687	6.948	21.9
1|9	290.2	289	4.071	11.21	21.9
1|10	322.4	321.2	4.493	18.19	21.9
1|11	354.4	353.2	4.994	29.57	21.9
1|12	386.3	385.1	5.548	47.99	21.9
1|13	418.4	417.2	6.186	77.86	21.9
1|14	450.5	449.3	6.976	126.3	21.9
1|15	482.5	481.3	7.965	204.9	21.9
1|16	514.5	513.3	9.204	332.3	21.9
1|17	546.6	545.4	10.91	538.9	21.9
1|18	578.7	577.5	13.04	874.2	21.9
1|19	610.6	609.4	15.61	1418	21.9
1|20	642.7	641.5	22.09	2300	21.9
2|1	674.5	30.74	22.17	2300	21.9
2|2	705.8	62.09	15.37	1418	21.9
2|3	737	93.32	12.82	874.2	21.9
2|4	768.2	124.5	10.73	538.9	21.9
2|5	799.5	155.7	9.045	332.3	21.9
2|6	830.7	186.9	7.763	204.8	21.9
2|7	861.9	218.2	6.789	126.3	21.9
2|8	893.1	249.4	5.973	77.86	21.9
2|9	924.2	280.5	5.33	48.01	21.9

2|10	955.5	311.8	4.802	29.58	21.9
2|11	986.8	343	4.31	18.22	21.9
2|12	1018	374.1	3.889	11.22	21.9
2|13	1049	405.4	3.491	6.915	21.9
2|14	1080	436.7	3.119	4.275	21.9
2|15	1112	467.9	2.805	2.621	21.9
2|16	1143	499.1	2.488	1.607	21.9
2|17	1174	530.4	2.178	0.977	21.9
2|18	1205	561.7	1.936	0.583	21.9
2|19	1237	592.9	1.687	0.357	21.9
2|20	1268	624	1.479	0.216	21.9
3|1	1299	31.16	1.46	0.221	21.9
3|2	1332	63.24	1.692	0.348	21.9
3|3	1364	95.28	1.953	0.583	21.9
3|4	1396	127.4	2.197	0.972	21.9
3|5	1428	159.5	2.499	1.63	21.9
3|6	1460	191.5	2.798	2.612	21.9
3|7	1492	223.7	3.134	4.256	21.9
3|8	1524	255.7	3.499	6.929	21.9
3|9	1556	287.7	3.87	11.2	21.9
3|10	1588	319.8	4.29	18.2	21.9
3|11	1620	351.9	4.771	29.58	21.9
3|12	1652	384	5.318	47.98	21.9
3|13	1684	416	5.953	77.86	21.9
3|14	1716	447.9	6.719	126.3	21.9
3|15	1748	479.9	7.672	204.9	21.9
3|16	1780	511.8	8.922	332.3	21.9
3|17	1812	543.9	10.58	538.9	21.9
3|18	1844	575.9	12.66	874.2	21.9
3|19	1877	608.3	15.14	1418	21.9
3|20	1909	640.6	21.96	2300	21.9
4|1	1941	30.74	22.17	2300	21.9

4|2	1972	62	14.94	1418	21.9
4|3	2003	93.15	12.46	874.2	21.9
4|4	2034	124.6	10.44	539	21.9
4|5	2066	156	8.815	332.3	21.9
4|6	2097	187.3	7.568	204.8	21.9
4|7	2128	218.6	6.617	126.3	21.9
4|8	2160	250	5.858	77.87	21.9
4|9	2191	281.4	5.229	47.96	21.9
4|10	2222	312.7	4.659	29.57	21.9
4|11	2254	344	4.202	18.18	21.9
4|12	2285	375.2	3.783	11.23	21.9
4|13	2316	406.5	3.401	6.934	21.9
4|14	2348	438	3.06	4.247	21.9
4|15	2379	469.3	2.713	2.593	21.9
4|16	2411	500.7	2.455	1.616	21.9
4|17	2442	532.1	2.163	0.968	21.9
4|18	2473	563.3	1.885	0.601	21.9
4|19	2504	594.6	1.629	0.357	21.9
4|20	2536	625.8	1.407	0.197	21.9

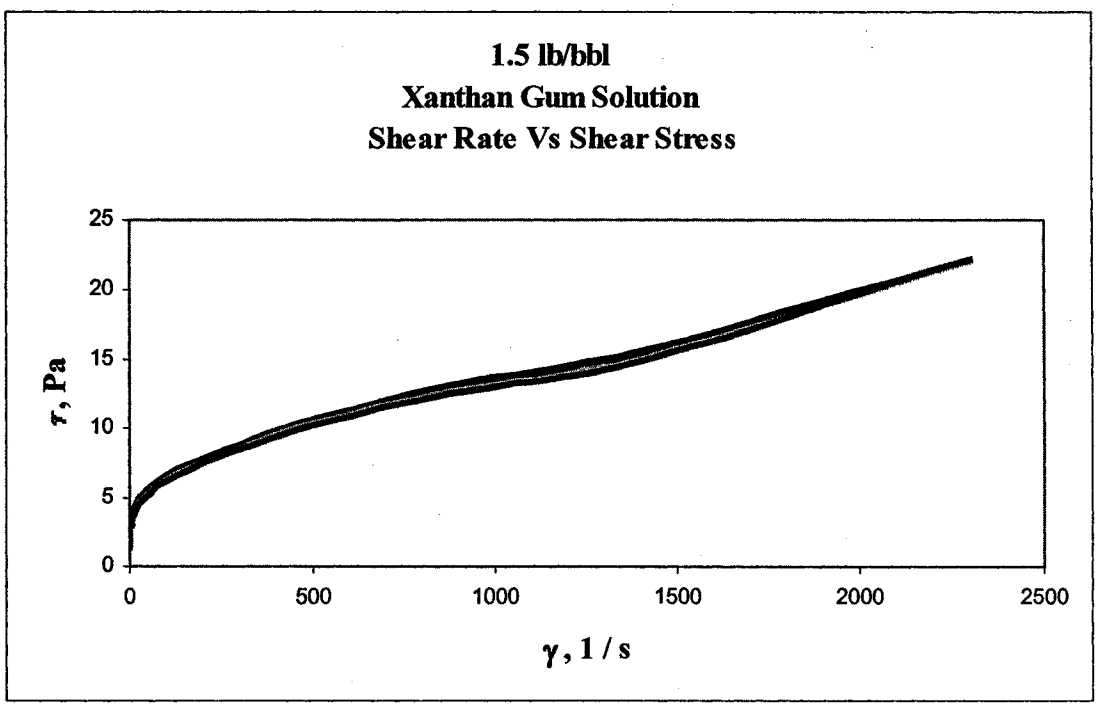

Figure N.2: Shear rate versus shear stress plot for 1.5 lb/bbl Xanthan Gum solution

Table N.3: Shear viscosity data for 3.0 lb/bbl Xanthan Gum solution

Nr-Seg	t [s]	t_seg [s]	τ [Pa]	γ [1/s]	T [°C]
1|1	32.58	31.37	7.215	0.244	21.5
1|2	65.31	64.11	7.08	0.362	21.5
1|3	97.69	96.48	7.546	0.601	21.5
1|4	130.1	128.9	8.128	0.968	21.5
1|5	162.6	161.4	8.692	1.635	21.5
1|6	195.1	193.9	9.275	2.617	21.4
1|7	227.5	226.3	9.924	4.261	21.5
1|8	261	259.8	10.63	6.934	21.5
1|9	294.7	293.5	11.48	11.2	21.5
1|10	327.1	325.9	12.45	18.2	21.5
1|11	359.6	358.4	13.47	29.59	21.5
1|12	392	390.8	14.42	47.99	21.5
1|13	424.3	423.1	15.39	77.86	21.5
1|14	456.9	455.7	16.45	126.3	21.5
1|15	489.6	488.4	17.7	204.8	21.5
1|16	522.9	521.7	19.68	332.3	21.5
1|17	555.4	554.2	22.22	539	21.5
1|18	587.9	586.7	24.96	874.2	21.5
1|19	620.3	619.1	28.73	1418	21.5
1|20	652.8	651.6	32.77	2300	21.5
2|1	685.1	31.09	32.51	2300	21.5
2|2	716.6	62.63	28.11	1418	21.5
2|3	748.1	94.09	24.1	874.2	21.5
2|4	779.5	125.5	20.82	538.9	21.5
2|5	811	157	18.41	332.3	21.5
2|6	842.5	188.5	16.66	204.8	21.5
2|7	873.8	219.8	15.34	126.3	21.5
2|8	905	251	14.24	77.85	21.5
2|9	936.6	282.6	13.16	47.97	21.5

2|10	968.1	314.1	12.08	29.6	21.5
2|11	999.5	345.5	11.02	18.21	21.5
2|12	1031	376.9	10.11	11.23	21.5
2|13	1062	408.4	9.3	6.915	21.5
2|14	1094	439.9	8.637	4.237	21.5
2|15	1125	471.3	8.041	2.593	21.5
2|16	1157	502.7	7.53	1.616	21.5
2|17	1188	533.9	6.994	0.958	21.5
2|18	1219	565.5	6.488	0.573	21.5
2|19	1251	596.8	5.933	0.376	21.5
2|20	1282	628.4	5.402	0.225	21.5
3|1	1315	31.3	5.458	0.211	21.5
3|2	1347	63.67	6.285	0.357	21.5
3|3	1379	95.94	6.961	0.611	21.5
3|4	1412	128.4	7.318	0.972	21.5
3|5	1444	161	7.695	1.635	21.5
3|6	1477	193.4	8.093	2.607	21.5
3|7	1509	225.9	8.626	4.251	21.5
3|8	1541	258.2	9.333	6.939	21.5
3|9	1574	290.7	10.09	11.2	21.5
3|10	1607	323.2	11.07	18.19	21.5
3|11	1639	355.7	12.12	29.58	21.5
3|12	1672	388.3	13.22	48	21.5
3|13	1705	421.3	14.31	77.87	21.5
3|14	1738	454.3	15.38	126.3	21.5
3|15	1770	486.8	16.67	204.9	21.5
3|16	1803	519.4	18.44	332.3	21.5
3|17	1835	551.8	20.86	538.9	21.5
3|18	1868	584.3	24.12	874.2	21.5
3|19	1900	616.8	27.93	1418	21.5
3|20	1932	649.2	32.1	2300	21.5
4|1	1965	30.9	32.04	2300	21.5

4|2	1996	62.18	27.8	1418	21.5
4|3	2027	93.55	23.89	874.2	21.5
4|4	2059	125.1	20.67	538.9	21.5
4|5	2090	156.5	18.29	332.3	21.5
4|6	2122	188	16.58	204.8	21.5
4|7	2153	219.3	15.29	126.3	21.5
4|8	2185	250.8	14.17	77.87	21.5
4|9	2216	282.2	13.11	47.97	21.5
4|10	2247	313.6	11.99	29.55	21.5
4|11	2279	345	10.93	18.22	21.5
4|12	2310	376.5	9.964	11.21	21.5
4|13	2342	407.9	9.201	6.943	21.5
4|14	2373	439.3	8.518	4.237	21.5
4|15	2404	470.6	7.933	2.612	21.5
4|16	2436	502.1	7.431	1.616	21.5
4|17	2467	533.5	6.893	0.968	21.5
4|18	2499	564.9	6.369	0.573	21.5
4|19	2530	596.4	5.807	0.366	21.5
4|20	2562	627.9	5.296	0.188	21.5

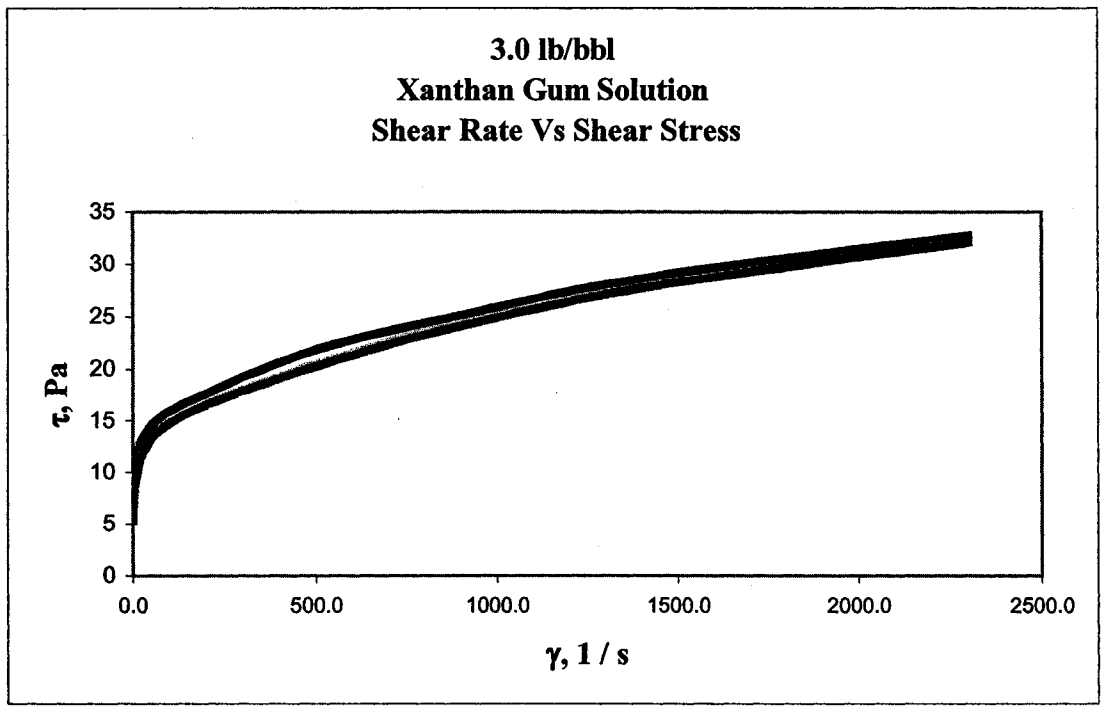

Figure N.3: Shear rate versus shear stress plot for 3.0 lb/bbl Xanthan Gum solution

APPENDIX O: HAAKE VISCOMETER SHEAR VISCOSITY DATA (PHPA)

Table O.1: Shear viscosity data for 0.5 lb/bbl PHPA solution

Nr-Seg	t [s]	t_seg [s]	τ [Pa]	γ [1/s]	T [°C]
1|1	32.6	31.5	0.00	0.22	21.9
1|2	64.8	63.7	0.00	0.35	21.9
1|3	97.0	95.9	0.04	0.59	21.9
1|4	129.2	128.1	0.01	0.96	21.9
1|5	161.2	160.1	0.05	1.61	22.0
1|6	193.1	192.0	0.03	2.61	22.0
1|7	225.2	224.1	0.06	4.26	22.0
1|8	257.2	256.1	0.10	6.93	22.0
1|9	289.2	288.1	0.16	11.20	22.0
1|10	321.1	320.0	0.24	18.18	22.0
1|11	353.1	352.0	0.35	29.59	21.9
1|12	385.1	384.0	0.53	47.98	21.9
1|13	417.2	416.1	0.75	77.86	21.9
1|14	449.2	448.1	1.04	126.30	22.0
1|15	481.3	480.2	1.50	204.80	22.0
1|16	513.4	512.3	2.15	332.30	21.9
1|17	545.4	544.3	3.07	539.00	21.9
1|18	577.5	576.4	5.81	874.20	21.9
1|19	609.6	608.5	9.85	1418.00	22.0
1|20	641.7	640.6	16.43	2300.00	22.0
2|1	673.6	30.8	16.49	2300.00	21.9
2|2	704.8	62.0	9.57	1418.00	21.9
2|3	736.1	93.3	5.49	874.20	22.0
2|4	767.3	124.5	3.02	539.00	22.0

2|5	798.4	155.6	2.12	332.30	21.9
2|6	829.6	186.8	1.49	204.80	21.9
2|7	860.8	218.0	1.06	126.30	22.0
2|8	892.1	249.3	0.76	77.85	22.0
2|9	923.2	280.4	0.51	47.99	21.9
2|10	954.5	311.7	0.34	29.57	21.9
2|11	985.6	342.8	0.23	18.21	22.0
2|12	1017.0	374.0	0.16	11.20	22.0
2|13	1048.0	405.3	0.12	6.93	21.9
2|14	1079.0	436.5	0.07	4.25	21.9
2|15	1111.0	467.7	0.05	2.61	22.0
2|16	1142.0	499.2	0.02	1.62	22.0
2|17	1173.0	530.6	0.01	0.98	21.9
2|18	1205.0	561.8	0.00	0.58	21.9
2|19	1236.0	593.1	0.00	0.35	22.0
2|20	1267.0	624.3	0.00	0.23	22.0
3|1	1299.0	31.2	0.00	0.21	21.9
3|2	1331.0	63.2	0.01	0.36	21.9
3|3	1363.0	95.2	0.01	0.58	22.0
3|4	1395.0	127.5	0.00	0.96	22.0
3|5	1428.0	160.0	0.01	1.63	21.9
3|6	1460.0	192.1	0.03	2.62	22.0
3|7	1492.0	224.1	0.07	4.25	22.0
3|8	1524.0	256.2	0.10	6.92	21.9
3|9	1556.0	288.3	0.16	11.20	21.9
3|10	1588.0	320.4	0.22	18.20	22.0
3|11	1620.0	352.5	0.38	29.58	22.0
3|12	1652.0	384.5	0.51	48.00	21.9
3|13	1684.0	416.5	0.76	77.86	21.9
3|14	1716.0	448.5	1.04	126.30	21.9
3|15	1748.0	480.6	1.50	204.80	22.0
3|16	1780.0	512.7	2.14	332.30	22.0

3|17	1812.0	544.7	3.05	539.00	21.9
3|18	1845.0	576.9	5.59	874.20	22.0
3|19	1877.0	608.9	9.56	1418.00	22.0
3|20	1909.0	641.0	16.50	2300.00	21.9
4|1	1940.0	30.6	16.52	2300.00	21.9
4|2	1972.0	61.9	9.57	1418.00	22.0
4|3	2003.0	93.0	5.56	874.20	22.0
4|4	2034.0	124.4	3.02	539.00	21.9
4|5	2065.0	155.8	2.10	332.30	21.9
4|6	2097.0	187.0	1.48	204.90	22.0
4|7	2128.0	218.1	1.05	126.30	22.0
4|8	2159.0	249.6	0.74	77.87	21.9
4|9	2190.0	280.8	0.52	47.99	21.9
4|10	2222.0	312.4	0.33	29.55	22.0
4|11	2254.0	344.0	0.24	18.20	22.0
4|12	2285.0	375.2	0.15	11.21	21.9
4|13	2316.0	406.4	0.10	6.92	21.9
4|14	2347.0	437.7	0.07	4.24	22.0
4|15	2378.0	468.7	0.04	2.59	22.0
4|16	2410.0	499.9	0.03	1.62	21.9
4|17	2441.0	531.1	0.00	0.98	21.9
4|18	2472.0	562.4	0.00	0.59	22.0
4|19	2503.0	593.7	0.00	0.35	22.0
4|20	2535.0	624.9	0.00	0.21	22.0

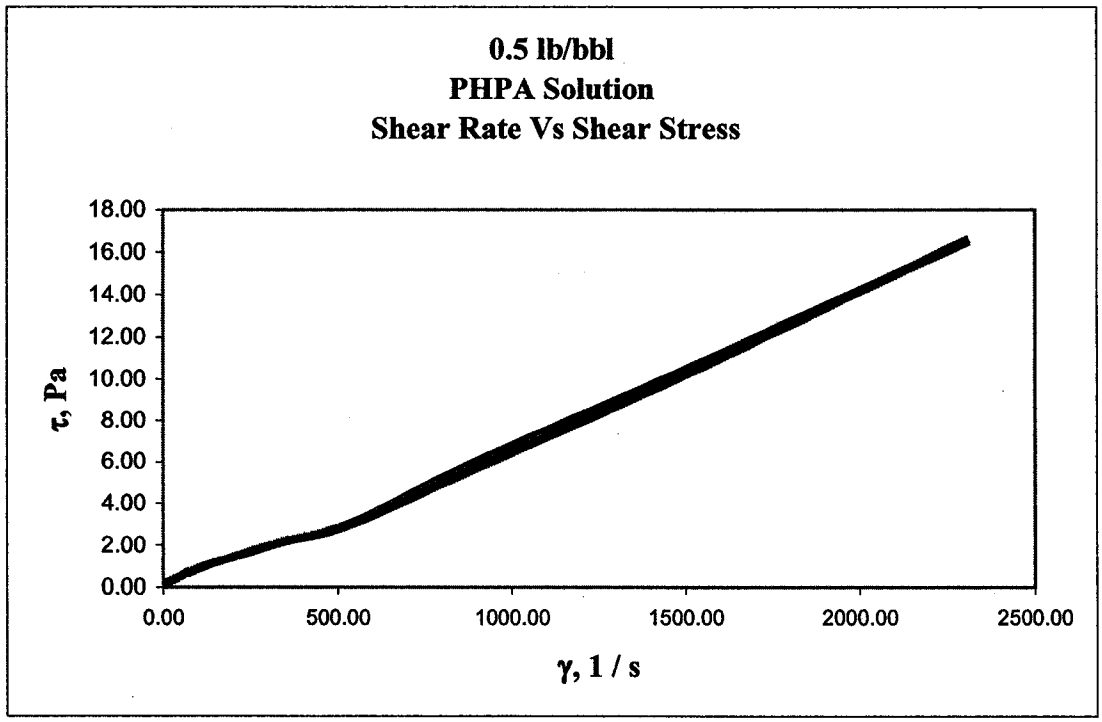

Figure O.1: Shear rate versus shear stress plot for 0.5 lb/bbl PHPA solution

Table O.2: Shear viscosity data for 1.5 lb/bbl PHPA solution

Nr-Seg	t [s]	t_seg [s]	τ [Pa]	γ [1/s]	T [°C]
1|1	32.590	31.420	0.005	0.21	21.9
1|2	64.900	63.730	0.001	0.36	21.9
1|3	97.330	96.160	0.013	0.60	21.9
1|4	130.200	129.100	0.077	0.96	21.9
1|5	162.900	161.700	0.082	1.62	21.9
1|6	195.500	194.300	0.136	2.61	21.9
1|7	228.100	226.900	0.195	4.26	21.9
1|8	260.600	259.400	0.304	6.93	21.9
1|9	293.100	292.000	0.466	11.21	21.9
1|10	325.700	324.500	0.719	18.21	21.9
1|11	358.400	357.200	1.100	29.57	21.9
1|12	390.800	389.700	1.577	47.99	21.9
1|13	423.500	422.400	2.277	77.86	21.9
1|14	456.200	455.000	3.187	126.30	21.9
1|15	488.800	487.600	4.401	204.80	21.9
1|16	521.400	520.300	5.995	332.30	21.9
1|17	553.900	552.800	8.116	539.00	21.9
1|18	586.600	585.400	10.810	874.30	21.9
1|19	619.100	617.900	14.170	1418.00	21.9
1|20	651.700	650.600	28.510	2300.00	21.9
2|1	684.000	30.940	28.450	2300.00	21.9
2|2	715.700	62.600	14.240	1418.00	21.9
2|3	747.200	94.130	10.870	874.20	21.9
2|4	778.700	125.600	8.171	538.90	21.9
2|5	810.200	157.200	6.044	332.30	21.9
2|6	841.800	188.800	4.399	204.90	21.9
2|7	873.300	220.200	3.207	126.30	21.9
2|8	904.700	251.600	2.276	77.87	21.9
2|9	936.400	283.400	1.591	47.99	21.9

2|10	967.900	314.800	1.093	29.57	21.9
2|11	999.400	346.400	0.710	18.23	21.9
2|12	1031.000	377.900	0.462	11.21	21.9
2|13	1062.000	409.300	0.294	6.94	21.9
2|14	1094.000	440.800	0.188	4.26	21.9
2|15	1125.000	472.000	0.114	2.60	21.9
2|16	1156.000	503.100	0.054	1.63	21.9
2|17	1187.000	534.400	0.045	0.96	21.9
2|18	1219.000	565.600	0.019	0.58	21.9
2|19	1250.000	596.800	0.010	0.35	21.9
2|20	1281.000	628.100	0.006	0.23	21.9
3|1	1313.000	31.220	0.000	0.22	21.9
3|2	1345.000	63.260	0.000	0.35	21.9
3|3	1377.000	95.380	0.014	0.60	21.9
3|4	1409.000	127.400	0.026	0.95	21.9
3|5	1441.000	159.400	0.079	1.62	21.9
3|6	1473.000	191.400	0.108	2.62	21.9
3|7	1505.000	223.400	0.182	4.26	21.9
3|8	1537.000	255.400	0.297	6.92	21.9
3|9	1569.000	287.500	0.453	11.19	21.9
3|10	1601.000	319.600	0.737	18.18	21.9
3|11	1633.000	351.600	1.071	29.59	21.9
3|12	1666.000	383.700	1.609	47.98	21.9
3|13	1698.000	415.700	2.274	77.86	21.9
3|14	1730.000	447.800	3.213	126.30	21.9
3|15	1762.000	479.900	4.422	204.80	21.9
3|16	1794.000	511.900	6.035	332.30	21.9
3|17	1826.000	544.000	8.186	539.00	21.9
3|18	1858.000	576.000	10.890	874.20	21.9
3|19	1890.000	608.200	14.240	1418.00	21.9
3|20	1922.000	640.400	28.140	2300.00	21.9
4|1	1954.000	30.900	27.990	2300.00	21.9

4|2	1985.000	62.060	14.210	1418.00	21.9
4|3	2017.000	93.400	10.860	874.30	21.9
4|4	2048.000	124.600	8.164	538.90	21.9
4|5	2079.000	156.100	6.030	332.30	21.9
4|6	2111.000	187.500	4.407	204.90	21.9
4|7	2142.000	218.900	3.210	126.30	21.9
4|8	2173.000	250.200	2.276	77.87	21.9
4|9	2205.000	281.600	1.581	48.01	21.9
4|10	2236.000	313.100	1.082	29.58	21.9
4|11	2268.000	344.600	0.722	18.20	21.9
4|12	2299.000	375.800	0.449	11.20	21.9
4|13	2331.000	407.300	0.309	6.94	21.9
4|14	2362.000	438.800	0.197	4.27	21.9
4|15	2394.000	470.200	0.110	2.59	21.9
4|16	2425.000	501.400	0.057	1.61	21.9
4|17	2456.000	532.800	0.047	0.95	21.9
4|18	2488.000	564.300	0.028	0.59	21.9
4|19	2519.000	595.700	0.004	0.36	21.9
4|20	2551.000	627.200	0.000	0.23	21.9

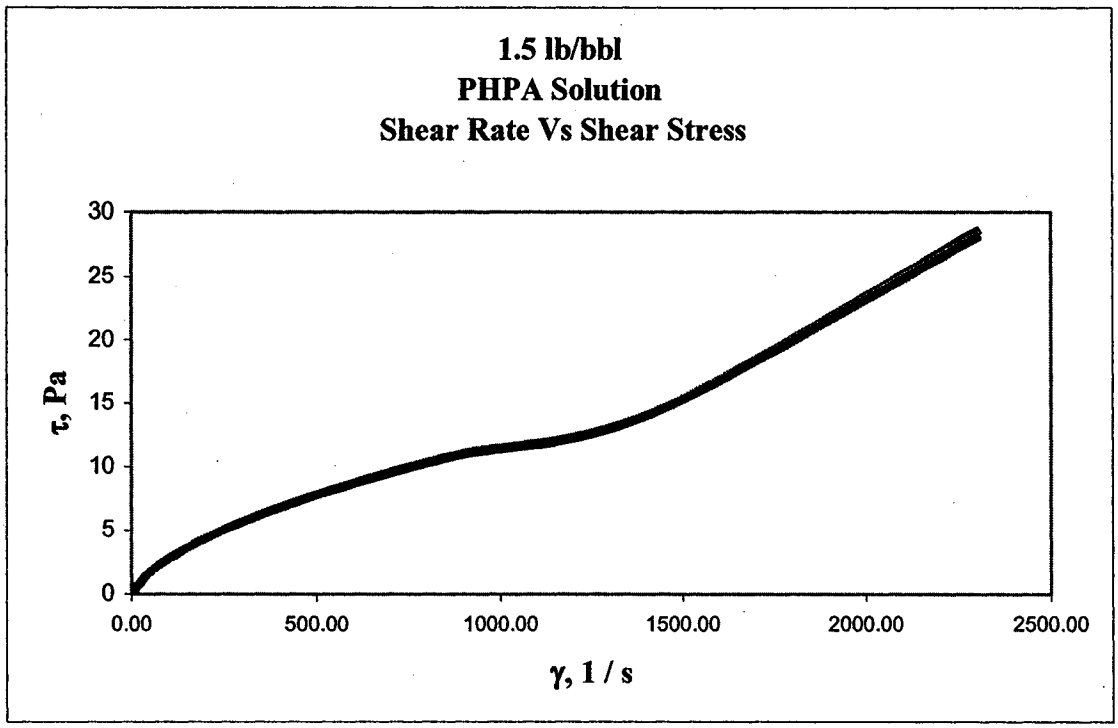

Figure O.2: Shear rate versus shear stress plot for 1.5 lb/bbl PHPA solution

Table O.3: Shear viscosity data for 3.0 lb/bbl PHPA solution

Nr-Seg	t [s]	t_seg [s]	τ [Pa]	γ [1/s]	T [°C]
1|1	32.51	31.32	0.07	0.21	21.9
1|2	64.87	63.68	0.11	0.36	21.9
1|3	97.12	95.93	0.20	0.58	21.9
1|4	129.30	128.10	0.28	0.97	21.9
1|5	161.30	160.20	0.46	1.62	21.9
1|6	193.40	192.20	0.70	2.62	21.9
1|7	225.40	224.20	1.07	4.26	21.9
1|8	257.50	256.30	1.54	6.93	21.9
1|9	289.50	288.30	2.19	11.22	21.9
1|10	321.50	320.30	3.02	18.22	21.9
1|11	353.70	352.50	4.09	29.56	21.9
1|12	385.80	384.60	5.37	47.98	21.9
1|13	418.00	416.80	6.97	77.86	21.9
1|14	450.10	448.90	8.88	126.30	21.9
1|15	482.20	481.00	11.24	204.80	21.9
1|16	514.20	513.00	14.12	332.30	21.9
1|17	546.40	545.20	17.79	538.90	21.9
1|18	578.40	577.20	22.52	874.20	21.9
1|19	610.60	609.40	28.35	1418.00	21.9
1|20	642.70	641.50	38.82	2300.00	21.9
2|1	675.30	31.16	38.02	2300.00	21.9
2|2	706.90	62.76	28.05	1418.00	21.9
2|3	738.10	94.00	22.30	874.20	21.9
2|4	769.30	125.20	17.75	538.90	21.9
2|5	800.60	156.50	14.12	332.30	21.9
2|6	831.70	187.60	11.20	204.90	21.9
2|7	863.00	218.90	8.87	126.30	21.9
2|8	894.30	250.20	6.93	77.86	21.9
2|9	925.50	281.40	5.36	47.98	21.9

2|10	956.80	312.70	4.04	29.57	21.9
2|11	988.00	343.90	3.01	18.20	21.9
2|12	1019.00	375.10	2.18	11.18	21.9
2|13	1050.00	406.30	1.55	6.93	21.9
2|14	1082.00	437.70	1.05	4.27	21.9
2|15	1113.00	469.10	0.69	2.59	21.9
2|16	1145.00	500.50	0.46	1.63	21.9
2|17	1176.00	531.70	0.28	0.96	21.9
2|18	1207.00	562.90	0.17	0.60	21.9
2|19	1238.00	594.20	0.11	0.36	21.9
2|20	1270.00	625.50	0.08	0.19	21.9
3|1	1301.00	31.23	0.07	0.21	21.9
3|2	1333.00	63.23	0.11	0.35	21.9
3|3	1365.00	95.27	0.16	0.59	21.9
3|4	1398.00	127.60	0.28	0.95	21.9
3|5	1430.00	159.80	0.45	1.62	21.9
3|6	1462.00	192.20	0.70	2.62	21.9
3|7	1494.00	224.10	1.05	4.25	21.9
3|8	1526.00	256.10	1.54	6.91	21.9
3|9	1558.00	288.30	2.18	11.21	21.9
3|10	1591.00	320.40	3.00	18.22	21.9
3|11	1623.00	352.70	4.03	29.57	21.9
3|12	1655.00	385.00	5.35	47.97	21.9
3|13	1687.00	417.10	6.95	77.87	21.9
3|14	1719.00	449.10	8.87	126.30	21.9
3|15	1751.00	481.30	11.19	204.90	21.9
3|16	1783.00	513.30	14.08	332.30	21.9
3|17	1816.00	545.40	17.71	539.00	21.9
3|18	1848.00	577.50	22.29	874.20	21.9
3|19	1880.00	609.50	28.04	1418.00	21.9
3|20	1912.00	641.60	35.50	2300.00	21.9
4|1	1944.00	30.83	35.53	2300.00	21.9

4|2	1975.00	62.05	27.96	1418.00	21.9
4|3	2006.00	93.37	22.26	874.20	21.9
4|4	2037.00	124.60	17.69	539.00	21.9
4|5	2069.00	155.90	14.07	332.30	21.9
4|6	2100.00	187.10	11.19	204.80	21.9
4|7	2131.00	218.30	8.82	126.30	21.9
4|8	2162.00	249.70	6.93	77.87	21.9
4|9	2194.00	281.10	5.35	47.98	21.9
4|10	2225.00	312.50	4.04	29.57	21.9
4|11	2257.00	343.80	3.01	18.21	21.9
4|12	2288.00	375.10	2.16	11.18	21.9
4|13	2319.00	406.30	1.52	6.92	21.9
4|14	2350.00	437.50	1.04	4.25	21.9
4|15	2381.00	468.70	0.67	2.62	21.9
4|16	2413.00	500.00	0.45	1.63	21.9
4|17	2444.00	531.20	0.27	0.96	21.9
4|18	2475.00	562.50	0.16	0.59	21.9
4|19	2506.00	593.70	0.09	0.35	21.9
4|20	2538.00	625.00	0.06	0.19	21.9

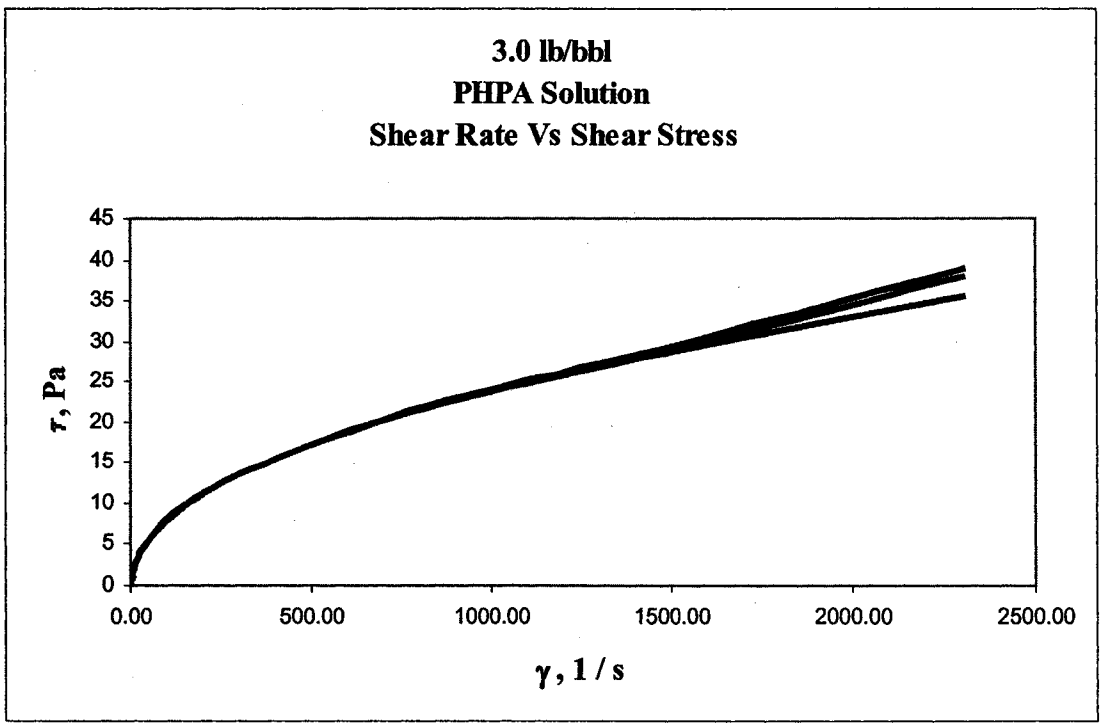

Figure O.3: Shear rate versus shear stress plot for3.0 lb/bbl PHPA solution